NACA RM L55H05

NACA

RESEARCH MEMORANDUM

LOW-SPEED STUDY OF THE EFFECT OF FREQUENCY ON THE STABILITY DERIVATIVES OF WINGS OSCILLATING IN YAW WITH PARTICULAR REFERENCE TO HIGH ANGLE-OF-ATTACK CONDITIONS

By John P. Campbell, Joseph L. Johnson, Jr., and Donald E. Hewes

Langley Aeronautical Laboratory
Langley Field, Va.

NATIONAL ADVISORY COMMITTEE FOR AERONAUTICS

WASHINGTON

November 1, 1955
Declassified June 20, 1957

NATIONAL ADVISORY COMMITTEE FOR AERONAUTICS

RESEARCH MEMORANDUM

LOW-SPEED STUDY OF THE EFFECT OF FREQUENCY ON THE STABILITY DERIVATIVES OF WINGS OSCILLATING IN YAW WITH PARTICULAR REFERENCE TO HIGH ANGLE-OF-ATTACK CONDITIONS

By John P. Campbell, Joseph L. Johnson, Jr., and Donald E. Hewes

SUMMARY

A low-speed investigation has been conducted in the Langley free-flight tunnel to provide some basic information regarding the effects of frequency on wings oscillating in yaw. The investigation consisted of both free-oscillation tests and forced-oscillation tests of a 60° delta wing, a 45° sweptback wing of aspect ratio 2.61, and an unswept wing of aspect ratio 3 over an angle-of-attack range from 0° to 30°. The investigation covered a range of the reduced-frequency parameter $\omega b/2V$ of 0.08 to 0.30 for the free-oscillation tests and of 0.01 to 0.12 for the forced-oscillation tests.

At very low values of reduced frequency, the directional stability derivative $C_{n_\beta} + k^2 C_{n_{\dot{r}}}$ and the effective dihedral derivative $-\left(C_{l_\beta} + k^2 C_{l_{\dot{r}}}\right)$ measured in the oscillation tests tended to approach the steady state values of C_{n_β} and $-C_{l_\beta}$ measured in conventional static force tests. At these very low frequencies, extremely large values of the damping-in-yaw derivative $C_{n_r} - C_{n_{\dot{\beta}}}$ and the cross derivative $C_{l_r} - C_{l_{\dot{\beta}}}$ were obtained with the delta and swept wings at high angles of attack where considerable flow separation was present. For these conditions, increasing the frequency from the very low values caused large reductions in the absolute magnitude of all four of these derivatives. These results were attributed to a lag in the alternating increase and decrease in separated flow over the wing panels as the models oscillated in yaw. In general, only minor effects of frequency were obtained with the delta and swept wings at low angles of attack or with the unswept wing at any angle of attack.

INTRODUCTION

Several investigations have been made in the past few years to determine the dynamic-stability derivatives of airplanes or components of airplanes performing oscillations in yaw or sideslip. (See refs. 1 to 11.) Some of these investigations (refs. 1 to 7) have indicated that large values of the important damping-in-yaw parameter $C_{n_r} - C_{n_{\dot{\beta}}}$ can be produced at moderate and high angles of attack by swept or delta wings. Although three of these studies (refs. 3, 4, and 7) have provided some information on the effects of oscillation frequency on the derivatives, no systematic investigation of the effects of frequency has been made at the higher angles of attack where the derivatives are largest. The present investigation was therefore undertaken to provide some basic information regarding the effects of frequency on the stability derivatives of wings oscillating in yaw at angles of attack from 0° to 30°.

The investigation consisted of both free-oscillation and forced-oscillation tests of a 60° delta wing, a 45° swept wing of aspect ratio 2.61, and an unswept wing of aspect ratio 3. The tests were made at relatively low Reynolds numbers in the Langley free-flight tunnel and covered a range of the reduced-frequency parameter $\omega b/2V$ of 0.08 to 0.30 for the free-oscillation tests and 0.01 to 0.12 for the forced-oscillation tests. This overall range of reduced frequency is believed to cover the frequencies likely to be obtained in the lateral oscillations of airplanes having wing plan forms similar to those used in this investigation. In the testing techniques used in this investigation in which the model is oscillated in yaw about a fixed axis, the angle of sideslip is equal and opposite to the angle of yaw so that stability derivatives are measured in the following combinations: $C_{n_\beta} + k^2 C_{n_{\dot{r}}}$ and $C_{l_\beta} + k^2 C_{l_{\dot{r}}}$ (derivatives in phase with displacement) and $C_{n_r} - C_{n_{\dot{\beta}}}$ and $C_{l_r} - C_{l_{\dot{\beta}}}$ (derivatives 90° out of phase with displacement). In the forced-oscillation tests all four of these derivatives were measured, but in the free-oscillation tests only the damping-in-yaw derivative $C_{n_r} - C_{n_{\dot{\beta}}}$ was measured. Conventional static force tests were also made with the three wings to provide static longitudinal and lateral stability data for use in correlation with the oscillation data.

SYMBOLS

All stability parameters and coefficients are referred to the stability system of axes originating at a center-of-gravity position of 25.0 percent of the mean aerodynamic chord and in the chord plane of wings investigated. (See fig. 1.)

b	wing span, ft
$\bar{c}$	mean aerodynamic chord, ft
c	torsion spring constant, ft-lb/rad
e	modulated input voltage for strain-gage balance, volts
e_1	maximum input voltage for yawing-moment strain gages, volts
e_2	maximum input voltage for rolling-moment strain gages, volts
i	output current from strain gages, amps
k_n, k_l	overall calibration constants for strain gages and amplifier, amps/volt-foot-pound
k	reduced frequency parameter ($\omega b/2V$)
a	logarithmic decrement per second, wind-on test
a_f	logarithmic decrement per second, wind-off test
m	mass of model, slugs
q	dynamic pressure, lb/sq ft
ρ_o	air density, slug/cu ft
t	time, sec
I_Z	moment of inertia about Z-axis, slug-ft^2
I_{XZ}	product of inertia relative to stability axes, slug-ft^2
P	period, sec
S	wing area, sq ft
α	angle of attack, deg
β	angle of sideslip (for the present tests, $\beta = -\psi$), deg
ψ	angle of yaw, deg
$\dot{\beta}$	rate of change of sideslip angle, rad/sec

$\dot{\psi}$,r rate of change of yaw angle, rad/sec

$\ddot{\psi}$,$\dot{r}$ yawing acceleration, rad/sec^2

τ time lag between model displacement and resultant moment, sec (in this report it is assumed that for zero lag, positive yawing moment is produced by positive angle of yaw)

ϕ phase angle between model displacement and resultant moment, deg $\left(\frac{360\tau}{P}\right)$

τ_s calculated time lag associated with separation effects, sec (time lag between model displacement and the moment obtained by subtracting calculated moment from experimental moment, see fig. 29)

ϕ_s phase angle associated with separation effects, deg $\left(\text{phase angle between model displacement and the moment obtained by subtracting calculated moment from experimental moment } \frac{360\tau_s}{P}\right)$

ω angular velocity, rad/sec

V airspeed, feet per sec

X longitudinal force, lb

Y lateral force, lb

Z force along Z-axis, lb

M pitching moment, lb-ft

N yawing moment, lb-ft

L rolling moment, lb-ft

C_L lift coefficient, Lift/qS

C_D drag coefficient, Drag/qS

C_m pitching-moment coefficient, $\frac{M}{qS\bar{c}}$

C_n yawing-moment coefficient, $\frac{N}{qSb}$

C_l rolling-moment coefficient, $\frac{L}{qSb}$

$N_\beta = \frac{\partial N}{\partial \beta}$, lb-ft/rad

$N_{\dot{\beta}} = \frac{\partial N}{\partial\left(\frac{d\beta}{dt}\right)}$, lb-ft/rad/sec

$N_{\dot{\psi}} = \frac{\partial N}{\partial\left(\frac{d\psi}{dt}\right)}$, lb-ft/rad/sec

$L_\beta = \frac{\partial L}{\partial \beta}$, lb-ft/rad

$L_{\dot{\beta}} = \frac{\partial L}{\partial\left(\frac{d\beta}{dt}\right)}$, lb-ft/rad/sec

$L_{\dot{\psi}} = \frac{\partial L}{\partial\left(\frac{d\psi}{dt}\right)}$, lb-ft/rad/sec

$C_{n_\beta} = \frac{\partial C_n}{\partial \beta}$

$C_{n_{\dot{\beta}}} = \frac{\partial C_n}{\partial \frac{\dot{\beta} b}{2V}}$

$C_{n_r} = \frac{\partial C_n}{\partial \frac{rb}{2V}}$

$C_{n_{\dot{r}}} = \frac{\partial C_n}{\partial \frac{\dot{r} b^2}{4V^2}}$

$C_{l_\beta} = \frac{\partial C_l}{\partial \beta}$

$C_{l_{\dot{\beta}}} = \frac{\partial C_l}{\partial \frac{\dot{\beta} b}{2V}}$

$$C_{l_r} = \frac{\partial C_l}{\partial \frac{rb}{2V}}$$

$$C_{l_{\dot{r}}} = \frac{\partial C_l}{\partial \frac{\dot{r}b^2}{4V^2}}$$

Subscripts:

l	related to rolling moment
n	related to yawing moment
ψ_{max}	quantity measured when ψ is maximum
$\psi = 0$	quantity measured when ψ is zero during oscillation
max	maximum
av.	average
calc.	calculated
exp.	experimental

APPARATUS AND MODELS

The free-to-damp and forced-oscillation tests were conducted in the Langley free-flight tunnel. The installation of the forced-oscillation apparatus in the tunnel is shown in figure 2. The dimensional characteristics of the three wing models used in the investigation are given in table I. The delta- and swept-wing models were constructed of solid mahogany while the unswept wing model was of built-up balsa construction. There were provisions in each model for mounting an internal strain-gage moment balance at 0.25 mean aerodynamic chord. The model was rotated with respect to the balance to change angle of attack so that all measurements were made with respect to the stability axes.

Free-To-Damp Oscillation Equipment

Drawings of the free-to-damp oscillation apparatus are presented in figure 3(a). The wing models were attached to the horizontal sting which was mounted in ball bearings in the head of the supporting structure

and was alined at right angles to the airstream so that the model would rotate about the yaw stability axis. A torsion rod which had a spring constant of one foot-pound per degree was attached to the sting and the bearing housing, as shown in figure 3(a), to provide the spring restraint for the rotating sting. A cross bar to which different weights were added was attached to the sting so that the inertia of the system could be changed to vary the oscillation frequency. A light cable attached to the inertia bar and passing into the tunnel control room was used to displace the model in yaw to start the oscillations. The displacement of the model in yaw was measured by means of a slide-wire pick-up, and the time histories of this motion were recorded on an oscillograph.

Forced-Oscillation Equipment

The forced-oscillation apparatus was the same as that used for the free-to-damp tests except that the wings were mounted to the sting by means of a strain-gage balance, the inertia bar was removed, and the bearing housing containing the torsion spring was replaced with one containing the oscillator unit shown in figure 3(b). The oscillator consisted of a drum-type cam, which produced one cycle of sinusoidal motion per revolution, and two roller cam followers connected to the ends of a thin steel strap which was wrapped around the shaft of the sting and pinned to it at the midpoint of the strap. Both followers were forced against the cam face to eliminate play in the system by preloading the strap in tension. The cam followers were supported in carefully machined tracks which permitted the followers to move only in the vertical direction. The cam was rotated at speeds between about 0.06 and 0.50 revolution per second by a 5-horsepower electrical drive unit built into the lower portion of the sting support and connected to the cam by a drive shaft passing through the tubular support structure.

Two different methods for obtaining data were used in the forced oscillation tests. Block diagrams showing the instrumentation for each method are given in figure 4. In the first method, which will be called method A, the input voltage was kept constant and the output signals from the rolling- and yawing-moment strain gages as well as the displacement signal from the slidewire pick-off were fed into a multichannel oscillograph through a control box for gain control and circuit balancing. Low pass filters with cut-off at 10 cycles per second were employed to minimize record hash due to tunnel vibration and turbulence.

The second method, method B, involved the use of a system for resolving the balance output signals into components in and out of phase with displacement. This method required much less data reduction time than method A because it provided for direct measurement of the moments used to calculate the various derivatives. In this case, the slidewire pick-up which provided the in-phase signal and a rate pick-up which

provided the out-of-phase signal were used to modulate the output of two power supplies which furnished voltage for the strain gages. The rate pick-up which measured the angular velocity of the sting was essentially a direct-current generator similar in construction to a D'Arsonval galvanometer. Gain controls on the power supplies were adjusted to equalize the maximum amplitudes of the modulated voltages and a monitoring cathode-ray oscilloscope was used for measuring the amplitudes. A selector switch was provided on the control box so that either of the two voltages could be applied to the strain gages and a potentiometer for balancing the circuit was also provided. Because the power input to the balance was limited to a relatively low value by the modulated power supply, it was necessary to use a direct-current amplifier to amplify the strain-gage signals before measuring them on a heavily damped microammeter.

TESTS

All static tests, free-to-damp oscillation tests, and forced-oscillation tests were made over an angle-of-attack range from 0° to 30°. The static tests and forced-oscillation tests were made for the unswept, sweptback, and delta-wing configurations. The free-to-damp oscillation tests were made for the delta wing only.

Force tests were made to determine the static longitudinal and lateral stability characteristics of the three wings investigated over the angle-of-attack range. The lateral stability characteristics were measured over an angle-of-sideslip range from -10° to 10°.

Free-to-damp oscillation tests were made to determine the effect of frequency on the damping-in-yaw derivative of the delta wing over the angle-of-attack range. The frequency range investigated was from 0.53 to 1.67 cycles per second which corresponds to a range of the reduced frequency parameter k from about 0.08 to 0.30. For these oscillation tests the model was displaced in yaw about 30° and then released and allowed to damp to 0° amplitude.

Forced-oscillation tests were made to determine the effect of frequency on the static and yawing stability derivatives. These oscillation tests were made over a frequency range from 0.067 to 0.57 cycle per second which corresponds to a range of the reduced frequency parameter k from about 0.01 to 0.12. All the forced-oscillation tests were made with a yawing amplitude of $\pm 10^\circ$.

Most of the tests were made at dynamic pressures from 4.3 to 4.6 pounds per square foot which corresponds to an airspeed range from 61 to 63 feet per second. Some of the free-to-damp oscillation tests

were made at a dynamic pressure of 3.2 pounds per square foot which corresponds to an airspeed of 53 feet per second and some of the forced-oscillation tests were made at a dynamic pressure of 2.5 pounds per square foot which corresponds to an airspeed of 47 feet per second. The Reynolds number range covered in the tests varied from about 510,000 to 708,000 based on the mean aerodynamic chords of the wings investigated.

REDUCTION OF DATA

Corrections

Corrections for tunnel blockage and interference effects and for support strut tares were not applied to the measurements of the derivatives, although with the test setup used in the present investigation the support strut did introduce appreciable asymmetry in the static lateral stability data. Corrections to account for this interference effect could have been applied to the static data but no information was available on which to base similar corrections for the oscillation data which were obtained with the same test setup. The static data were therefore left uncorrected in order that they be directly comparable with the oscillation data presented in this report. This point is covered in more detail later in the report in connection with the presentation of the static force test results. Corrections to the forced oscillation data, to account for the effects of the flexibility of the model support system on the moment measurements, were considered to be negligible since the natural frequencies of the system were at least ten times greater than the highest forced oscillation frequency.

Free-To-Damp Oscillation Data

The measurement of the damping derivatives using the free-to-damp oscillation technique, which has been used extensively, is fully discussed in several reports, for example references 1 and 3. The expression for the damping derivatives for a yawing oscillation is given as,

$$C_{n_r} - C_{n_{\dot{\beta}}} = \frac{-4I_Z V(a - a_f)}{qSb^2} \qquad (1)$$

The values of a and a_f are determined from the wind-on and wind-off test runs, respectively, using the following expression,

$$a \text{ or } a_f = \frac{\log \psi_o - \log \psi_t}{t} \qquad (2)$$

where ψ_t is the amplitude of the oscillation at some time t following the initial amplitude of ψ_o at $t = 0$.

The value of I_Z is determined from the wind-off test runs from the following expression:

$$I_Z = \frac{-cP^2}{4\pi^2} \tag{3}$$

where c is the torsion spring constant and P is the period of oscillation.

For all the free-oscillation tests the model was displaced in yaw about 30° before being released and allowed to damp to 0° amplitude. The envelopes of the oscillations were plotted on semilogarithmic paper and were found to be fairly linear through the amplitude range investigated except for small amplitudes where the tunnel turbulence caused the data to be erratic. Because of the nonlinearity of the data at the small amplitudes, the logarithmic decrements or damping factors used to determine the damping derivatives of this investigation were obtained from the slope of the envelope curves for amplitudes above approximately $\pm 2^\circ$ or $\pm 3^\circ$.

Forced-Oscillation Data

The equations for calculating the stability derivatives from the forced-oscillation data were obtained from the following expressions for the sum of the aerodynamic and inertia moments acting on the model about the roll and yaw axes for a sinusoidal yawing motion:

Yaw Axis

$$\omega^2(I_Z - N_{\ddot{\psi}})\psi_{max} \sin \omega t + \omega(N_{\dot{\psi}} - N_{\dot{\beta}})\psi_{max} \cos \omega t - N_\beta \psi_{max} \sin \omega t = N \tag{4}$$

Roll Axis

$$\omega^2(I_{XZ} - L_{\ddot{\psi}})\psi_{max} \sin \omega t + \omega(L_{\dot{\psi}} - L_{\dot{\beta}})\psi_{max} \cos \omega t - L_\beta \psi_{max} \sin \omega T = L \tag{5}$$

where the yaw displacement is $\psi = \psi_{max} \sin \omega t$ and N and L represent the resultant moments which are transmitted to the support structure through the strain-gage balance.

For the case in which the aerodynamic moments are reduced to zero, as in the case of wind-off tests, the equations may be written as;

Yaw Axis:

$$\omega^2 I_Z \psi_{max} \sin \omega t = \bar{N} \tag{6}$$

Roll Axis:

$$\omega^2 I_{XZ} \psi_{max} \sin \omega t = \bar{L} \tag{7}$$

where the bar (-) indicates the resultant moments for the wind-off condition. The differences between equations (4) and (6) and equations (5) and (7) yield the following relations for the resultant aerodynamic moments:

Yaw Axis:

$$-\omega^2 N_{\dot{\psi}} \psi_{max} \sin \omega t + \omega(N_{\dot{\psi}} - N_{\dot{\beta}}) \psi_{max} \cos \omega t - N_\beta \psi_{max} \sin \omega t =$$

$$N_{max} \sin (\omega t + \phi_n) \tag{8}$$

Roll Axis:

$$-\omega^2 L_{\dot{\psi}} \psi_{max} \sin \omega t + \omega(L_{\dot{\psi}} - L_{\dot{\beta}}) \psi_{max} \cos \omega t - L_\beta \psi_{max} \sin \omega t =$$

$$L_{max} \sin (\omega t + \phi_l) \tag{9}$$

where $N_{max} \sin (\omega t + \phi_n)$ and $L_{max} \sin (\omega t + \phi_l)$ have been substituted for the terms $(N - \bar{N})$ and $(L - \bar{L})$, respectively.

The equations for the components of the resultant moments which are in phase and out of phase with the displacement of the model are obtained by setting ωt equal to $\frac{\pi}{2}$ and 0, respectively, in equations (8) and (9);

In phase:

$$-(N_\beta + N_{\dot{\psi}} \omega^2) \psi_{max} = N_{max} \cos \phi_n \tag{10}$$

$$-(L_\beta + L_{\dot{\psi}} \omega^2) \psi_{max} = L_{max} \cos \phi_l \tag{11}$$

Out of phase:

$$\omega(N_{\dot{\psi}} - N_{\dot{\beta}})\psi_{max} = N_{max} \sin \phi_n \tag{12}$$

$$\omega(L_{\dot{\psi}} - L_{\dot{\beta}})\psi_{max} = L_{max} \sin \phi_l \tag{13}$$

Reducing the left side of equations (10) to (13) to coefficient form gives the following equations for calculating the stability derivatives from the forced oscillation data:

$$C_{n_\beta} + C_{n_{\dot{r}}}k^2 = -\frac{1}{qSb\psi_{max}} N_{max} \cos \phi_n \tag{14}$$

$$C_{l_\beta} + C_{l_{\dot{r}}}k^2 = -\frac{1}{qSb\psi_{max}} L_{max} \cos \phi_l \tag{15}$$

$$C_{n_r} - C_{n_{\dot{\beta}}} = \frac{1}{kqSb\psi_{max}} N_{max} \sin \phi_n \tag{16}$$

$$C_{l_r} - C_{l_{\dot{\beta}}} = \frac{1}{kqSb\psi_{max}} L_{max} \sin \phi_l \tag{17}$$

Forced-oscillation method A.- Two data reduction techniques were employed in the case of method A to measure the unknown quantities N_{max}, L_{max}, ϕ_n, and ϕ_l from the oscillographic records. Figure 5 which represents a sample of typical displacement and yawing-moment traces from an oscillographic record for an ideal linear system, is used to illustrate the two methods used. In both cases the moment traces are marked along the abscissa time scale to indicate the points where the model displacement is at zero and maximum amplitude. The wind-off moment traces are superimposed on the wind-on traces using the displacement traces to match the two records. The first technique consists of measuring the maximum difference in amplitude between the wind-on and wind-off traces to obtain the quantity N_{max}. The time interval τ between the point where the two traces cross and the point on the moment traces where the displacement is zero is also measured to obtain the quantity ϕ_n where $\phi_n = \frac{360\tau}{P}$.

The second technique consists of measuring the differences in amplitude of the two moment traces at the points where displacement is zero to obtain the quantity $N_{max} \sin \phi_n$ and also where the displacement is maximum to obtain the quantity $N_{max} \cos \phi_n$. The procedures for taking the measurements from the rolling-moment traces were exactly the same as discussed for the yawing moments. The average of the quantities measured from several cycles of the oscillation were substituted directly in equations (10) through (13) to calculate the stability derivatives.

Use of either of these two data reduction techniques would yield the same results provided the test conditions were the same as those assumed in deriving equations (14) through (17) - that is, a linear system oscillating with a constant amplitude sinusoidal motion. In general, the data worked up by the two techniques agreed closely for the lower angles of attack but were markedly different in some cases at the higher angles of attack. This disagreement at the higher angles of attack can be attributed to nonlinear characteristics of the system which result from the flow separation over the model and which are evidenced in the test data by the distortion of the rolling and yawing traces from sinusoidal curves, as illustrated in figure 6. This figure shows retraces of some typical oscillograph records obtained from tests at 30° angle of attack and at two different frequencies.

In general, the value of a given derivative obtained using the first data reduction technique was smaller than that obtained using the second technique. Actually, analysis indicates that a value somewhere between these two values would be obtained with an equivalent linear system, that is, a linear system in which the energy exchange in one cycle of the motion is equal to that of the nonlinear system. The data obtained with the two techniques were therefore averaged and only one data point presented for each test condition.

Forced-oscillation method B.- The equations for calculating the stability derivatives from the test data of method B were derived from the following analysis. If the input voltage e to the strain gages measuring the resultant moment $N_{max} \sin (\omega t + \phi_n)$ is made to vary directly with the displacement such that $e = e_1 \sin \omega t$, the output current i_n will be

$$i_n = (k_n)(e_1 \sin \omega t)\left[N_{max} \sin (\omega t + \phi_n)\right]$$

$$= \frac{1}{2} k_n e_1 \left[N_{max}(\cos \phi_n - \cos \phi_n \cos 2\omega t + \sin \phi_n \sin 2\omega t)\right] \qquad (18)$$

where k_n is the gage calibration factor in terms of amperes per volt-foot-pound. The average value of the current, is

$$i_{n_{av}} = \frac{1}{2} k_n e_1 (N_{max} \cos \phi_n) \tag{19}$$

If the input voltage is changed so that it varies exactly out of phase with the displacement or in phase with the angular velocity, i.e., $e = e_2 \cos \omega t$, the output current will be

$$i_n = (k_n)(e_2 \cos \omega t)\left[N_{max} \sin (\omega t + \phi_n)\right]$$

$$= \frac{1}{2} k_n e_2 N_{max} (\sin \phi_n + \cos \phi_n \sin 2\omega t + \sin \phi_n \cos 2\omega t) \tag{20}$$

and the average current is

$$i_{n_{av}} = \frac{1}{2} k_n e_2 N_{max} (\sin \phi_n) \tag{21}$$

Likewise, the average output current of the strain gages measuring the resultant moment $L_{max} \sin (\omega t + \phi)$ for input voltages of $e = e_1 \sin \omega t$ and $e = e_2 \cos \omega t$ will be, respectively,

$$i_{l_{av}} = \frac{1}{2} k_l e_1 (L_{max} \cos \phi_l) \tag{22}$$

and

$$i_{l_{av}} = \frac{1}{2} k_l e_2 (L_{max} \sin \phi_l) \tag{23}$$

where k_l is the roll gage calibration factor.

The stability derivatives were calculated from the following equations which were obtained from equations (14) through (23)

$$C_{n_\beta} + C_{n_r} k^2 = - \frac{1}{qSb\psi_{max}} \left(\frac{2 i_{n_{av}}}{e_1 k_n} \right) \tag{24}$$

$$C_{l_\beta} + C_{l_{\dot{r}}} k^2 = - \frac{1}{qSb\psi_{max}} \left(\frac{2i_{l_{av}}}{e_1 k_l} \right) \tag{25}$$

$$C_{n_r} - C_{n_{\dot{\beta}}} = \left(\frac{1}{k} \right) \left(\frac{1}{qSb\psi_{max}} \right) \left(\frac{2i_{n_{av}}}{e_2 k_n} \right) \tag{26}$$

$$C_{l_r} - C_{l_{\dot{\beta}}} = \left(\frac{1}{k} \right) \left(\frac{1}{qSb\psi_{max}} \right) \left(\frac{2i_{l_{av}}}{e_2 k_l} \right) \tag{27}$$

where e_1 is the maximum in-phase voltage and e_2 is the maximum out-of-phase voltage. The values for the output currents $i_{n_{av}}$ and $i_{l_{av}}$ were obtained by subtracting the wind-off tare measurements from the wind-on data.

RESULTS AND DISCUSSION

Presentation of Data

The results of the investigation are presented in figures 7 to 25. Static force test data for the three wings are shown in figures 7, 8, and 9. Oscillation test data are shown for $C_{n_r} - C_{n_{\dot{\beta}}}$ in figures 10 to 13, for $C_{n_\beta} + k^2 C_{n_{\dot{r}}}$ in figures 14 and 17, for $C_{l_r} - C_{l_{\dot{\beta}}}$ in figures 18 to 21, and for $C_{l_\beta} + k^2 C_{l_{\dot{r}}}$ in figures 22 to 25. Information used in the analysis and explanation of the test results are presented in figures 26 to 31.

Static Force Test Results

The static longitudinal data presented in figure 7 show that the unswept wing stalled at about 16° angle of attack and the swept wing at about 25° angle of attack. The delta wing was not completely stalled at the maximum angle of attack (30°) reached in the tests. These angles of attack should be kept in mind in studying the oscillation test results presented later since these results will be plotted against angle of attack rather than lift coefficient.

The basic static lateral stability data for the three wings are presented in figure 8. For all the wings, the rolling-moment and yawing-moment curves are displaced so that the moments are not zero at 0° sideslip as they should be. This asymmetry is attributed in most cases to the particular test setup used in the present investigation. (See fig. 3.) In this setup, which was used for both the static tests and the oscillation tests, the support structure near one wing tip apparently causes appreciable changes in the velocity and the angularity of the air flow over the wing. Additional static tests made with a symmetrical support system indicated that the slopes of the curves of figure 8 are not greatly in error even though the displacement of the curves is large in some cases. The data of figure 8 were left uncorrected since the oscillation test data, which would also require corrections for support interference, could not be corrected reliably by existing procedures. In the uncorrected form presented in figure 8 the static data are directly comparable with the oscillation data presented later in the report. The large displacement of the yawing-moment curve for the unswept wing at 15° angle of attack is attributed principally to unsymmetrical wing stalling rather than support interference since a similar displacement was obtained in tests with a symmetrical support system.

The values of the static directional stability derivative C_{n_β} and the effective dihedral derivative C_{l_β} presented in figure 9 were obtained by taking the average slopes of the basic data curves of figure 8 over the sideslip angle range of $\pm 10°$ which corresponds to the range used in the forced-oscillation tests. The existence of a negative value rather than a zero value of C_{l_β} at 0° angle of attack for the three wings is attributed to the support interference discussed in the preceding paragraph.

Damping in Yaw $C_{n_r} - C_{n_{\dot\beta}}$

Delta wing.- The values of the damping-in-yaw derivative $C_{n_r} - C_{n_{\dot\beta}}$ obtained in the free-to-damp and forced-oscillation tests of the delta wing are plotted against the reduced frequency parameter k for various angles of attack in figure 10. In figures 10(a) and 10(c), the two sets of symbols are for data obtained at two tunnel airspeeds. In all cases a single curve is faired through the data points and these faired curves are replotted in figure 10(d) to provide a comparison of the results obtained by the different testing techniques. It should be noted that the scale for k in figures 10(a) and 10(d) is much more compressed than in figures 10(b) and 10(c) because the free-to-damp oscillation tests covered a much larger range of values of k than the forced-oscillation tests. The remainder of the data in the report are plotted to the same scale of k as figures 10(b) and 10(c). The basic data from figure 10

are cross plotted in figure 11 to show more clearly the variation of $C_{n_r} - C_{n_{\dot{\beta}}}$ with angle of attack for various values of k.

The results of figures 10 and 11 show the large increase in $C_{n_r} - C_{n_{\dot{\beta}}}$ with angle of attack that has been noted in previous investigations with delta wings. (See refs. 2, 6, and 7.) The pronounced effect of frequency on $C_{n_r} - C_{n_{\dot{\beta}}}$ shown by these results has not been previously shown, although, for an isolated case in reference 4, a similar effect of frequency on $C_{n_{\dot{\beta}}}$ was indicated. The comparison of $C_{n_r} - C_{n_{\dot{\beta}}}$ and $C_{n_{\dot{\beta}}}$ is felt to be justified on the basis that oscillation test data obtained to date have indicated that the major portion of the damping represented by the combination derivative $C_{n_r} - C_{n_{\dot{\beta}}}$ can generally be attributed to $C_{n_{\dot{\beta}}}$. The large increases in $C_{n_r} - C_{n_{\dot{\beta}}}$ with decreasing frequency in the present case result in very large values of the derivative being obtained at high angles of attack with the smaller values of k. The effect of frequency is least at the lower angles of attack and appears to increase progressively with increasing angle of attack. The data obtained with forced-oscillation method A (fig. 10(b)) show a reversed variation of $C_{n_r} - C_{n_{\dot{\beta}}}$ with frequency for the lower values of k at angles of attack of 10°, 15°, and 20°.

An indication of the order of magnitude of the values of $C_{n_r} - C_{n_{\dot{\beta}}}$ presented in these figures is the fact that references 3 and 12 show that complete airplane models with unswept wings and large vertical tails have values of $C_{n_r} - C_{n_{\dot{\beta}}}$ that are less than half as large as the values shown in figures 10 and 11 for the delta wing at high angles of attack and low values of reduced frequency.

The results presented in reference 2 for a 60° delta wing in combination with a fuselage show values of $C_{n_r} - C_{n_{\dot{\beta}}}$ that are larger than the values shown in figure 10(a) for the delta wing at the same value of k (0.21). These results indicate a significant contribution of the fuselage to damping in yaw and, in this respect, differ from the results of reference 12. The large effect of the fuselage shown by these more recent data might be a result of wing-fuselage interference which alters the lift distribution of the delta wing.

The summary plots in figures 10(d) and 11(d) show that the data obtained with the three different techniques are generally in fairly good agreement although in some cases the quantitative agreement does not appear to be so good. Actually, the differences between the three sets of data do not appear to be much greater than the scatter of some of the data shown in figures 10(a) and 10(c).

Swept wing.- The values of $C_{n_r} - C_{n_{\dot{\beta}}}$ for the swept wing obtained by forced-oscillation method A are presented in figure 12. In general, the variation with k and α is similar to that obtained with the delta wing. The results for the swept wing, however, show a reversed variation of $C_{n_r} - C_{n_{\dot{\beta}}}$ with k for small values of k at 25° angle of attack instead of 20° as for the delta wing. For given values of k and α, the swept wing has smaller values of $C_{n_r} - C_{n_{\dot{\beta}}}$ than the delta wing.

The data of reference 3 show that a 45° swept wing of aspect ratio 4 and taper ratio 0.6 in combination with a fuselage has values of $C_{n_r} - C_{n_{\dot{\beta}}}$ at 16° angle of attack that are generally larger than the values shown in figure 12 for the swept wing at 20° angle of attack. Part of this difference might be attributed to the difference in wing plan form but it is likely that most of the difference is caused by wing-fuselage interference as suggested previously in the case of the delta wing.

Unswept wing.- The values of $C_{n_r} - C_{n_{\dot{\beta}}}$ for the unswept wing obtained by forced-oscillation method A are presented in figure 13. Compared to the values of $C_{n_r} - C_{n_{\dot{\beta}}}$ for the delta and swept wings these values for the unswept wing are very small at all angles of attack and all values of reduced frequency covered in the tests. In fact, plotted to the scale for $C_{n_r} - C_{n_{\dot{\beta}}}$ used in the present report the values appear to be insignificantly small and within the experimental accuracy obtainable with forced-oscillation method A. Actually, the values shown are generally of the same order of magnitude as the values presented in references 3 and 12 for unswept wings and wing-fuselage combinations.

Directional Stability $C_{n_\beta} + k^2 C_{n_{\dot{r}}}$

Delta wing.- The values of the directional stability derivative $C_{n_\beta} + k^2 C_{n_{\dot{r}}}$ obtained in the forced-oscillation tests of the delta wing are presented in figures 14 and 15. Static directional stability data ($k = 0$) from figure 9 have also been plotted on these figures for comparison with the oscillation results.

The results of figures 14 and 15 show that for very low values of reduced frequency where k approaches zero the values of $C_{n_\beta} + k^2 C_{n_{\dot{r}}}$ measured in the oscillation tests generally tend to approach the values of C_{n_β} measured in the static force tests. Actually, for some angles of attack the quantitative agreement between the static values of C_{n_β} and the oscillation values extrapolated to $k = 0$ does not appear to be

very close but in all cases the same trends are shown. It is logical, of course, that as k approaches zero the value of $C_{n_\beta} + k^2 C_{n_{\dot{r}}}$ measured should tend to approach the static value since the yawing velocities involved in these very long period oscillations are so slow that the tests essentially correspond to static tests. For example, the value of k of 0.01 in the present tests was obtained with an oscillation period of about 15 seconds. As will be explained later, this same reasoning does not apply in the case of damping in yaw where the values of $C_{n_r} - C_{n_{\dot{\beta}}}$ at low values of k were generally several times as large as the steady-state values of C_{n_r}.

The results of figures 14 and 15 show that, for angles of attack of 20° or less the values of $C_{n_\beta} + k^2 C_{n_{\dot{r}}}$ did not vary very much with frequency. For angles of attack about 24°, however, there was a pronounced variation of $C_{n_\beta} + k^2 C_{n_{\dot{r}}}$ with k. For the higher angles of attack, as k was increased from very low values, $C_{n_\beta} + k^2 C_{n_{\dot{r}}}$ decreased from a highly negative value to zero and then increased positively. These results are in agreement with the trends indicated by the data of reference 4. An explanation for this variation will be presented in the Analysis of Results Section.

The comparisons presented in figures 14(c) and 15(c) show that the data obtained with the two forced-oscillation techniques are in fairly good agreement.

Swept wing.- The values of $C_{n_\beta} + k^2 C_{n_{\dot{r}}}$ for the swept wing obtained by forced-oscillation method A are presented in figure 16. The agreement between the static data and an extrapolation of the oscillation data to $k = 0$ appears to be fairly good. The variation of $C_{n_\beta} + k^2 C_{n_{\dot{r}}}$ with frequency is quite similar to that obtained for the delta wing. That is, there was little variation with frequency at angles of attack of 20° or less but there was a pronounced decrease in the negative value of $C_{n_\beta} + k^2 C_{n_{\dot{r}}}$ with increasing frequency for angles of attack of 25° and 30°.

Unswept wing.- The values of $C_{n_\beta} + k^2 C_{n_{\dot{r}}}$ for the unswept wing obtained by forced-oscillation method A are presented in figure 17. For this wing there is no large variation of $C_{n_\beta} + k^2 C_{n_{\dot{r}}}$ with frequency at any angle of attack. The oscillation data are in good agreement with the static data in this case.

Cross Derivative $C_{l_r} - C_{l_{\dot{\beta}}}$

Delta wing.- The values of $C_{l_r} - C_{l_{\dot{\beta}}}$ obtained for the delta wing by the two forced-oscillation methods are presented in figures 18 and 19. As in the case of $C_{n_r} - C_{n_{\dot{\beta}}}$ these results show the most pronounced effects of frequency at the higher angles of attack. Extremely large values of $C_{l_r} - C_{l_{\dot{\beta}}}$ are obtained at angles of attack from 25° to 30° at the lower values of k. In general, at the higher angles of attack, increasing the frequency causes a substantial decrease in the value of $C_{l_r} - C_{l_{\dot{\beta}}}$. At the lower angles of attack the effects of frequency are generally small but, for 10° angle of attack, there does appear to be a definite increase in $C_{l_r} - C_{l_{\dot{\beta}}}$ with increasing k. The results of reference 4 indicate generally similar effects of frequency on the lateral acceleration derivative $C_{l_{\dot{\beta}}}$ for a delta wing. Figures 18(c) and 19(c) show that the data obtained with the two forced-oscillation techniques indicate the same general trends but are in only fair quantitative agreement.

Swept wing.- The values of $C_{l_r} - C_{l_{\dot{\beta}}}$ for the swept wing obtained by forced-oscillation method A are shown in figure 20. The variations with angle of attack and frequency are similar to those obtained with the delta wing but, for each test condition, the value of $C_{l_r} - C_{l_{\dot{\beta}}}$ is smaller than that for the delta wing for the corresponding condition.

Unswept wing.- The values of $C_{l_r} - C_{l_{\dot{\beta}}}$ for the unswept wing obtained by forced-oscillation method A are presented in figure 21. The variations with k and α are markedly different from those for the delta and swept wings and the values of $C_{l_r} - C_{l_{\dot{\beta}}}$ are generally much smaller. At the higher angles of attack and low values of reduced frequency, the values of $C_{l_r} - C_{l_{\dot{\beta}}}$ are negative rather than highly positive as for the other wings. At these angles of attack, the unswept wing is fully stalled. (See fig. 7.)

Effective Dihedral $-\left(C_{l_\beta} + k^2 C_{l_{\dot{r}}}\right)$

Delta wing.- The values of the effective dihedral derivative $-\left(C_{l_\beta} + k^2 C_{l_{\dot{r}}}\right)$ obtained in forced-oscillation tests of the delta wing are presented in figures 22 and 23. Static stability data (k = 0) from figure 9 are also plotted on these figures for correlation with the oscillation test results.

As in the case of $C_{n_\beta} + k^2 C_{n_{\dot{r}}}$, the values of $C_{l_\beta} + k^2 C_{l_{\dot{r}}}$ for the very low values of k tend to approach the values measured in static force tests, but here again in some cases the quantitative agreement between the two sets of data is not very close.

The results of figures 22 and 23 show that at low angles of attack there was little or no variation of $C_{l_\beta} + k^2 C_{l_{\dot{r}}}$ with frequency, but at the high angles of attack, $C_{l_\beta} + k^2 C_{l_{\dot{r}}}$ decreased from a high positive value to zero and then increased negatively as the frequency was increased. The two sets of oscillation data are in fairly good agreement for the high angles of attack but, for angles of attack of 10° and 20°, different variations of $C_{l_\beta} + k^2 C_{l_{\dot{r}}}$ with k are indicated.

The large effect of frequency on $C_{l_\beta} + k^2 C_{l_{\dot{r}}}$ for the higher angles of attack is quite similar to that shown by the data of reference 4 for the C_{l_β} of the 60° delta wing.

Swept wing.- The values of $C_{l_\beta} + k^2 C_{l_{\dot{r}}}$ obtained by forced-oscillation method A for the swept wing are presented in figure 24. These results show the same general variation with α and k as for the delta wing.

Unswept wing.- The values of $C_{l_\beta} + k^2 C_{l_{\dot{r}}}$ obtained by forced-oscillation method A for the unswept wing are shown in figure 25. These data indicate a slight decrease in the negative value of $C_{l_\beta} + k^2 C_{l_{\dot{r}}}$ with increasing frequency for all angles of attack.

ANALYSIS OF RESULTS

Influence of Flow Separation

The data of figures 10 to 25 indicate only small effects of frequency for the delta and swept wings at low angles of attack or for the unswept wing at any angle of attack. For the delta and swept wings at high angles of attack, however, pronounced effects of frequency are obtained and the derivatives $C_{n_r} - C_{n_{\dot{\beta}}}$ and $C_{l_r} - C_{l_{\dot{\beta}}}$ become extremely large at the low frequencies. Since these results appear to be related to the occurrence of flow separation on the wings, an attempt was made to establish the nature of this relationship by correlating the static and oscillation test data.

The static stability data of figure 9 afford an indication of the angle of attack at which separation occurs for the three wings. In order to show the effects of separation more clearly the static data have been replotted in figure 26 together with the calculated values of the derivatives. These calculations were actually rough approximations made to extend the various curves beyond the break attributed to flow separation. The extensions to the curves (shown by the dotted lines) were made by assuming that C_{n_β} varies with C_L^2 and that C_{l_β} varies with C_L. The lift curves of figure 7 were used in making these calculations. The data of figure 26 show that separation caused decreases in the values of the derivatives for the delta and swept wings but caused increases in the case of the unswept wing.

In figure 27 values of $C_{n_r} - C_{n_{\dot\beta}}$ and $C_{l_r} - C_{l_{\dot\beta}}$ for a value of k of 0.02 are plotted against values of ΔC_{n_β} and ΔC_{l_β} obtained from figure 26 by taking the increments between calculated and measured values of the static derivatives. These plots show that the values of the oscillation derivatives increase with increasing values of the increments ΔC_{n_β} and ΔC_{l_β} in the case of the delta and swept wings. For the unswept wing, where the values of ΔC_{n_β} and ΔC_{l_β} are of opposite sign to those for the delta and swept wings, the variation of $C_{l_r} - C_{l_{\dot\beta}}$ with ΔC_{l_β} appears to be similar to that for the other wings, but there appears to be no correlation of $C_{n_r} - C_{n_{\dot\beta}}$ with ΔC_{n_β}. Actually the data of figure 21 indicate that for values of k much greater than 0.02 there would be no correlation of the unswept wing $C_{l_r} - C_{l_{\dot\beta}}$ data either. These results for the unswept wing are not surprising because the flow separation and stalling characteristics for an unswept wing are known to be quite different from those for the swept and delta wings.

Inasmuch as the values of $C_{n_r} - C_{n_{\dot\beta}}$ and $C_{l_r} - C_{l_{\dot\beta}}$ for the unswept wing are small in most cases and the values for the swept wing are generally similar to those for the delta wing, only the delta-wing data will be considered in the remainder of the analysis. The delta-wing data are used in preference to those for the swept wing because the delta-wing tests were much more extensive.

Type of Lag Involved

The results obtained with forced-oscillation method A appeared to provide the best data for making a detailed study of frequency effects. As explained previously the results obtained with this method were in the form of oscillograph traces of rolling and yawing moments and angle

of yaw recorded during forced sinusoidal oscillations on the wings. (See. fig. 5.) The basic data obtained for the yawing-moment traces for the delta wing are presented in figure 28. The quantity $C_{n_{max}}$ plotted in figure 28(a) is the maximum amplitude of the yawing-moment trace regardless of the angle of yaw at which it occurs. The lag of the yawing moment with respect to the angle of yaw is plotted in three different ways in figures 28(b), (c), and (d). Figure 28(d), which consists of a plot of time lag against frequency with cross-plotted curves for phase angles of 90° and 180°, shows that the lag involved is neither a constant phase lag nor a constant time lag in all cases. For angles of attack up to 15° there is essentially no lag (or 180° lag based on the assumption that for 0° phase lag a positive yawing moment is produced by a positive angle of yaw). For an angle of attack of 24° there appears to be a roughly constant phase lag, while for 26° and 30° angle of attack the lag is more nearly a constant time lag.

The basic lag data of figure 28 do not appear to afford a very clear indication of the nature of the phenomenon responsible for the large effects of frequency. It was found possible, however, to modify the basic data in such a way as to obtain more consistent values of lag for the various conditions. This modification of the data is illustrated in figure 29 which shows sample traces of yawing moment (converted to coefficient form) and angle of yaw against time for the delta wing at angles of attack of 20° and 30° for an oscillation period of 15 seconds ($k \cong 0.01$). The data for 20° angle of attack are presented as an example of cases where the value of C_{n_β} was positive while the 30° data serve as an example of negative C_{n_β}. In addition to these traces representing experimental data, traces are also shown in short dashed lines to represent the theoretical value of C_{n_β} at each angle of attack. These theoretical curves are exactly in phase with the yawing motion since they represent pure C_{n_β} with no damping. The amplitude of these curves was determined from the theoretical C_{n_β} curve for the delta wing shown in figure 26. The theoretical curves therefore represent the traces which would be obtained at the particular angle of attack if there were no separation and no damping. The difference (shown by the long dashed lines) between these curves and the experimental curves provides a direct indication of the effects of separation (and damping) on the yawing moments produced during the yawing oscillation. These traces indicate that the lag τ_s is the same order of magnitude for 20° and 30° angle of attack, whereas the basic data indicate that the measured lag τ is several times as great for 20° as for 30° angle of attack.

Values of lag determined in this manner from the yawing-moment data for the delta wing for various values of reduced frequency and angles of attack are presented in figure 30. These data show time lags

that vary only from about 0.2 to 0.4 second for all the different conditions as compared to the very large variation of time lag shown by the basic data of figure 28(c) and (d). It would appear then that the large values of $C_{n_r} - C_{n_{\dot{\beta}}}$ for the delta wing at high angles of attack can be attributed to an incremental destabilizing yawing moment which is produced by separated flow and which lags the yawing motion by a roughly constant time interval. These data indicate that the increase in the magnitude of $C_{n_r} - C_{n_{\dot{\beta}}}$ with increasing angle of attack is not caused by an increase in time lag and is therefore probably attributable solely to the increased increment of destabilizing yawing moment caused by separation at the higher angles of attack. (See fig. 27.) It appears that similar explanations would hold for the $C_{n_r} - C_{n_{\dot{\beta}}}$ data of the swept wing and for the $C_{l_r} - C_{l_{\dot{\beta}}}$ data of both the delta and swept wings.

Explanation of Frequency Effects

For the delta wing at 30° angle of attack, the data of figure 30 show a time lag τ_s that is fairly constant over the range of k(0.01 to 0.08) used in the tests with forced-oscillation method A. The trend of the data indicates a gradual reduction in the time lag with increasing frequency at the higher values of k. If, as a first approximation, the lag τ_s is assumed to be a constant value of 0.25 second for this angle of attack, the large effect of frequency for this condition can be partially explained.

Calculations based on a constant time lag of 0.25 second for the delta wing at 30° angle of attack are shown in figure 31 together with experimental data from figures 10(d) and 14(c) for comparison. The calculated variations of C_{n_β} and $C_{n_{\dot{\beta}}}$ with frequency (or period) are shown by the solid lines in the figure. The phase angle ϕ_s corresponding to 0.25 second time lag for the various values of k and P is also shown on the lower scale. The values of C_{n_β} and $C_{n_{\dot{\beta}}}$ were calculated from the expressions

$$C_{n_\beta} = \left(C_{n_{\beta_{calc}}}\right)_{k=0} - \left(\Delta C_{n_\beta}\right)_{k=0} \cos \phi_s \tag{28}$$

and

$$C_{n_{\dot{\beta}}} = \left(\Delta C_{n_\beta}\right)_{k=0} \frac{1}{k} \sin \phi_s \tag{29}$$

where

$$\left(\Delta C_{n_\beta}\right)_{k=0} = \left(C_{n_{\beta_{calc}}} - C_{n_{\beta_{exp}}}\right)_{k=0}$$

The values of $\left(C_{n_{\beta_{calc}}}\right)_{k=0}$ and $\left(\Delta C_{n_\beta}\right)_{k=0}$ were obtained from figure 26. For the case chosen (delta wing at 30° angle of attack), these terms had values of 0.096 and 0.148, respectively.

For values of k approaching zero, equation (29) can be modified by assuming that $\sin \phi_s = \phi_s$. Then by substituting $\frac{\pi b}{PV}$ for k and $\frac{2\pi\tau_s}{P}$ for ϕ_s and simplifying, the following equation can be obtained from equation (29):

$$\left(C_{n_{\dot{\beta}}}\right)_{k=0} = \left(\Delta C_{n_\beta}\right)_{k=0}\left(\frac{2V\tau_s}{b}\right) \tag{29a}$$

The calculated values of C_{n_β} and $C_{n_{\dot{\beta}}}$ show the same general variations with frequency as the experimental data but the quantitative agreement is only fair. The principal reason for the lack of good quantitative agreement is that the time lag is not exactly 0.25 second for all frequencies. Figure 30 shows that for 30° angle of attack the lag varies from about 0.19 to 0.26 second over the range of k from 0.01 to 0.08 and indicates that values of lag below 0.19 second would be obtained at values of k greater than 0.08. To illustrate the effect of such variations in lag, the curves of figure 31 have been replotted in figure 32 together with calculations for lags of 0.15, 0.20, and 0.30 second. The additional curves on this figure indicate that, generally, better agreement would be obtained between the experimental and calculated results if a lag greater than 0.25 second were used at low values of k and a lag less than 0.25 second were used at the higher values of k. In any event, the curves of either figure 31 or 32 serve to illustrate the relationship of damping in yaw to directional stability and also provide a general explanation for the large effects of frequency shown by the oscillation data for the swept and delta wings for the higher angles of attack.

Build Up and Decay of Lag Effects

In order to provide a further illustration of the type of phenomenon which is responsible for the oscillation test results obtained in this

investigation, tests were run with forced-oscillation method A to determine the variation of yawing and rolling moments during sudden starting and stopping of the oscillation. Two examples of yawing-moment records obtained during these tests are presented in figure 33. These records were obtained with the delta wing at 30° angle of attack for oscillation periods of 14 to 15 seconds. Plots of angle of yaw and yawing-moment coefficient against time and of yawing-moment coefficient against angle of yaw are shown. The records obtained during a continuous oscillation (dashed lines) serve as reference for the records of sudden starting and stopping of the oscillation (solid lines).

The records of figure 33(a) indicate that within about 1 second of the start of the oscillation the variation of angle of yaw with time was the same as that for the continuous oscillation. About a half a second longer elapsed, however, before the yawing moments of the two records came into approximate agreement. The data of figure 33(b) show a similar lag of the yawing moment in dropping off to about zero when the oscillation was stopped suddenly at zero angle of yaw. This lag appears to be of the same order of magnitude as that between the angle of yaw and the yawing moment in the continuous oscillation data.

The plots of yawing moment against angle of yaw on the right-hand side of figure 33 take the form of hysteresis loops which illustrate the static stability and damping in the oscillation. For the long period oscillation involved in this case, the slope of the major axis of the hysteresis loop is a measure of the static directional stability. The damping is a function of the area within the loop since this area is a measure of the energy absorbed from the oscillating wing by the airstream during each cycle. The solid lines in the hysteresis loops of figure 34 show the manner in which the loops build-up and decay during starting and stopping of oscillations.

CONCLUSIONS

The results of the low-speed investigation to determine the effects of frequency on the stability derivatives of wings oscillating in yaw at an amplitude of ±10° may be summarized as follows:

1. In general, the effects of frequency on the stability derivatives were most pronounced for the delta and swept wings at the higher angles of attack where considerable flow separation was present. No large effects of frequency were obtained with the unswept wing at any angle of attack or with the delta and swept wings at angles of attack where no flow separation was present.

2. At very low values of reduced frequency, the directional stability derivative $C_{n_\beta} + k^2 C_{n_{\dot{r}}}$ and the effective dihedral derivative $-\left(C_{l_\beta} + k^2 C_{l_{\dot{r}}}\right)$ tended to approach the steady state values of C_{n_β} and $-C_{l_\beta}$ measured in conventional static force tests. For these conditions extremely large values of the damping-in-yaw derivative $C_{n_r} - C_{n_{\dot{\beta}}}$ and the cross derivative $C_{l_r} - C_{l_{\dot{\beta}}}$ were obtained with the delta and swept wings at high angles of attack. Increasing the frequency from these very low values caused large reductions in the absolute magnitude of all four of these derivatives.

3. The large values of $C_{n_r} - C_{n_{\dot{\beta}}}$ and $C_{l_r} - C_{l_{\dot{\beta}}}$ at the high angles of attack for the delta and swept wings and the large variation of all the derivatives with frequency are attributed to a lag in the alternating increase and decrease in separated flow over the wing panels as the wing oscillates in yaw.

Langley Aeronautical Laboratory,
National Advisory Committee for Aeronautics,
Langley Field, Va., August 1, 1955.

REFERENCES

1. Hewes, Donald E.: Low-Speed Measurement of Static Stability and Damping Derivatives of a 60° Delta-Wing Model for Angles of Attack From 0° to 90°. NACA RM L54G22a, 1954.

2. Johnson, Joseph L., Jr.: Low-Speed Measurements of Rolling and Yawing Stability Derivatives of a 60° Delta-Wing Model. NACA RM L54G27, 1954.

3. Fisher, Lewis R., and Fletcher, Herman S.: Effect of Lag of Sidewash on the Vertical-Tail Contribution to the Oscillatory Damping in Yaw of Airplane Models. NACA TN 3356, 1954.

4. Riley, Donald R., Bird, John D., and Fisher, Lewis R.: Experimental Determination of the Aerodynamic Derivatives Arising From Accelerations in Sideslip for a Triangular, a Swept, and an Unswept Wing. NACA RM L55A07, 1955.

5. Bird, John D., Jaquet, Byron M., and Cowan, John W.: Effect of Fuselage and Tail Surfaces on Low-Speed Yawing Characteristics of a Swept-Wing Model As Determined in Curved-Flow Test Section of the Langley Stability Tunnel. NACA TN 2483, 1951. (Supersedes NACA RM L8G13.)

6. Beam, Benjamin H.: A Wind-Tunnel Test Technique for Measuring the Dynamic Rotary Stability Derivatives Including the Cross Derivatives at High Mach Numbers. NACA TN 3347, 1955.

7. Beam, Benjamin H., Reed, Verlin D., and Lopez, Armando E.: Wind-Tunnel Measurements at Subsonic Speeds of the Static and Dynamic-Rotary Stability Derivatives of a Triangular-Wing Airplane Model Having a Triangular Vertical Tail. NACA RM A55A28, 1955.

8. Lessing, Henry C., Fryer, Thomas B., and Mead, Merrill H.: A System for Measuring the Dynamic Lateral Stability Derivatives in High-Speed Wind Tunnels. NACA TN 3348, 1954.

9. Fisher, Lewis R., and Wolhart, Walter D.: Some Effects of Amplitude and Frequency on the Aerodynamic Damping of a Model Oscillating Continuously in Yaw. NACA TN 2766, 1952.

10. Fisher, Lewis R.: Some Effects of Aspect Ratio and Tail Length on the Contribution of a Vertical Tail to Unsteady Lateral Damping and Directional Stability of a Model Oscillating Continuously in Yaw. NACA TN 3121, 1954.

11. Bird, John D., Fisher, Lewis R., and Hubbard, Sadie M.: Some Effects of Frequency on the Contribution of a Vertical Tail to the Free Aerodynamic Damping of a Model Oscillating in Yaw. NACA Rep. 1130, 1953. (Supersedes NACA TN 2657.)

12. Cotter, William E., Jr.: Summary and Analysis of Data on Damping in Yaw and Pitch for a Number of Airplane Models. NACA TN 1080, 1946.

TABLE I.- DIMENSIONAL CHARACTERISTICS OF THE WINGS

[All dimensions in feet]

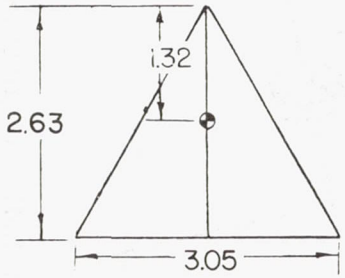

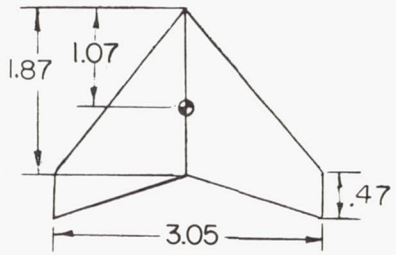

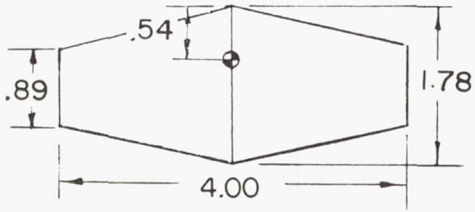

Type	Delta	Swept	Unswept
Sweep	60° (L.E.)	45° ($\bar{c}/4$)	0° ($\bar{c}/2$)
Area	4.05 sq ft	3.56 sq ft	5.35 sq ft
MAC	1.76 ft	1.31 ft	1.38 ft
Aspect ratio	2.31	2.61	3.00
λ	0	.25	.50
Airfoil	NACA 65-006.5	NACA 0012	NACA 0012

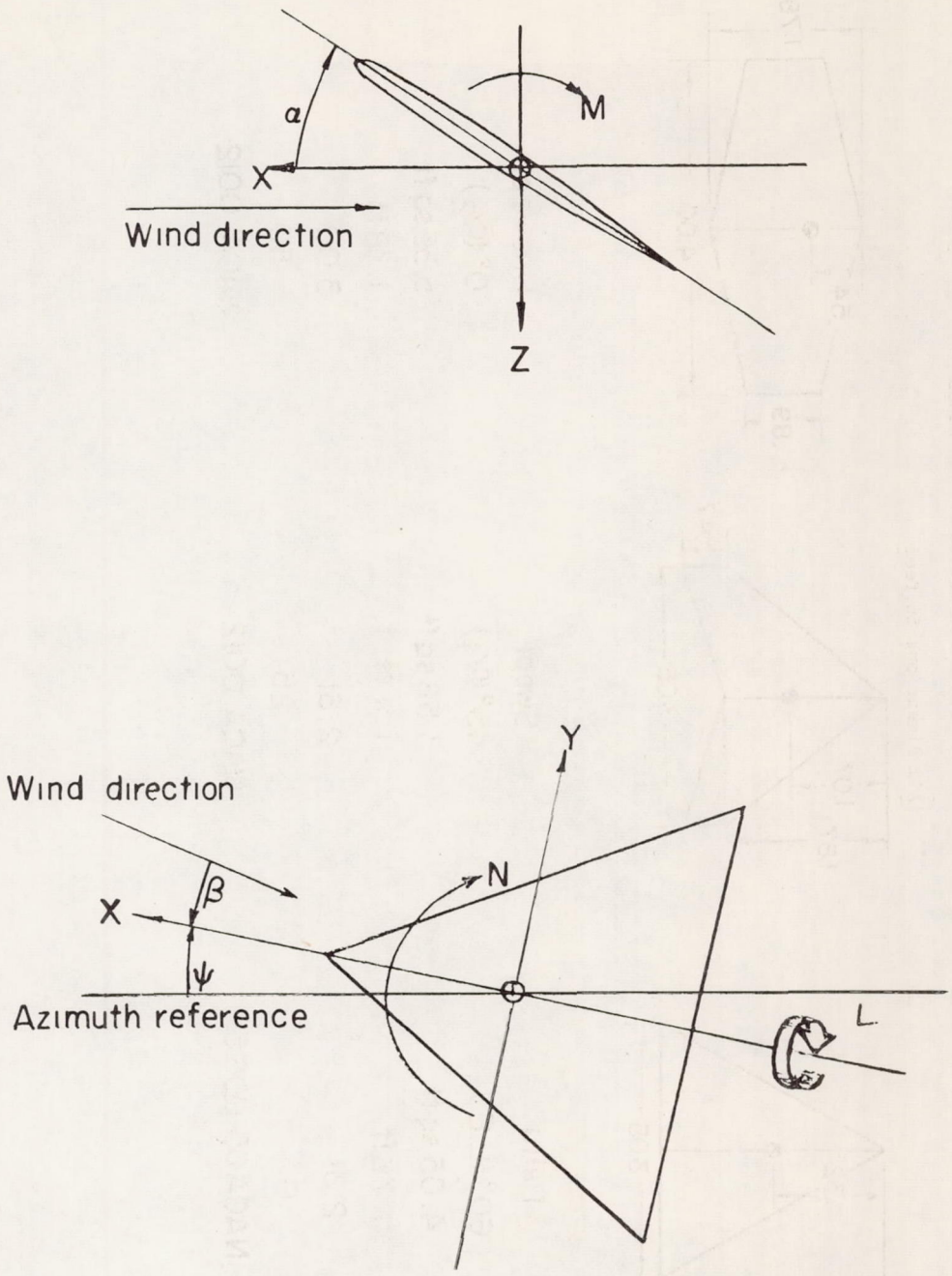

Figure 1.- The stability system of axes. Arrows indicate positive direction of moments, forces, and angles.

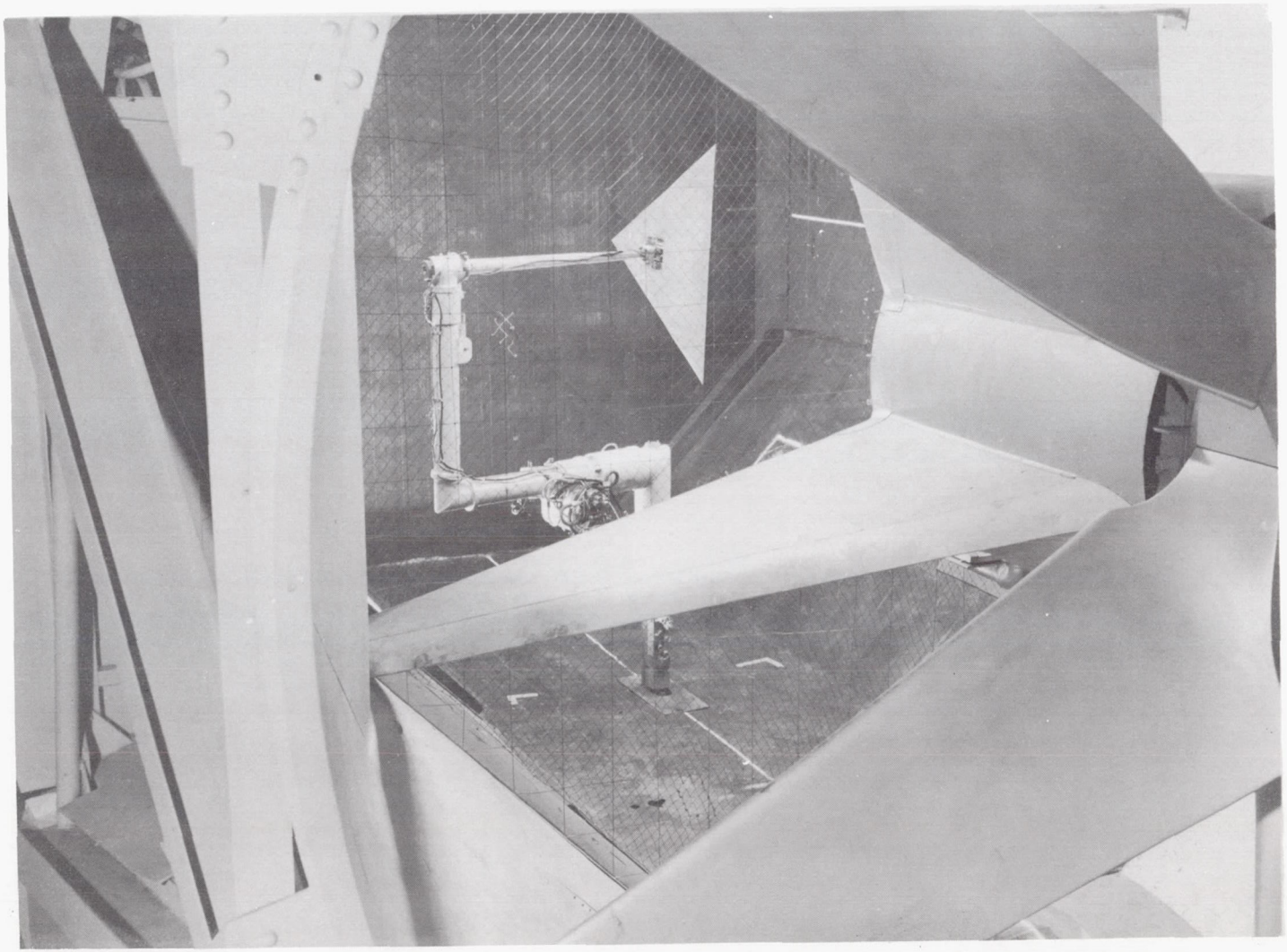

L-88052

Figure 2.- Installation of forced oscillation test apparatus in the tunnel.

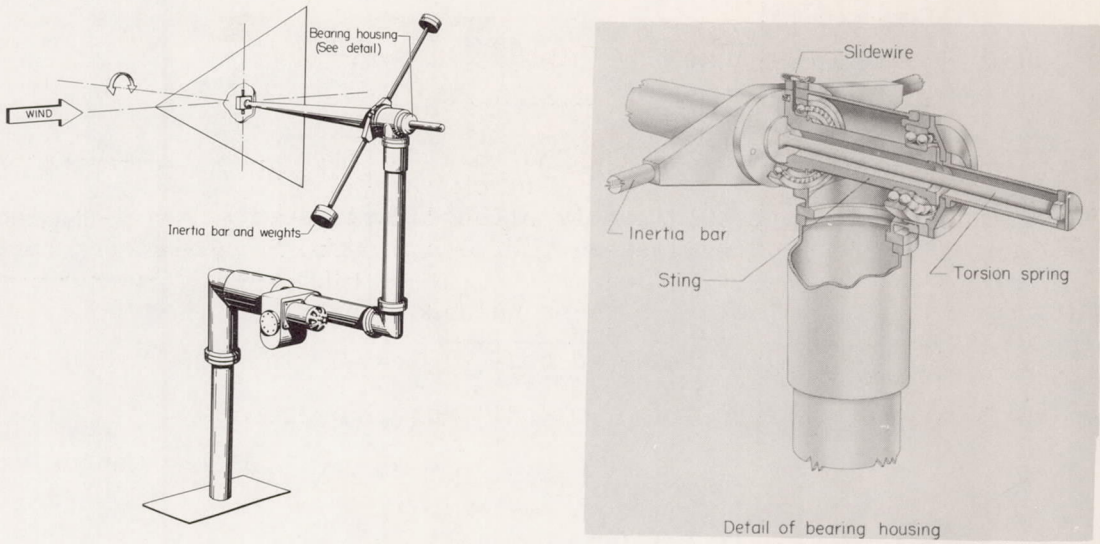

(a) Free-to-damp apparatus.

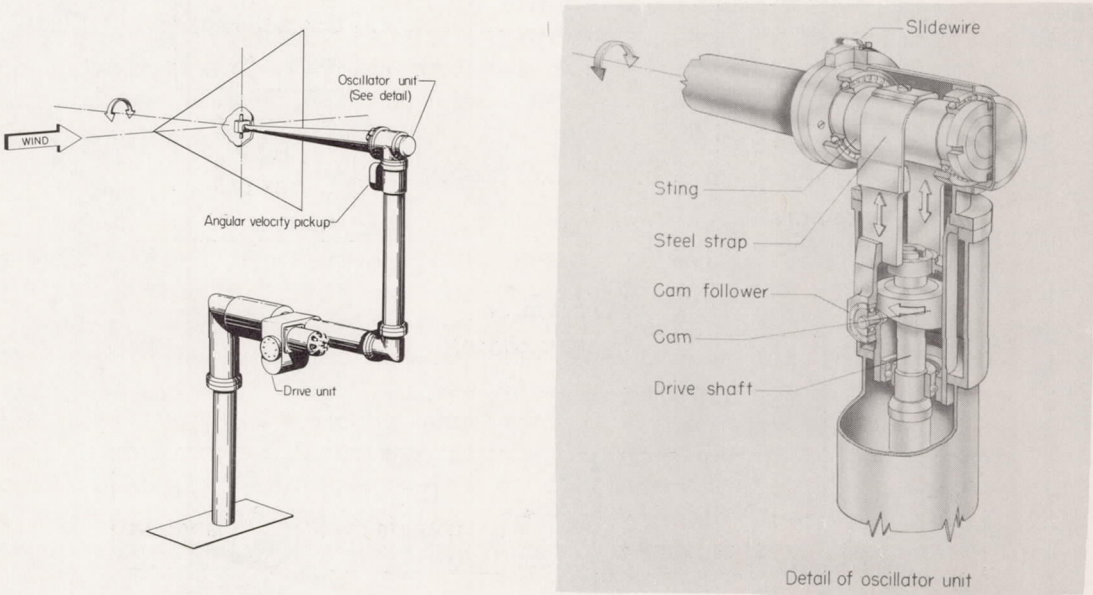

L-89380

(b) Forced-oscillation apparatus.

Figure 3.- Schematic drawings of the oscillation test apparatus.

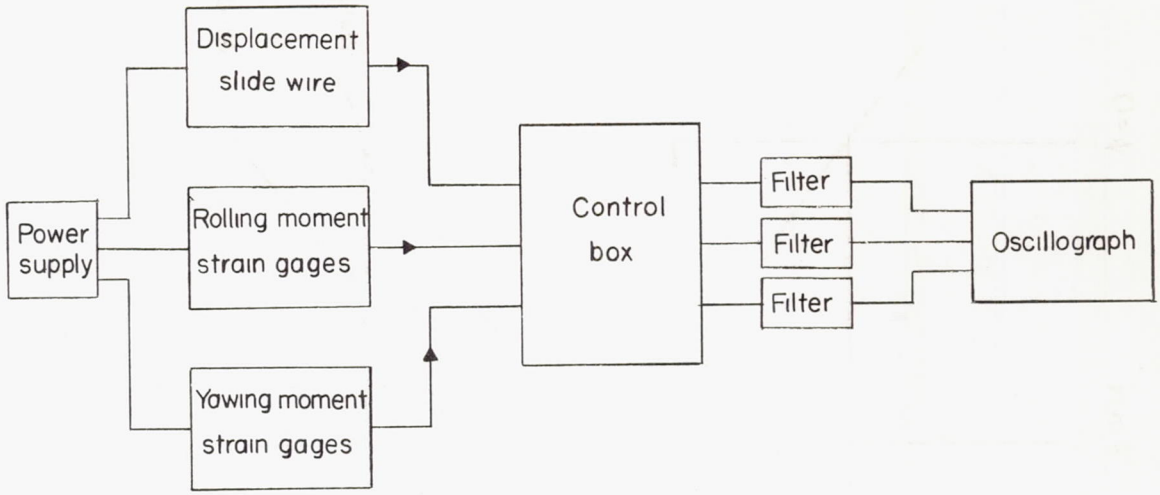

(a) Method A.

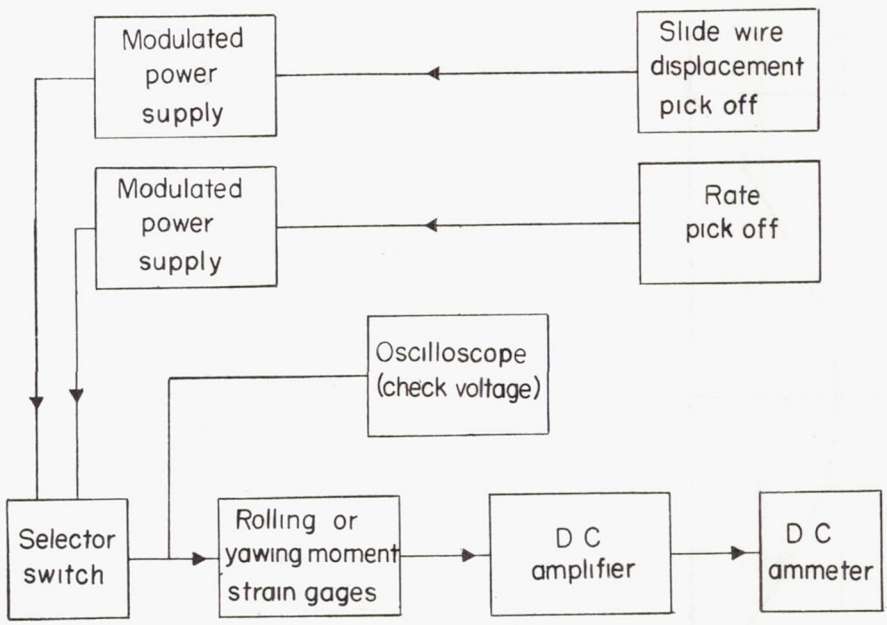

(b) Method B.

Figure 4.- Block diagrams for the two methods used in recording data by the forced oscillation method.

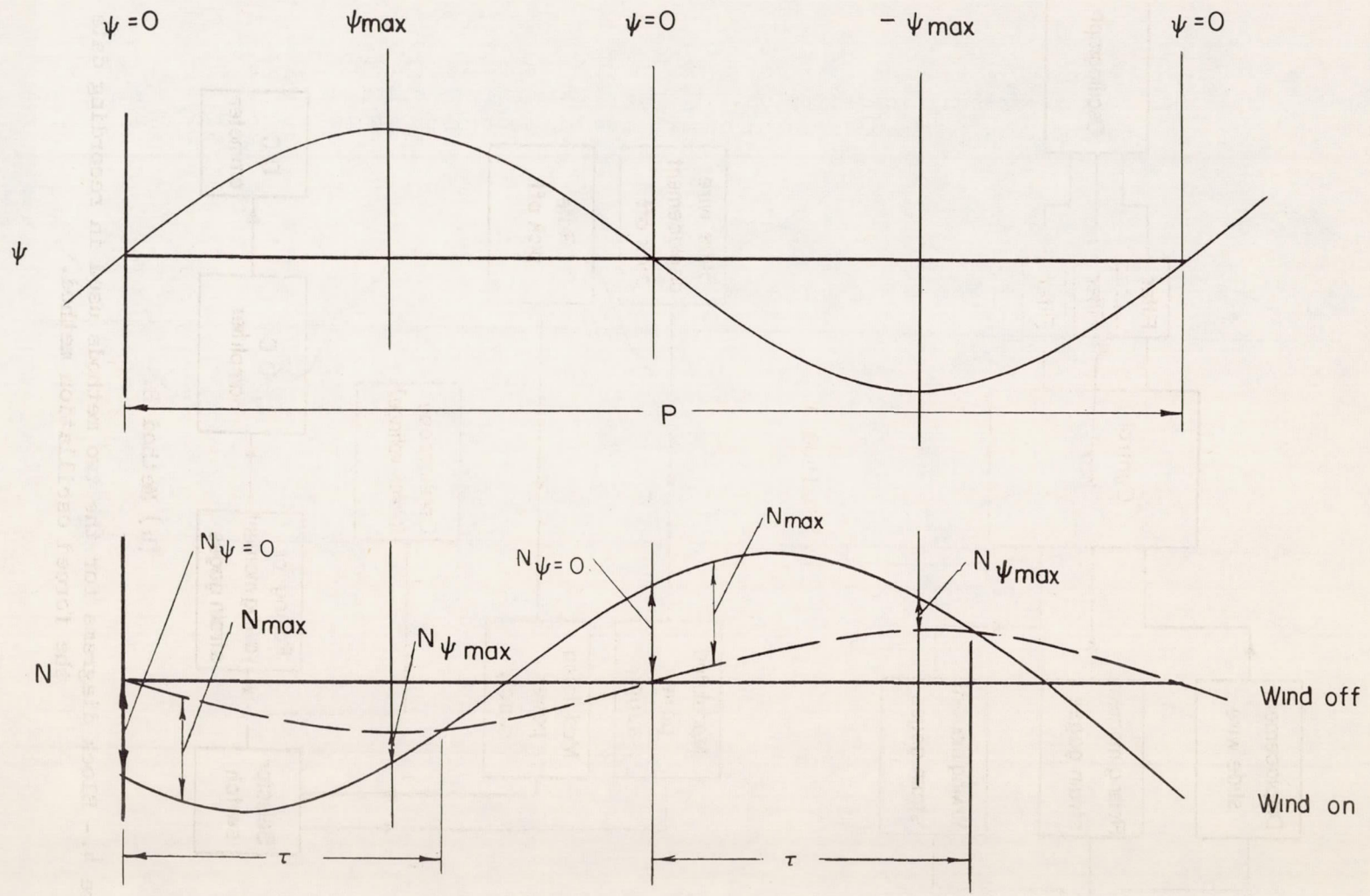

Figure 5.- Factors determined from forced oscillation records used in reduction of data.

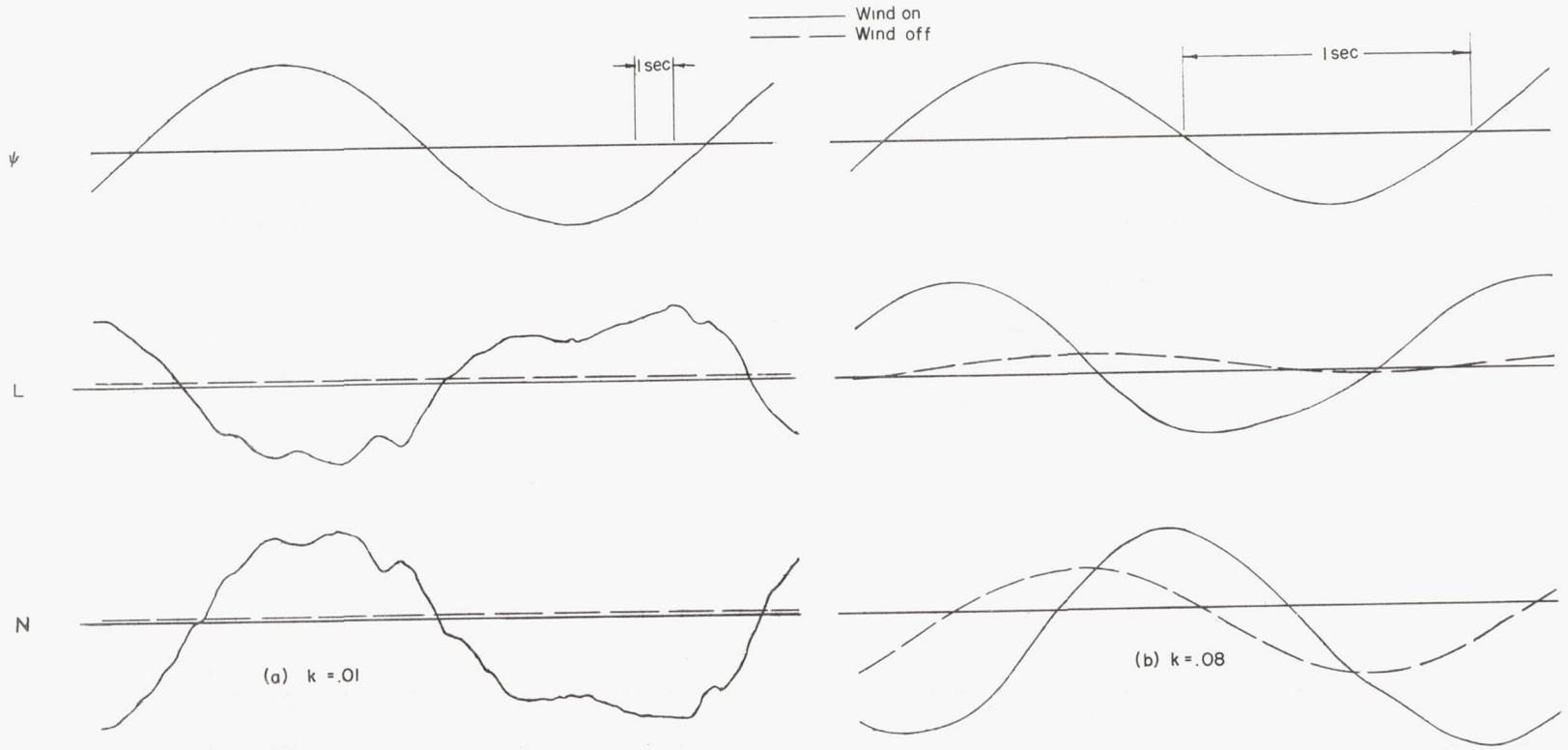

Figure 6.- Typical displacement and moment records obtained from forced oscillation tests of the delta wing at two different frequencies. $\alpha = 30^{\circ}$. Note difference in time scale for the two sets of data.

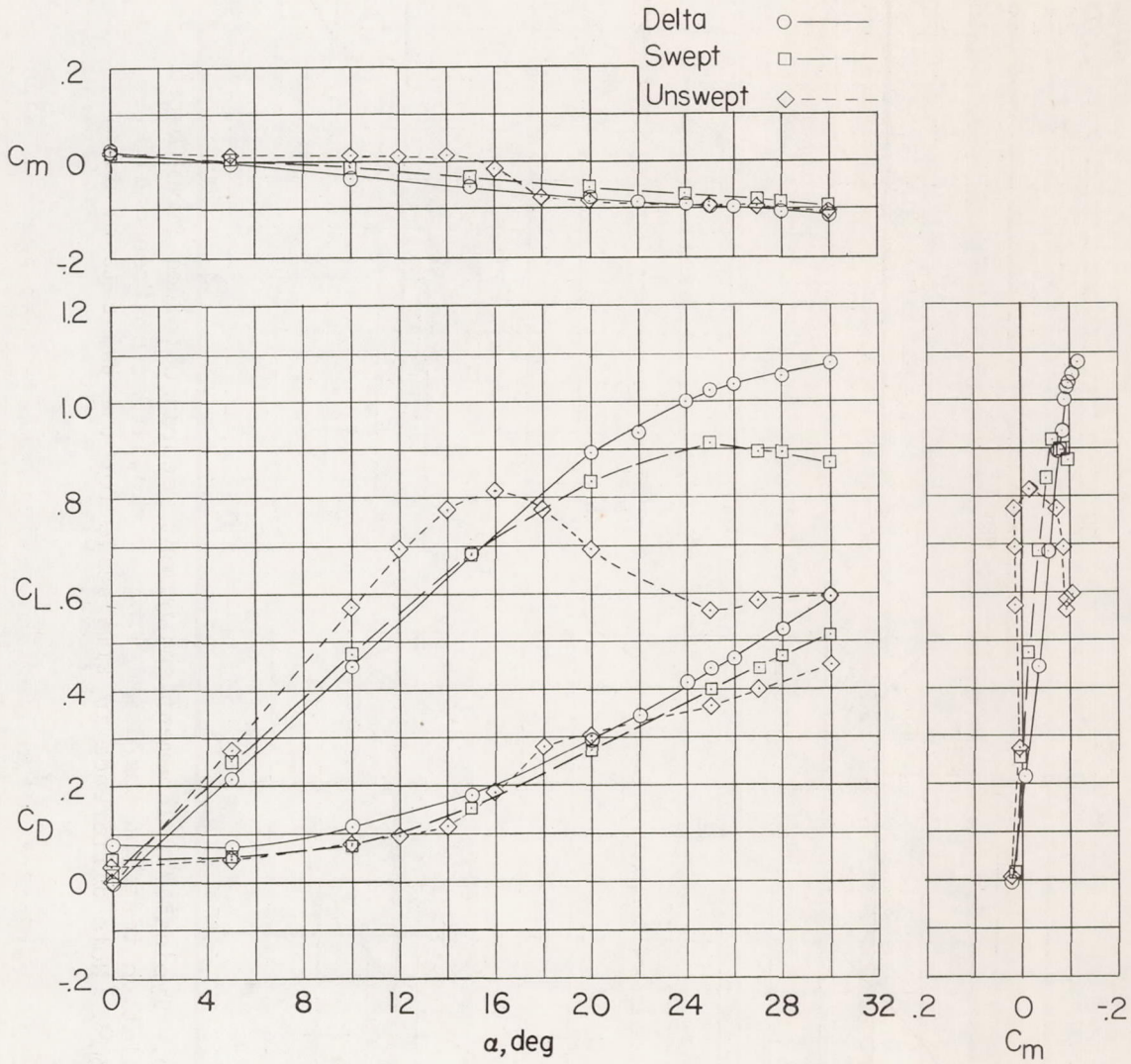

Figure 7.- Static longitudinal characteristics of the three wings.

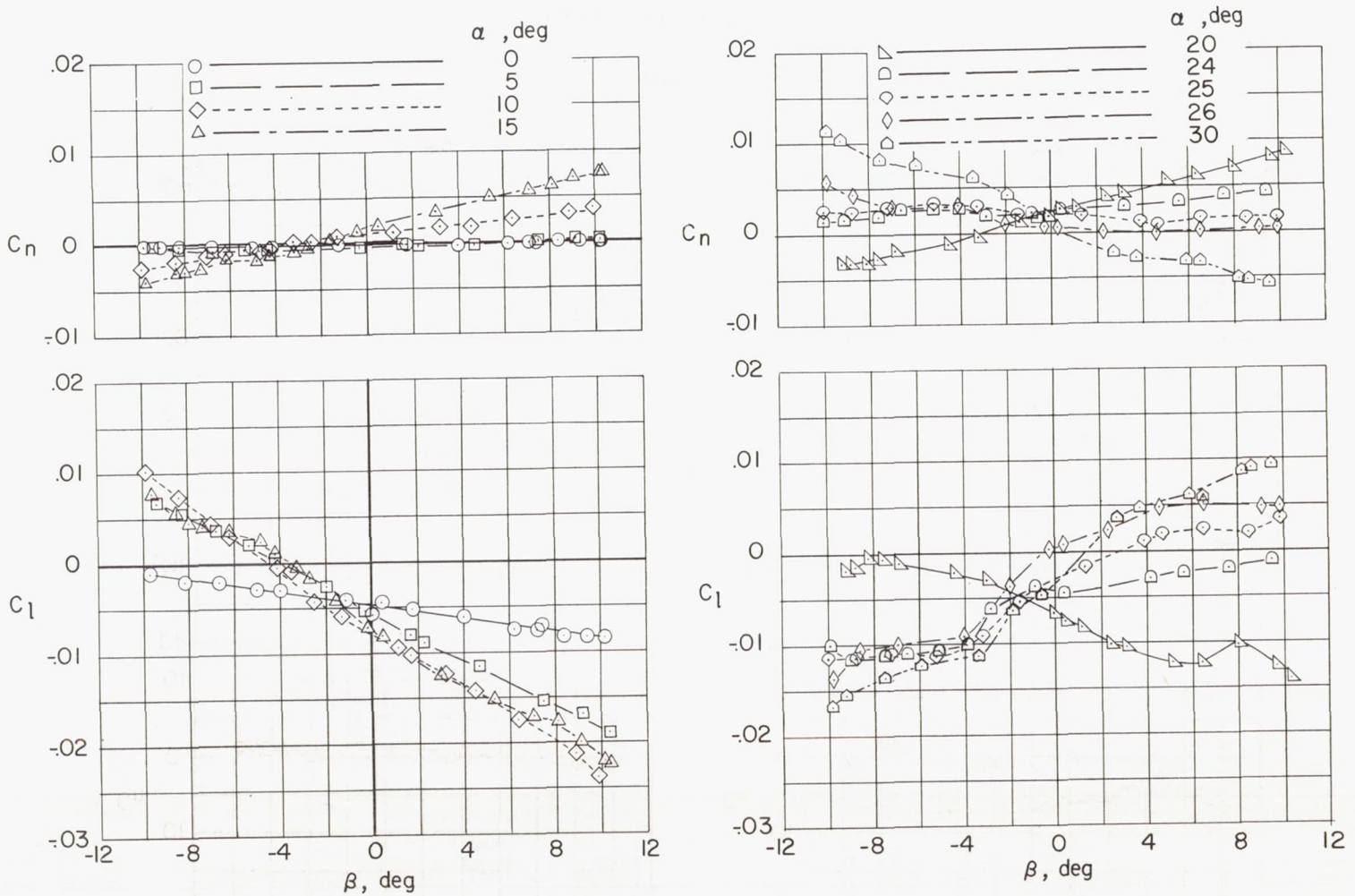

(a) Delta wing.

Figure 8.- Variation of rolling and yawing moments with angle of side-slip for the three wings.

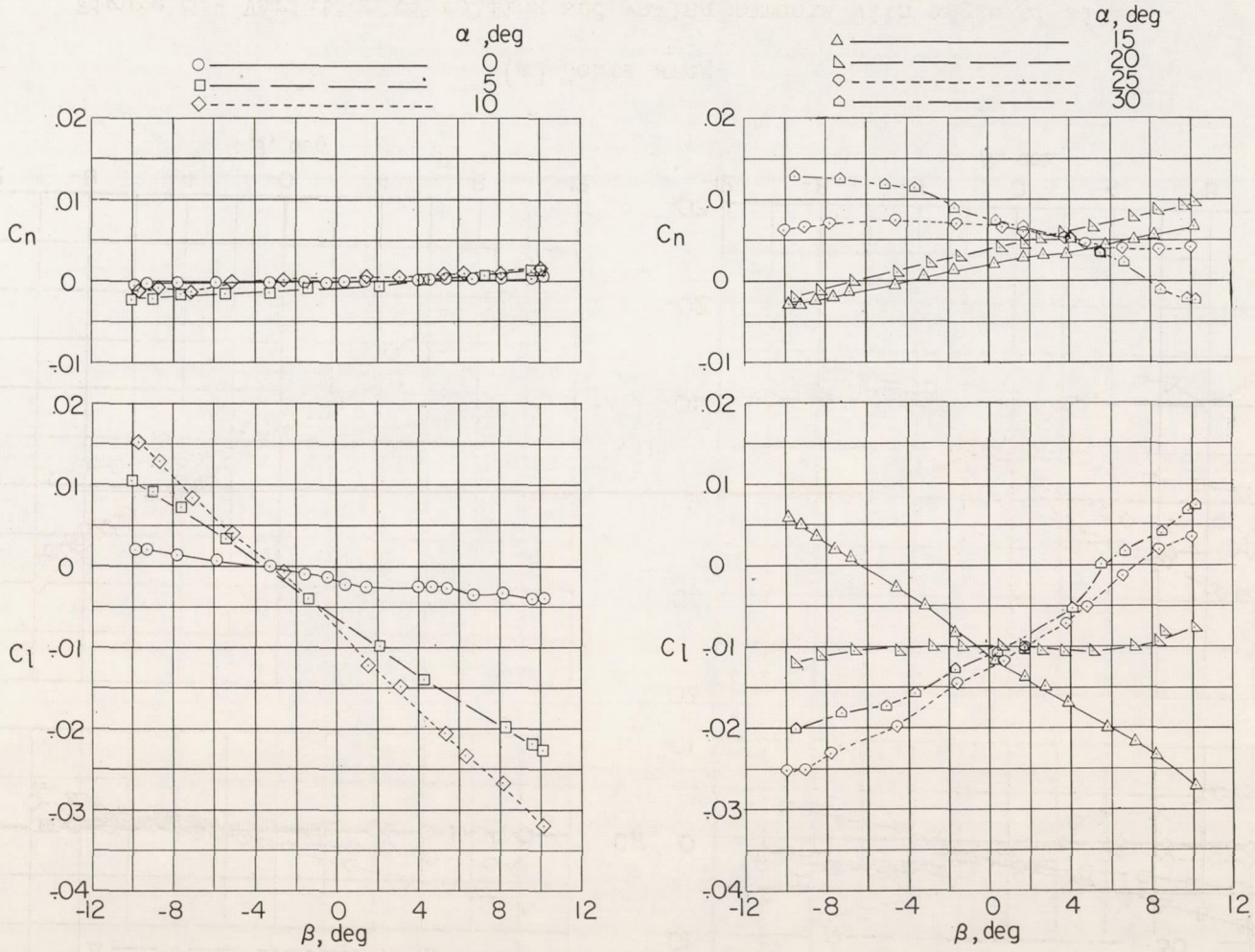

(b) Swept wing.

Figure 8.- Continued.

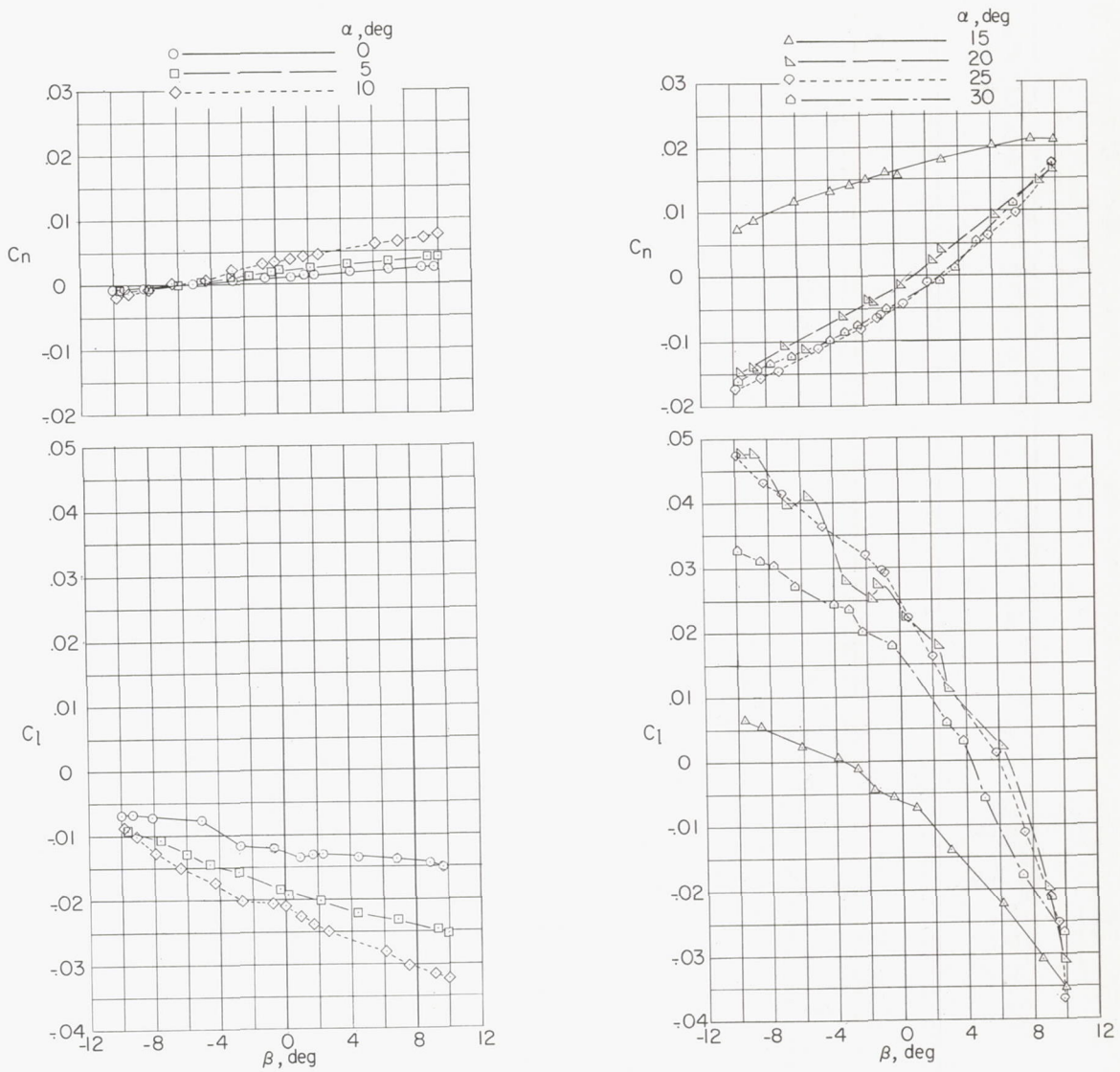

(c) Unswept wing.

Figure 8.- Concluded.

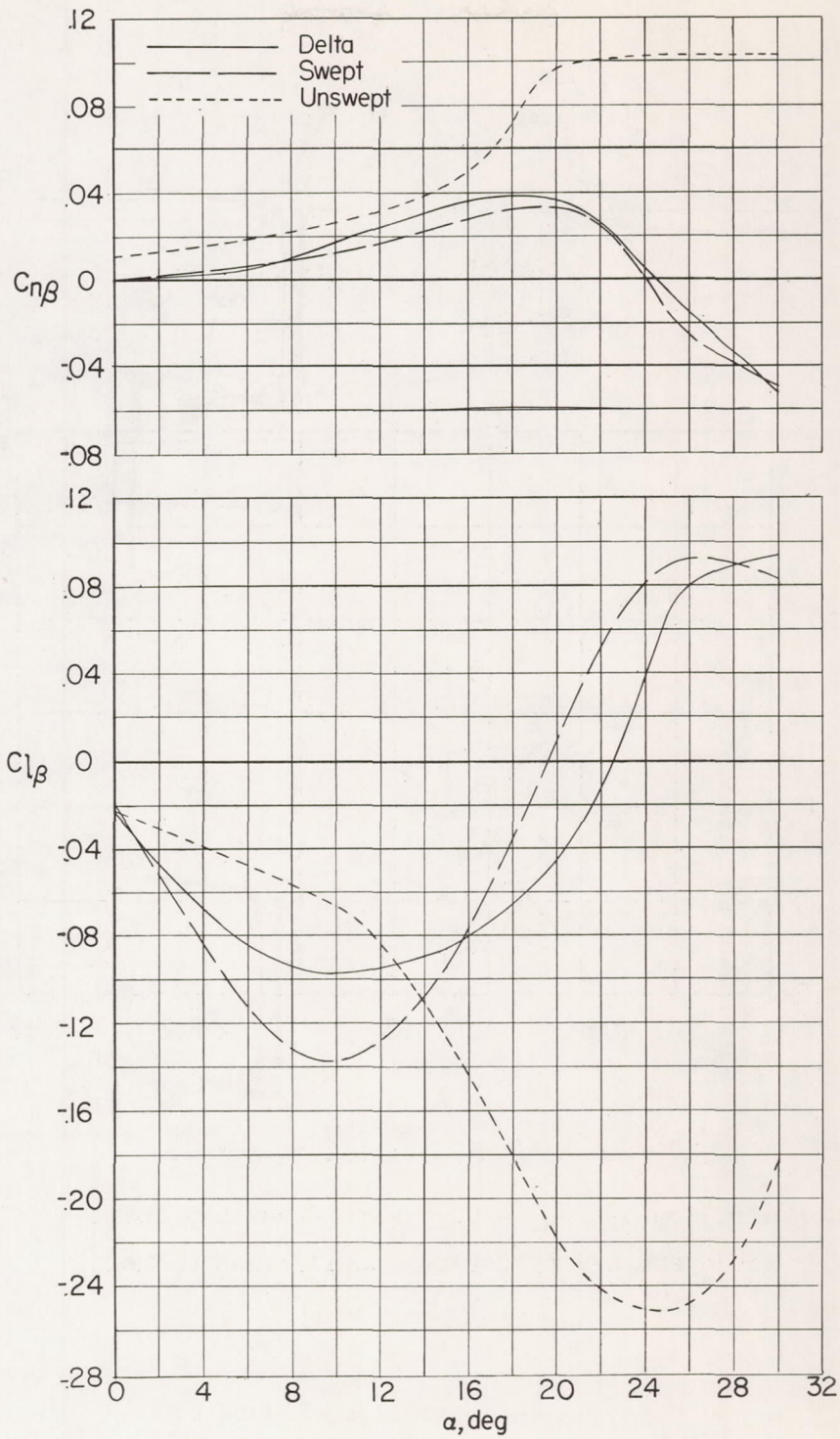

Figure 9.- Static lateral stability derivative of the three wings. (Values of $C_{n\beta}$ and $C_{l\beta}$ determined from average slopes between $\beta = 10^{\circ}$ and -10° of the curves of fig. 8.)

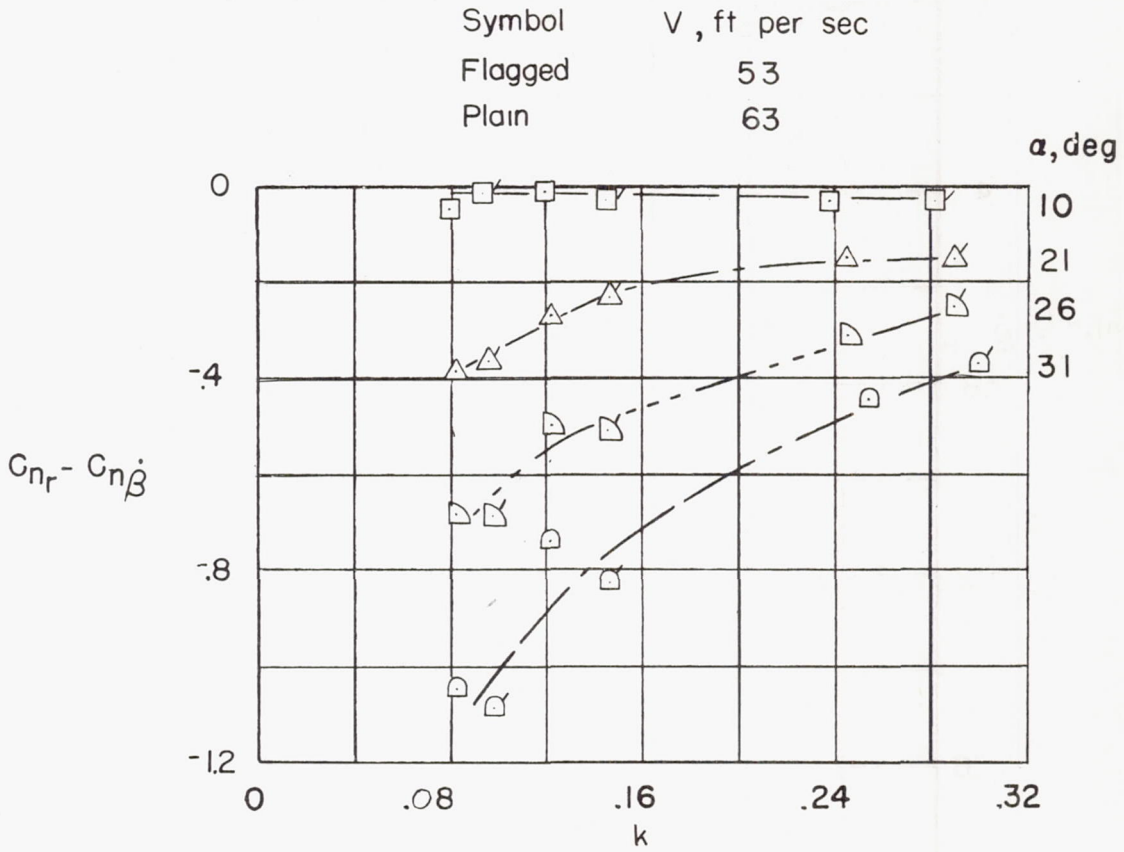

(a) Free-to-damp oscillation method.

Figure 10.- Variation of $C_{n_r} - C_{n_{\dot{\beta}}}$ with frequency for the delta wing as determined by various oscillation methods.

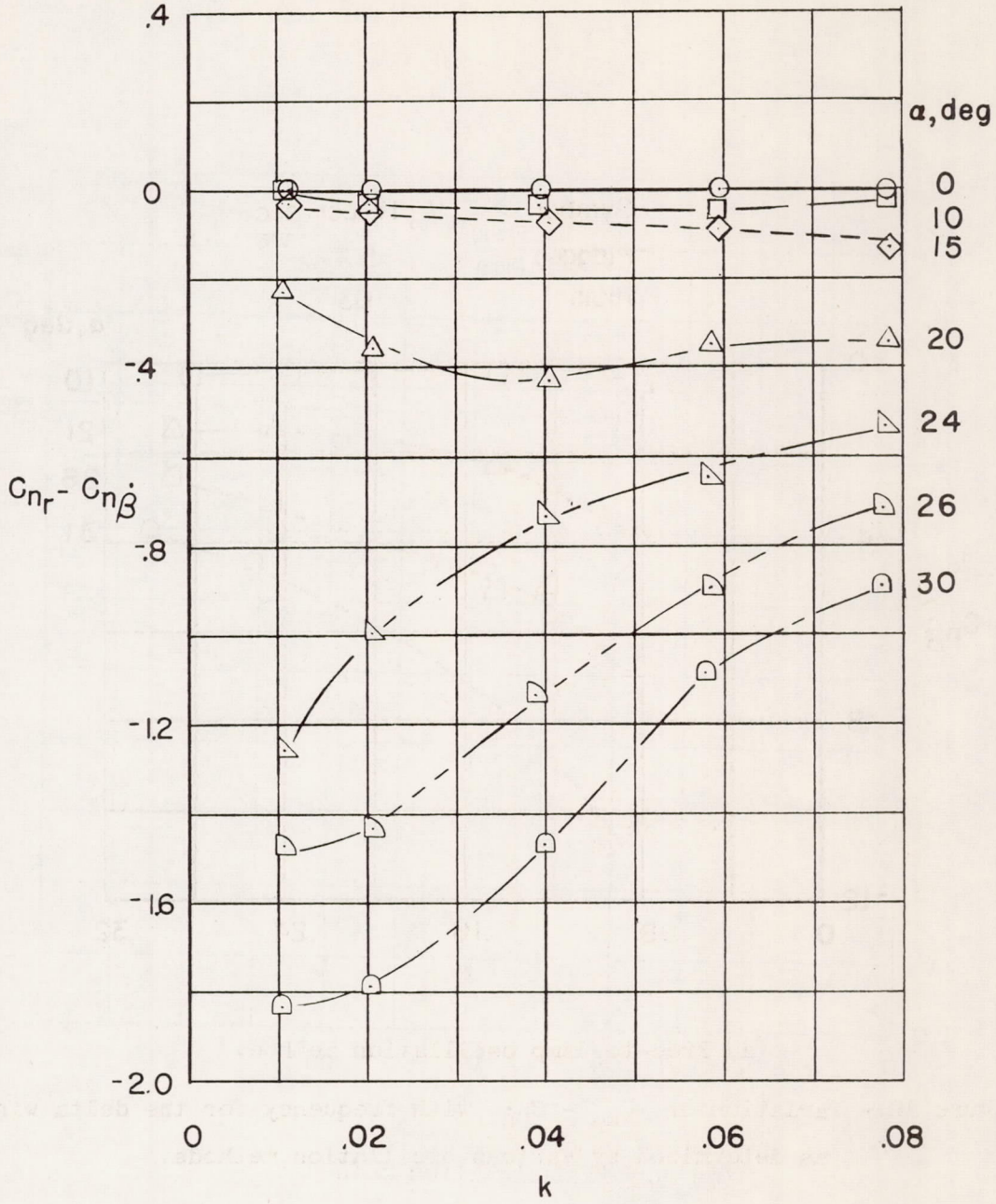

(b) Forced oscillation method A.

Figure 10.- Continued.

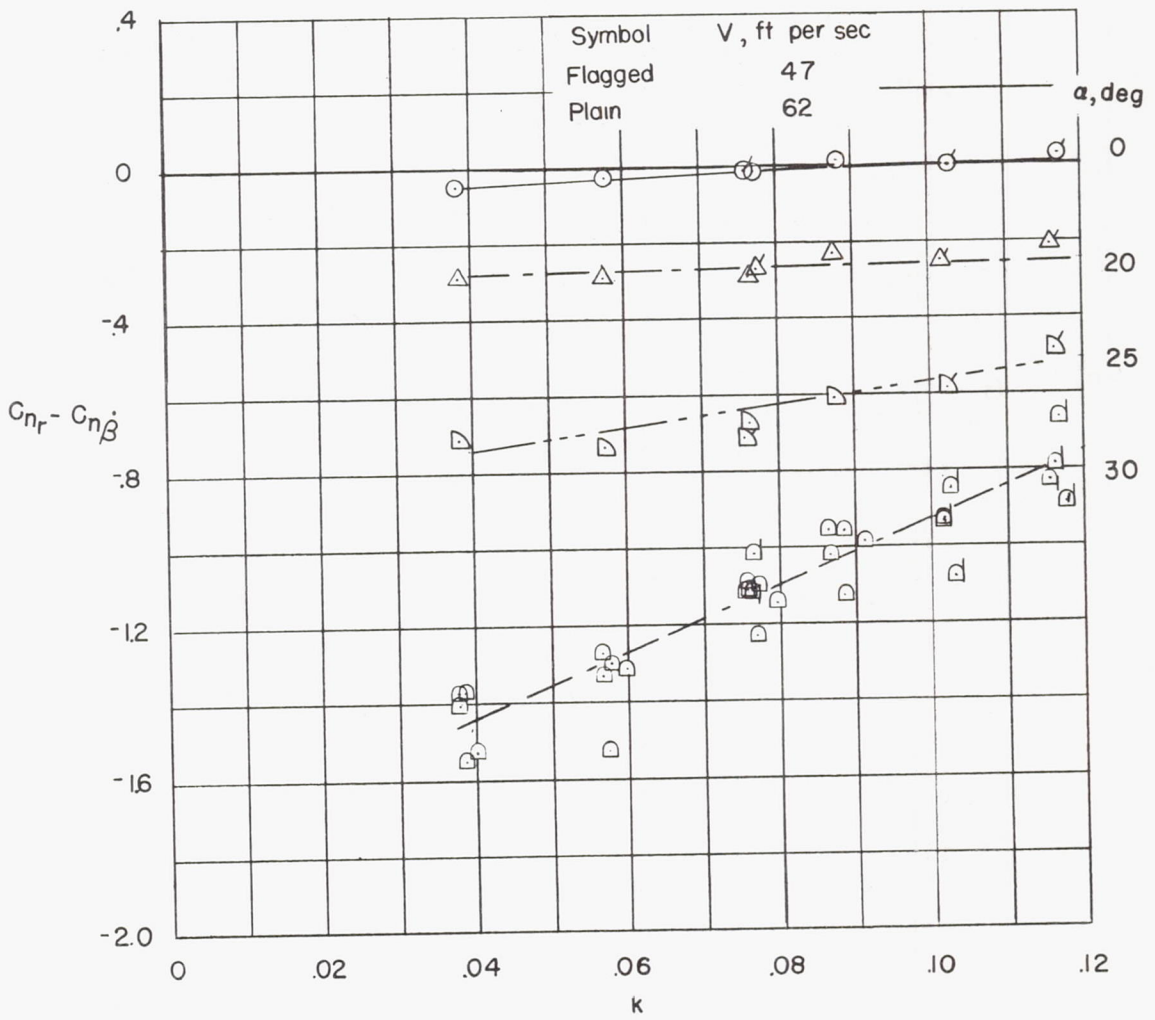

(c) Forced oscillation method B.

Figure 10.- Continued.

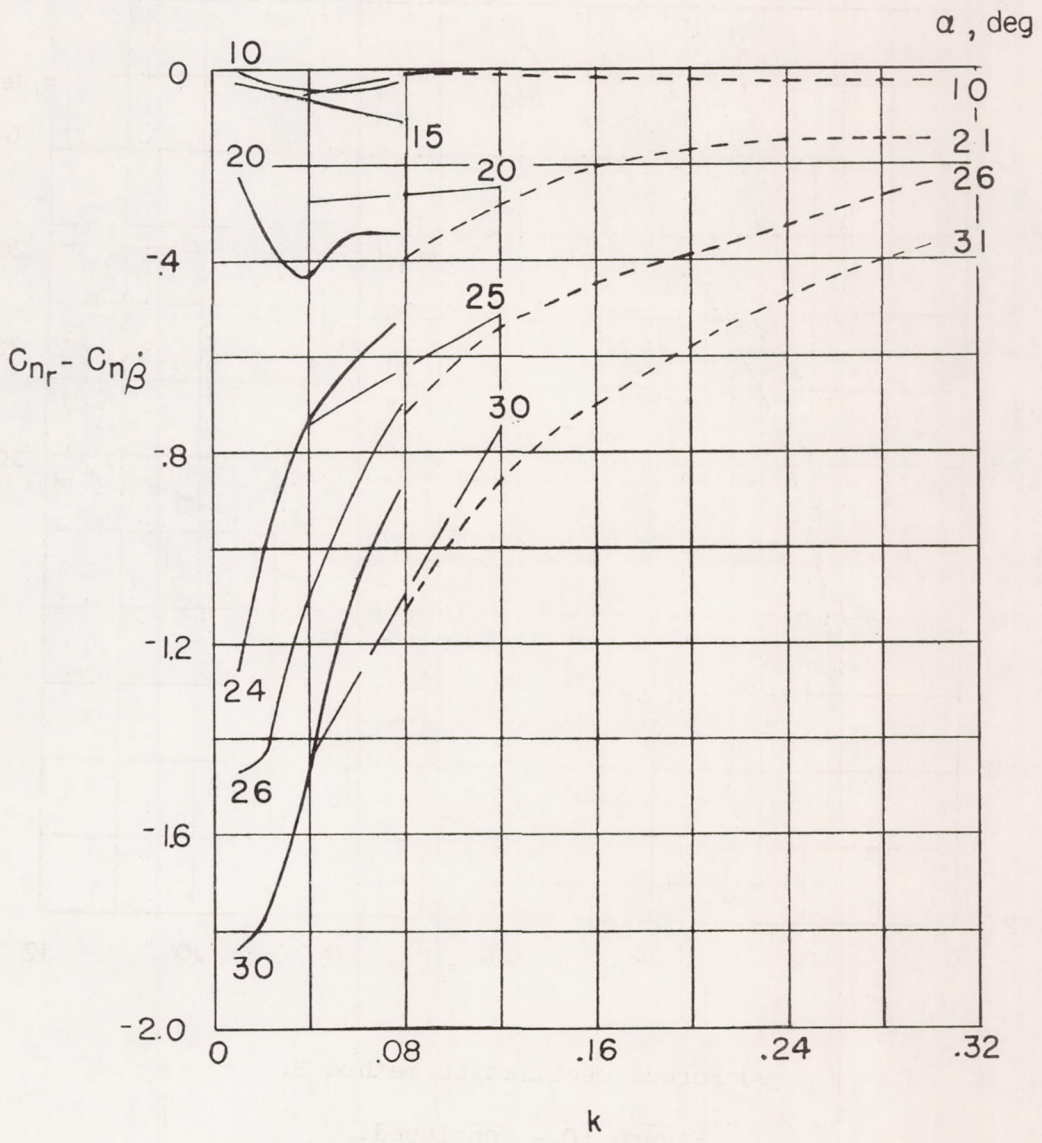

(d) Comparison of data obtained by various methods.

Figure 10.- Concluded.

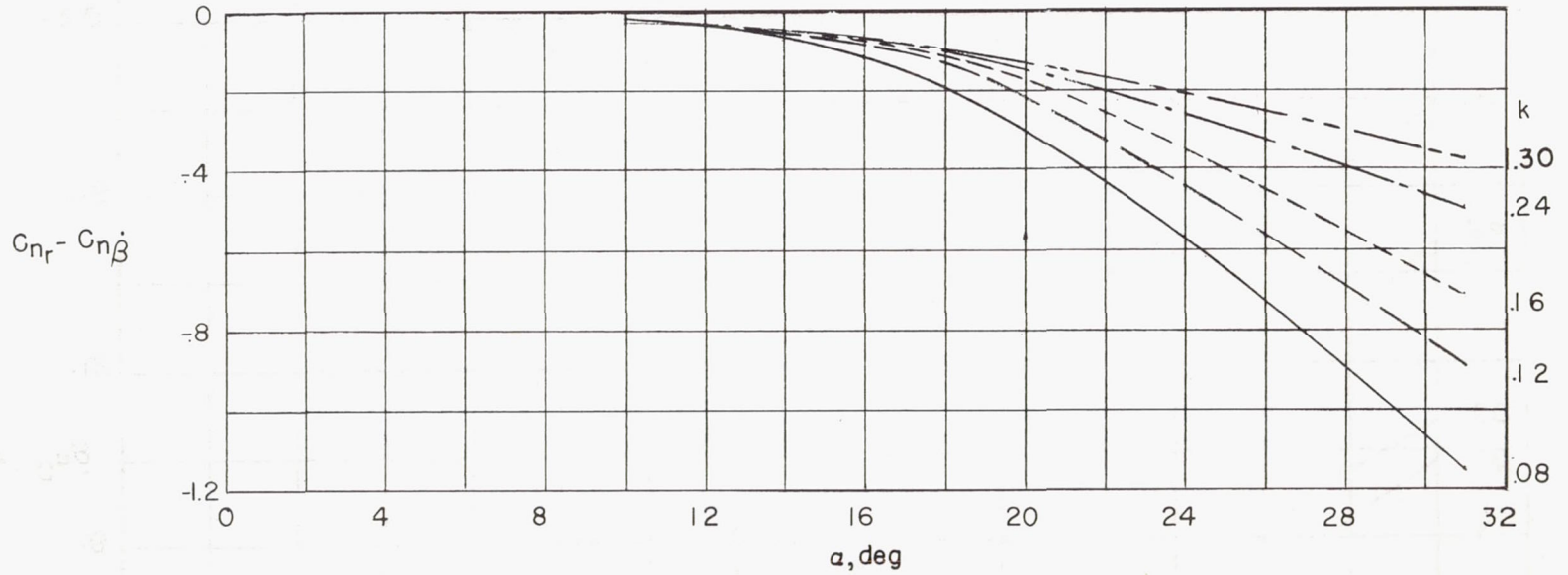

(a) Free-to-damp oscillation method.

Figure 11.- Variation of $C_{n_r} - C_{n\dot{\beta}}$ with angle of attack for the delta wing. (Cross plots of data of fig. 10.)

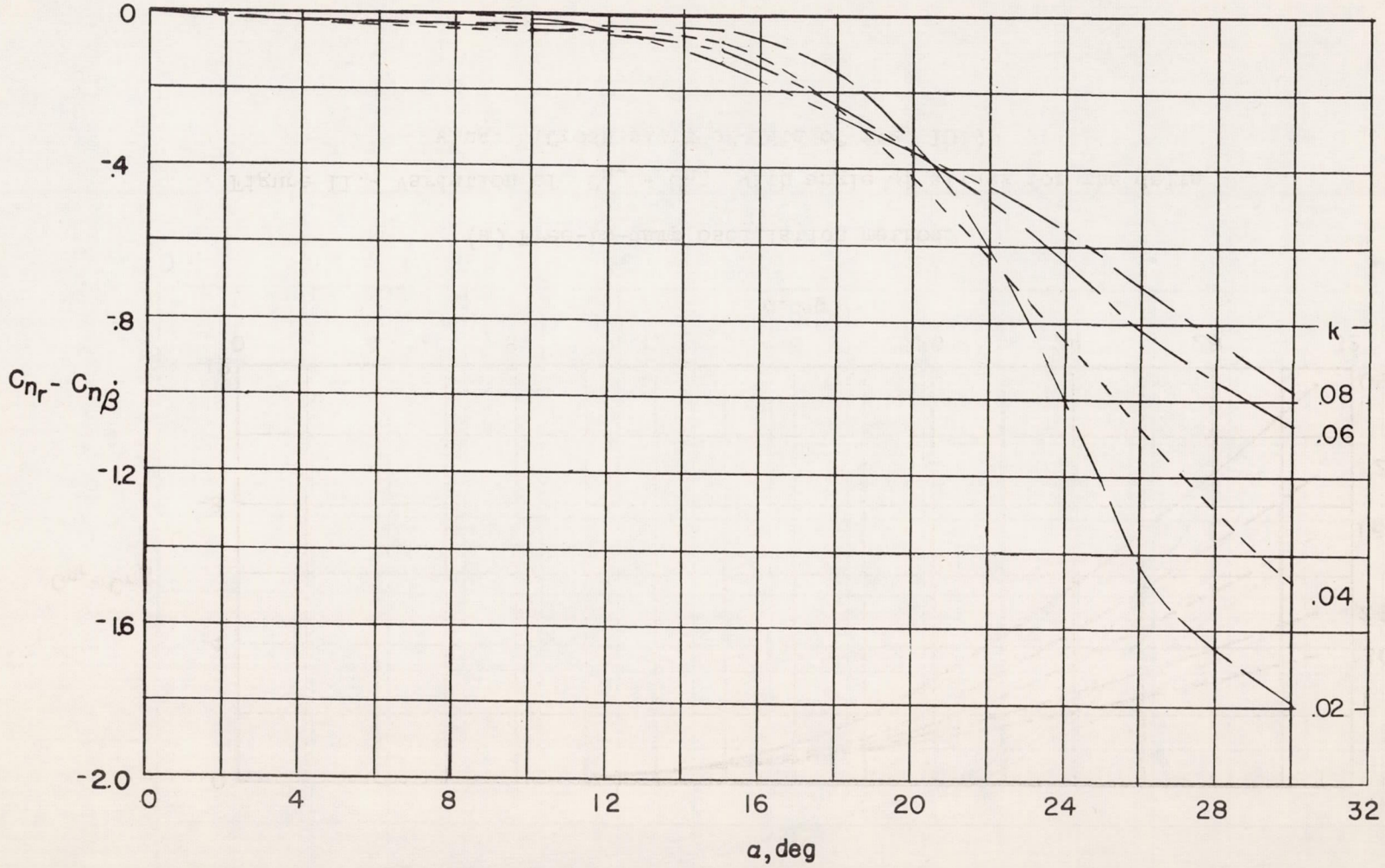

(b) Forced oscillation method A.

Figure 11.- Continued.

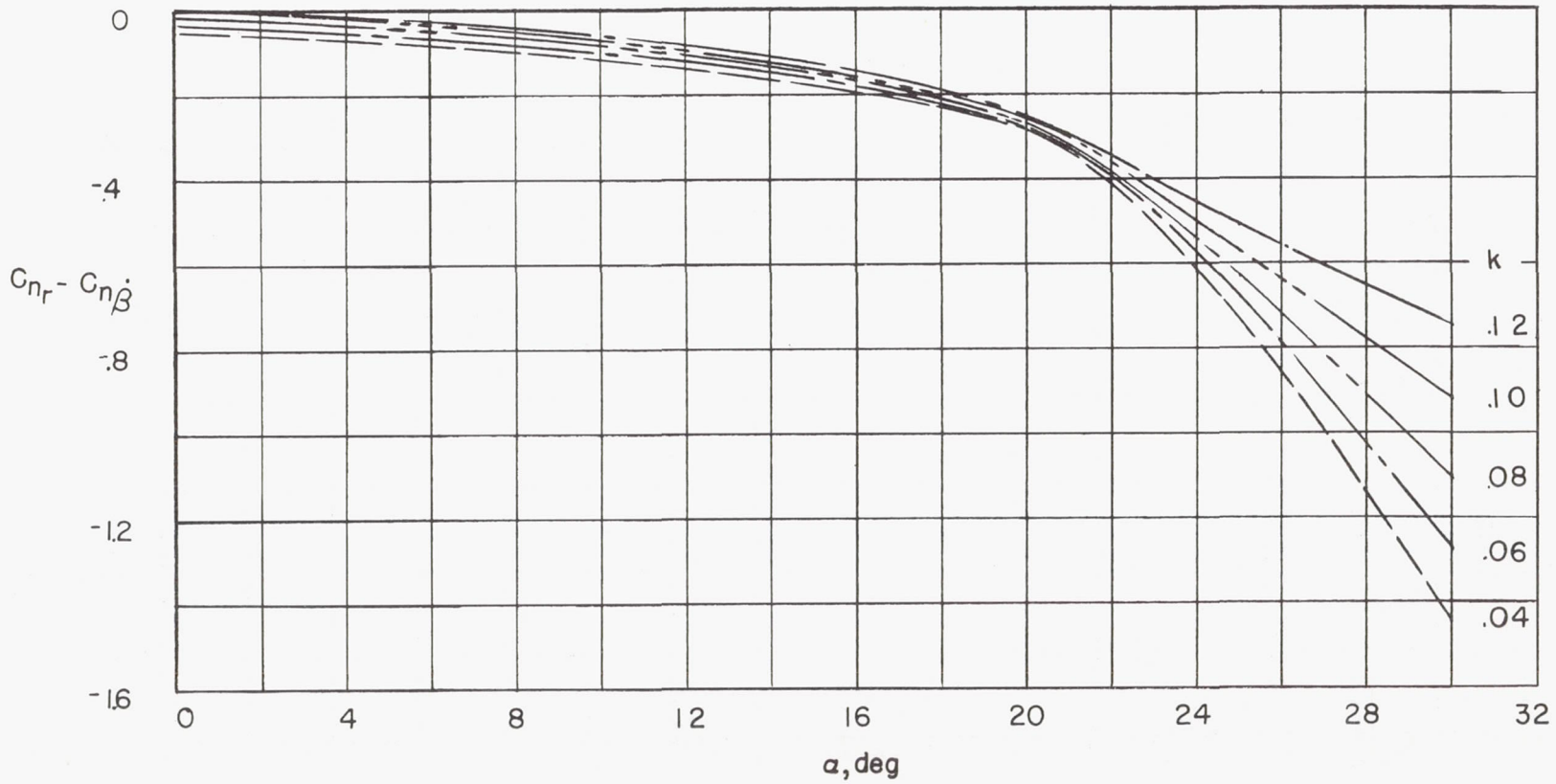

(c) Forced oscillation method B.

Figure 11.- Continued.

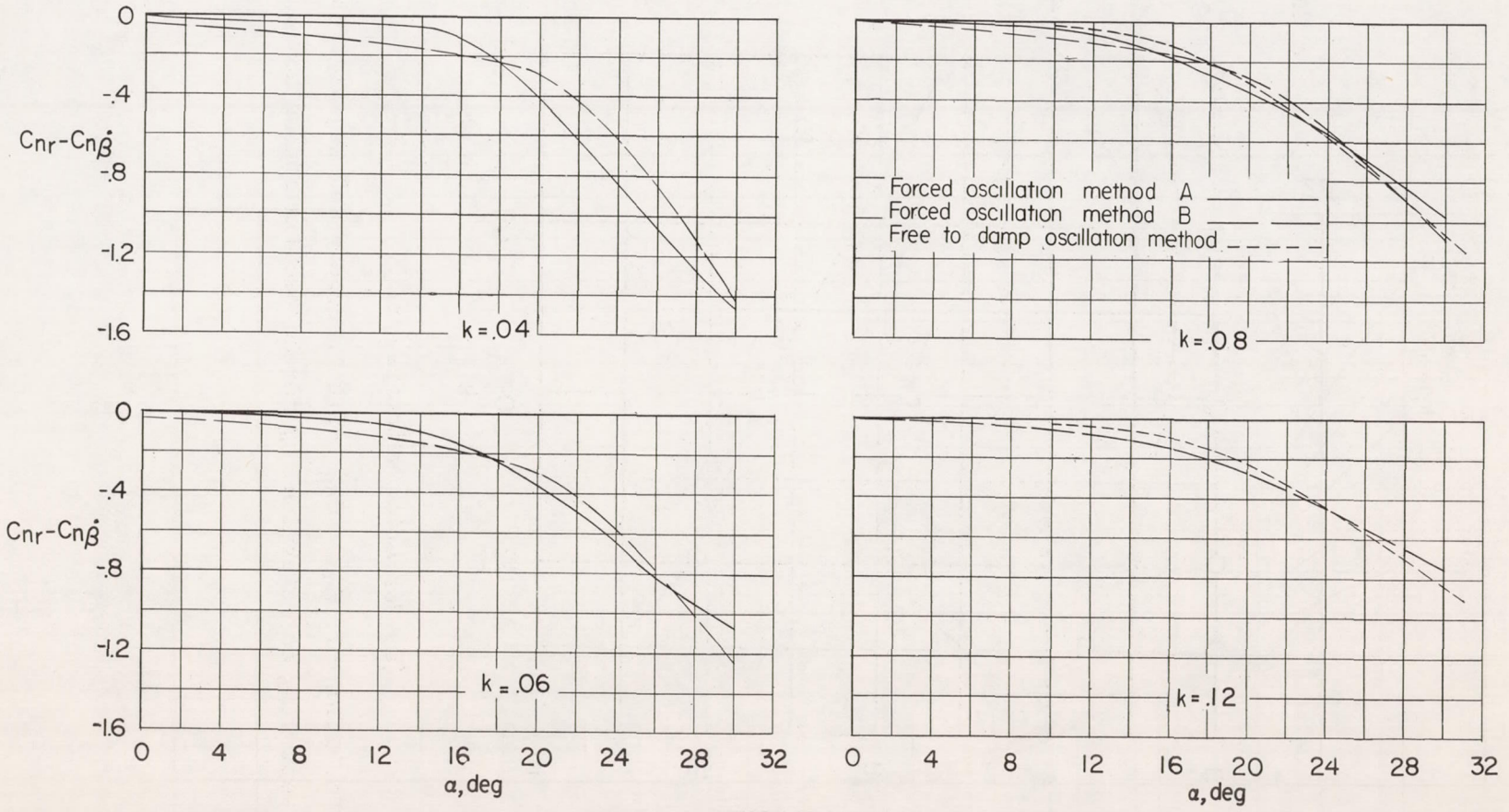

(d) Comparison of data obtained by various methods.

Figure 11.- Concluded.

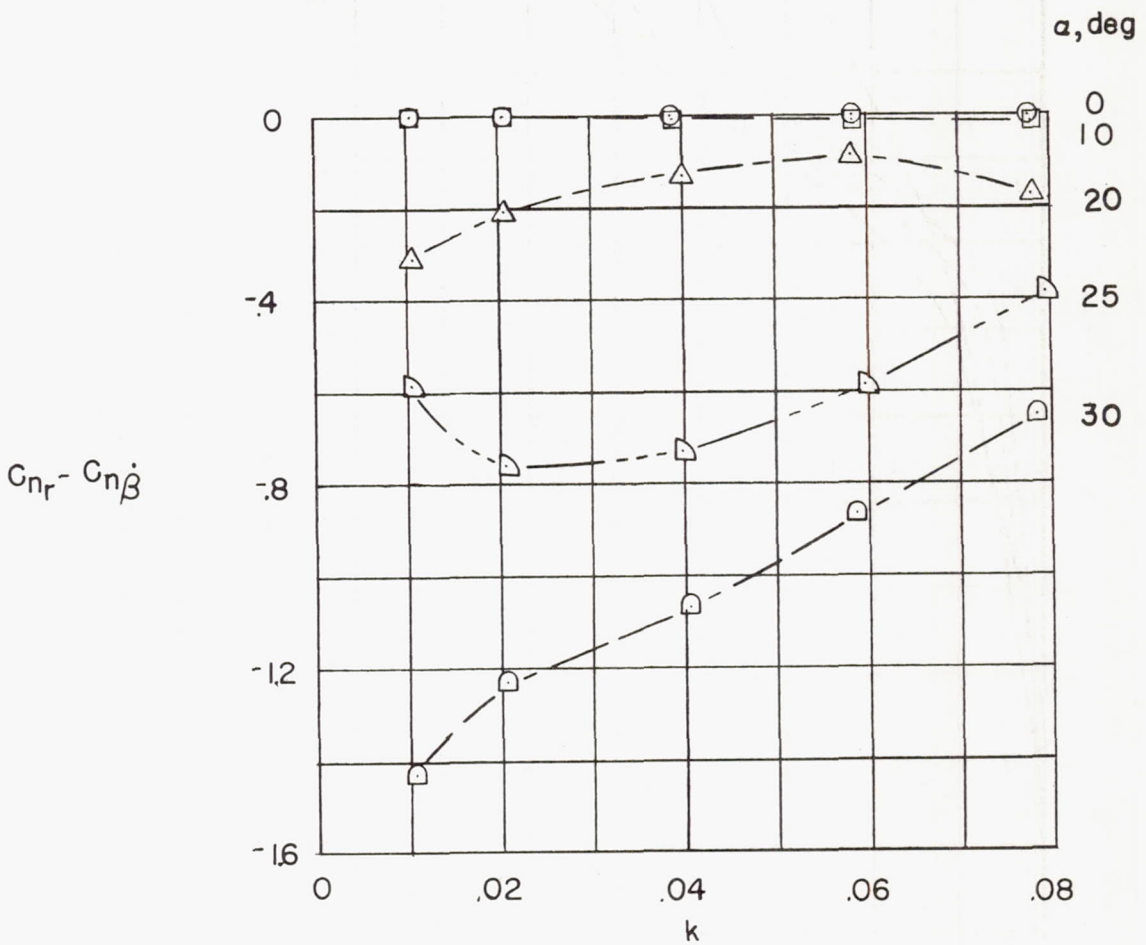

(a) Variation with frequency.

Figure 12.- Variation of $C_{n_r} - C_{n\dot{\beta}}$ with frequency and angle of attack for the swept wing as determined by forced oscillation method A.

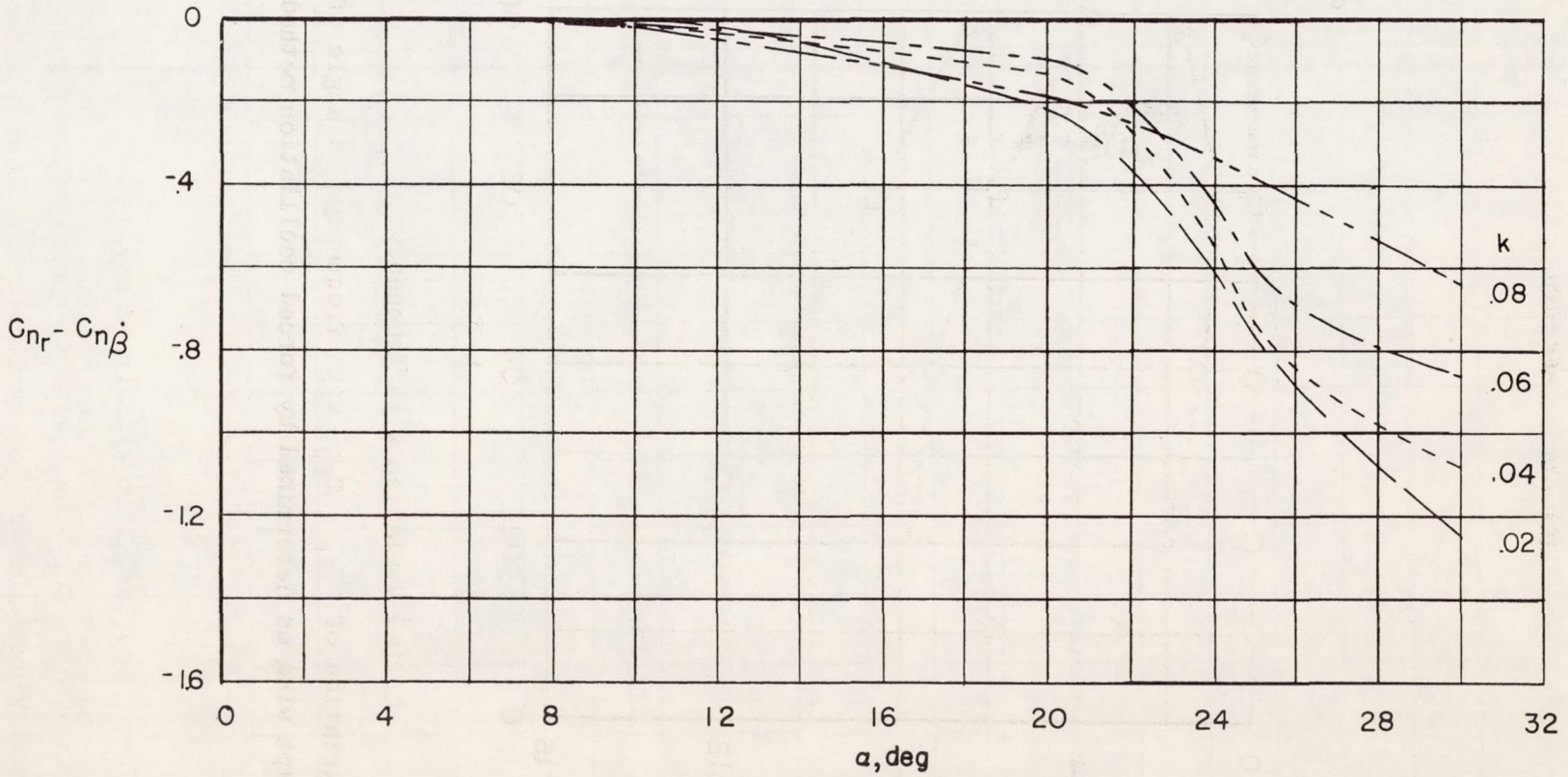

(b) Variation with angle of attack.

Figure 12.- Concluded.

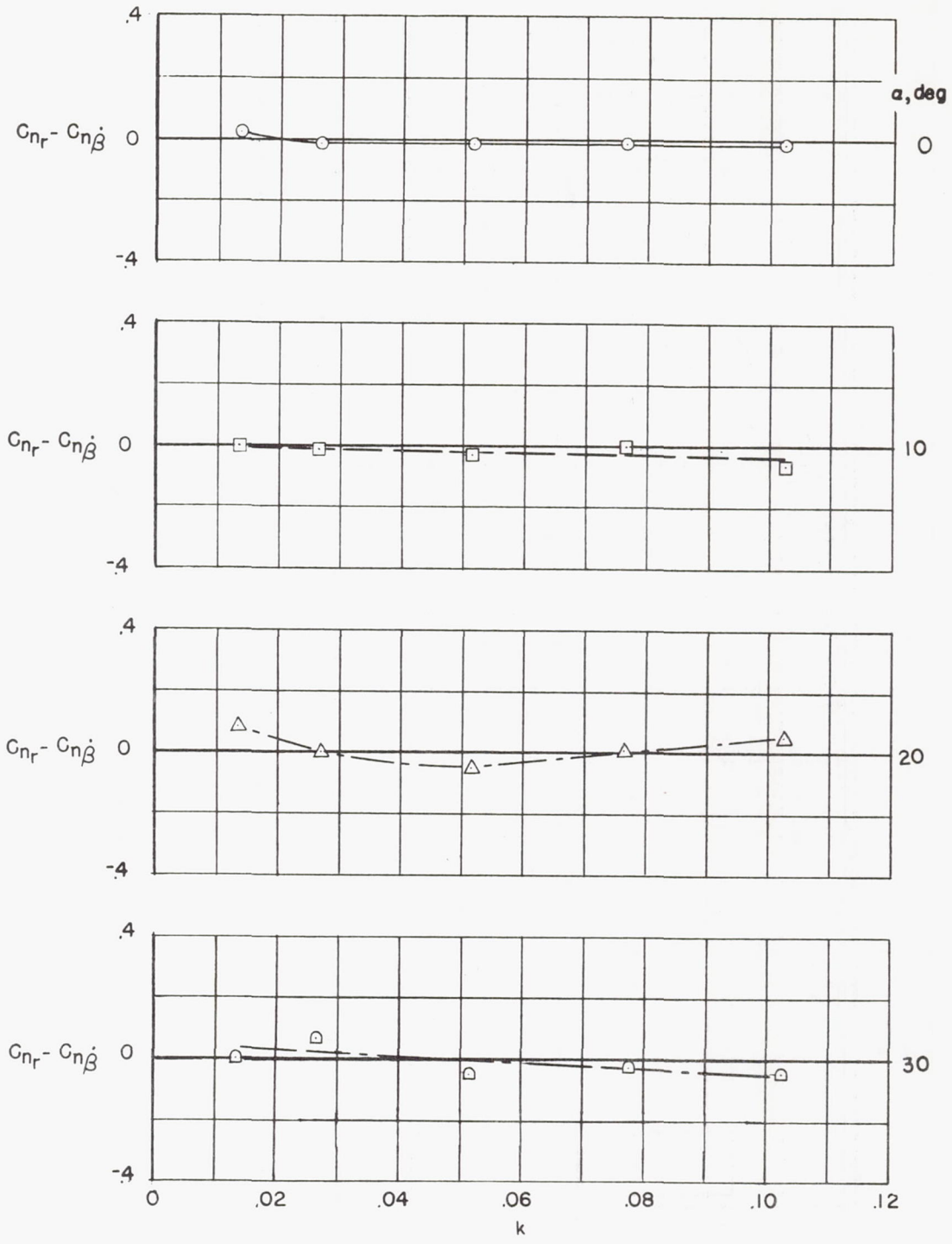

(a) Variation with frequency.

Figure 13.- Variation of $C_{n_r} - C_{n\dot{\beta}}$ with frequency and angle of attack for the unswept wing as determined by forced oscillation method A.

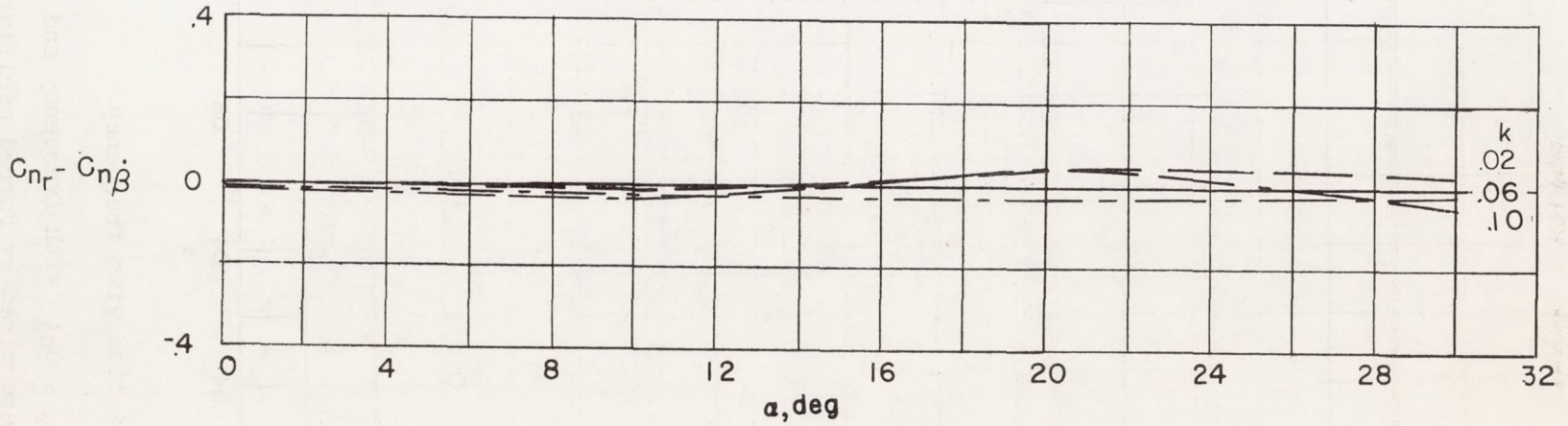

(b) Variation with angle of attack.

Figure 13.- Concluded.

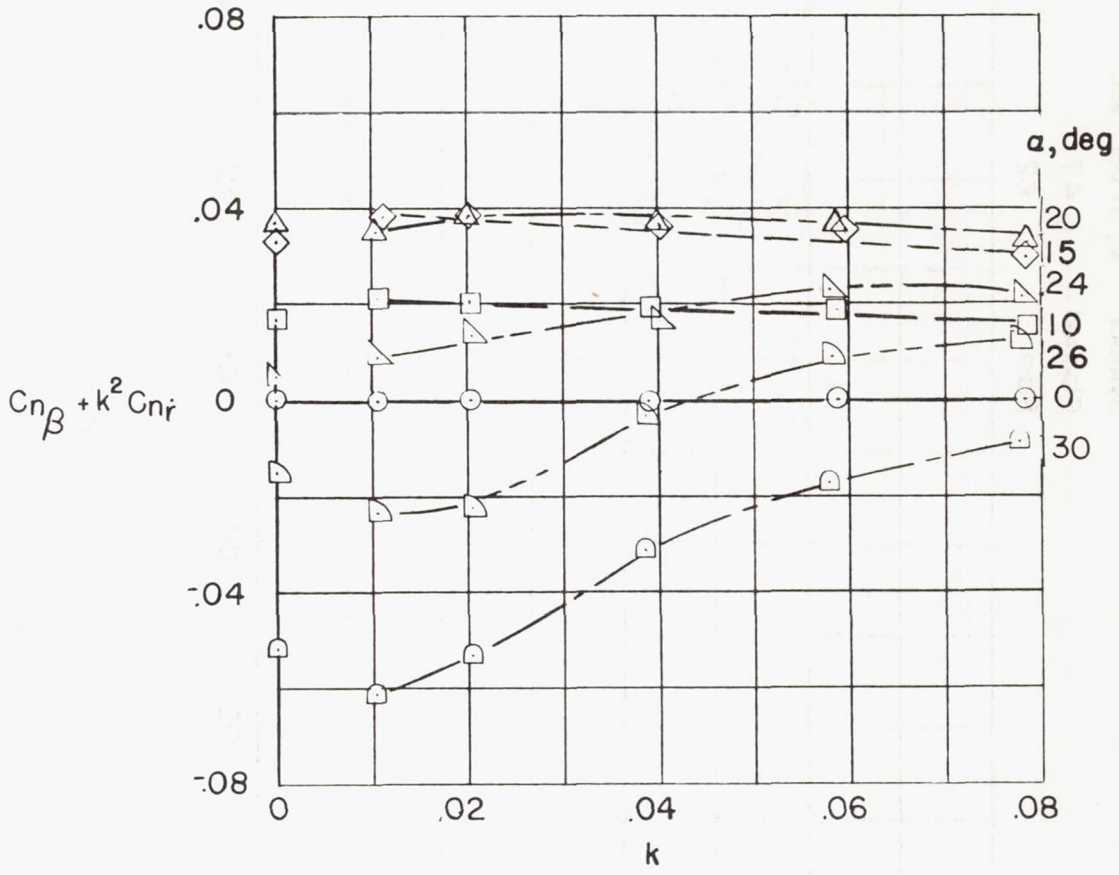

(a) Forced oscillation method A.

Figure 14.- Variation of $C_{n_\beta} + k^2 C_{n_{\dot{r}}}$ with frequency for the delta wing.

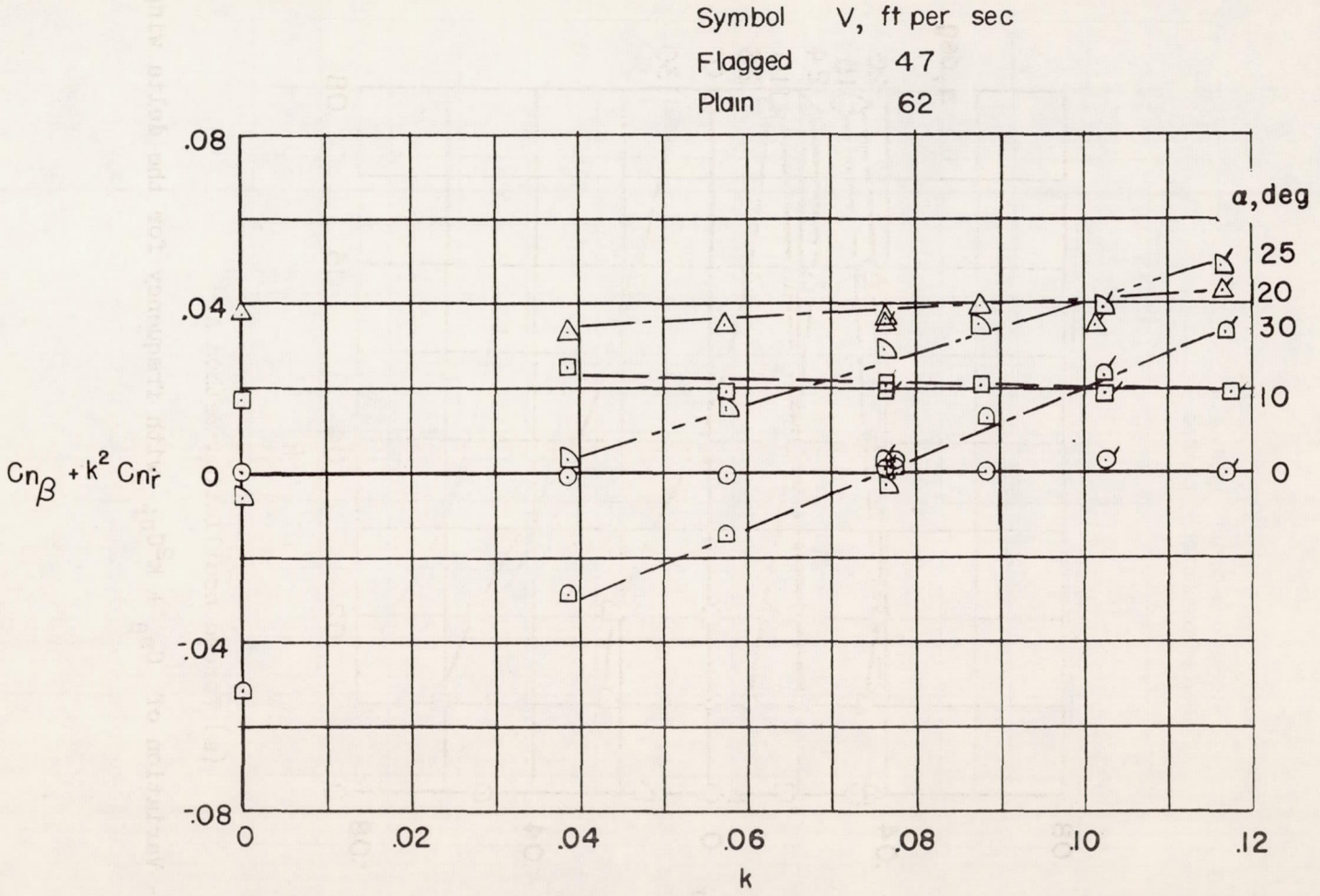

(b) Forced oscillation method B.

Figure 14.- Continued.

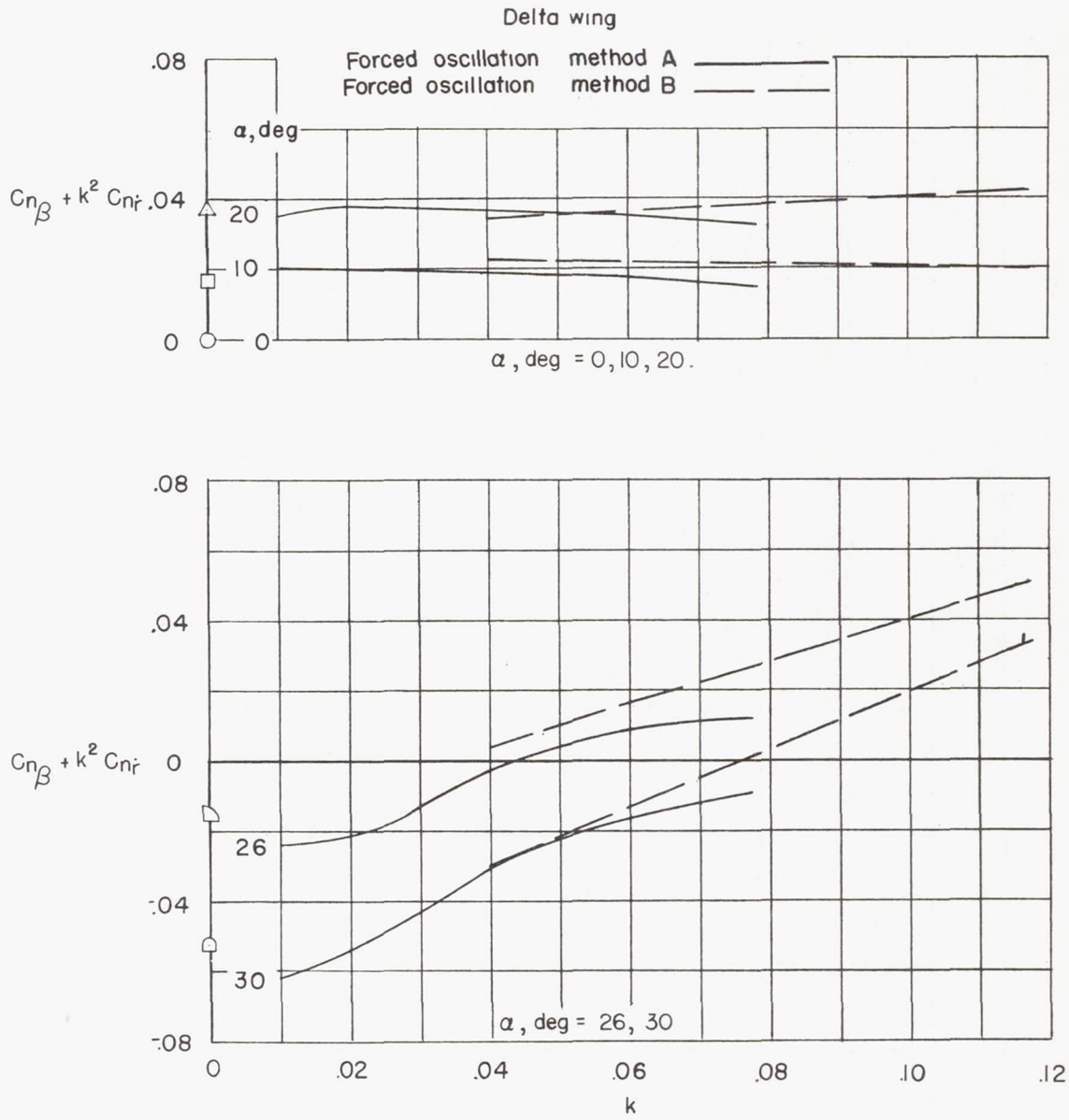

(c) Comparison of data obtained with two methods.

Figure 14.- Concluded.

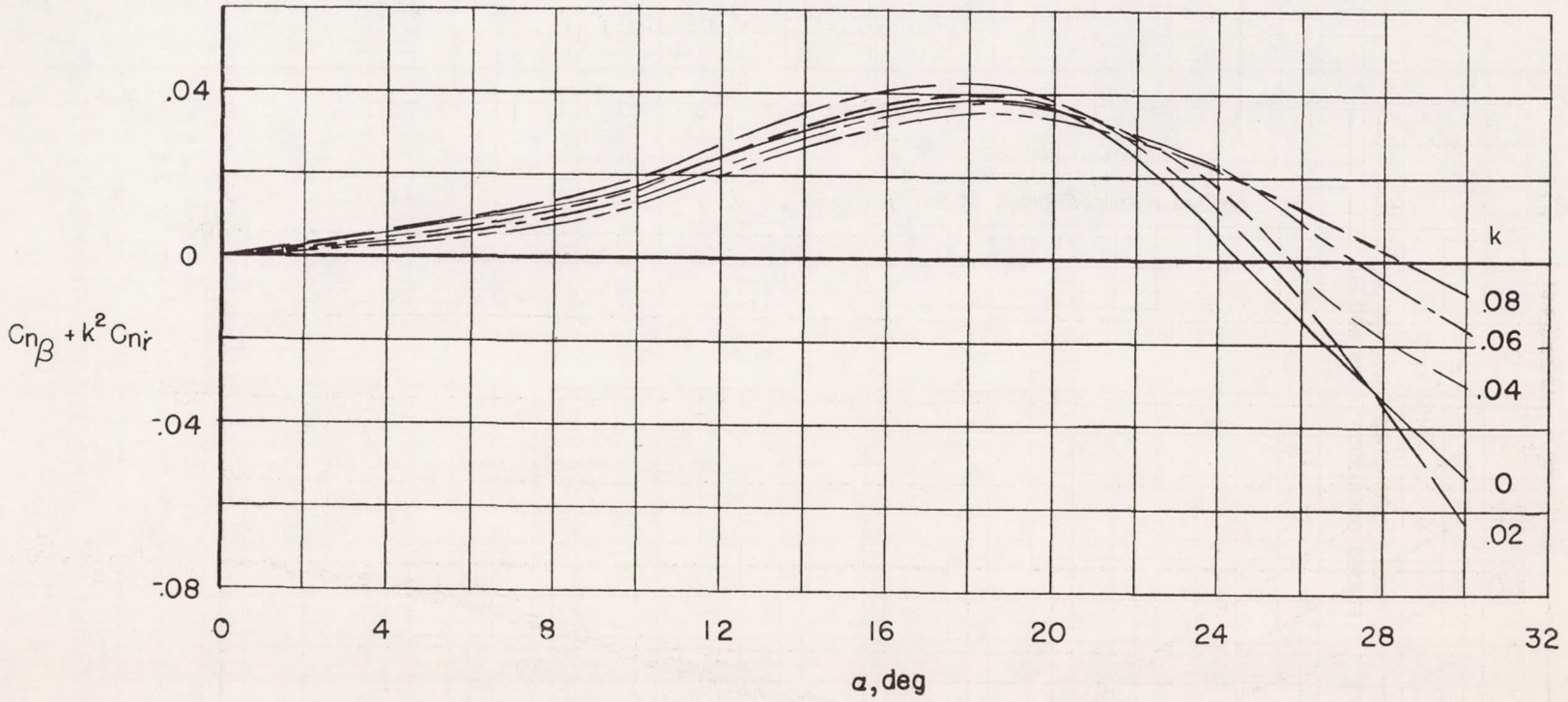

(a) Forced oscillation method A.

Figure 15.- Variation of $C_{n_\beta} + k^2 C_{n_{\dot{r}}}$ with angle of attack for the delta wing.

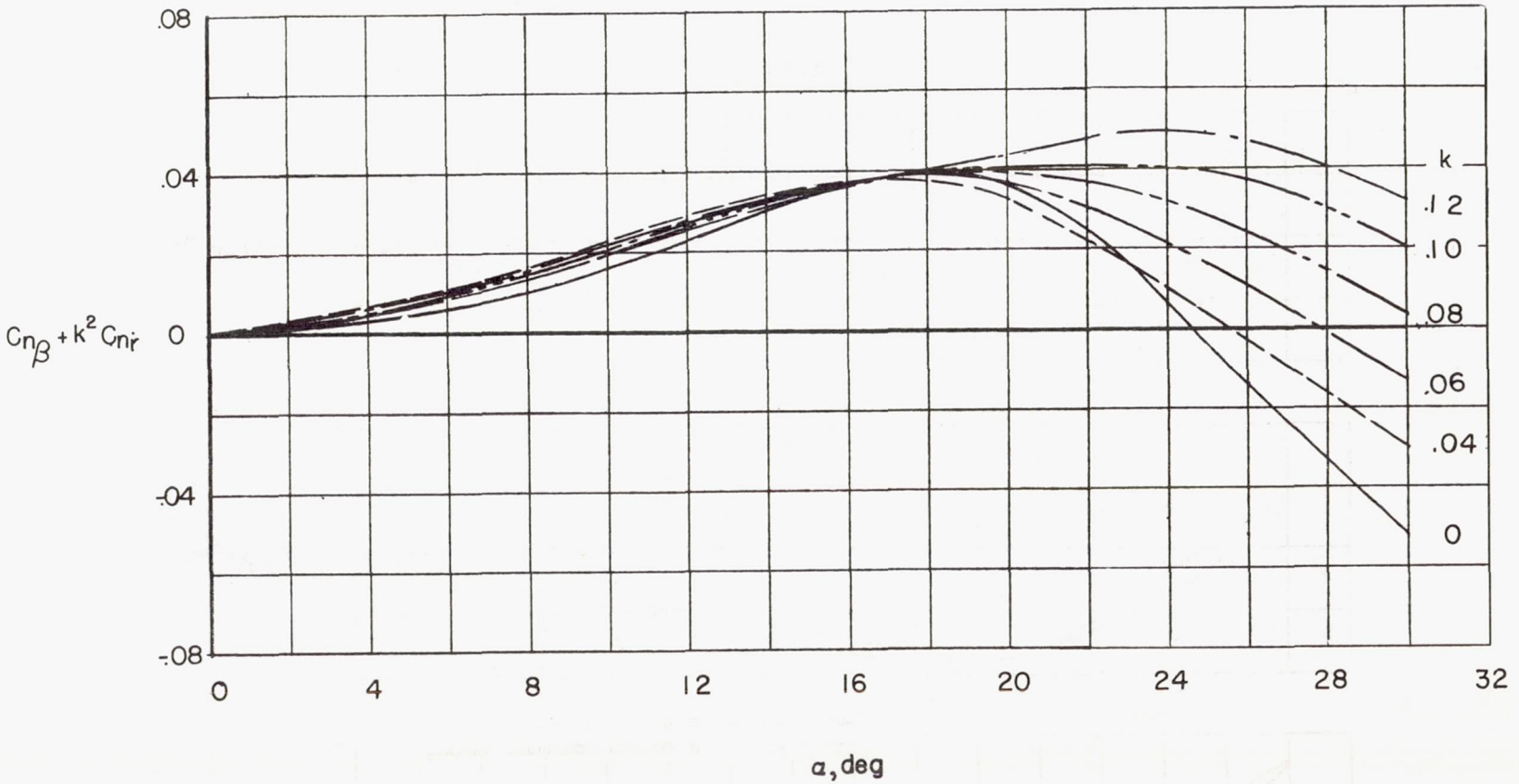

(b) Forced oscillation method B.

Figure 15.- Continued.

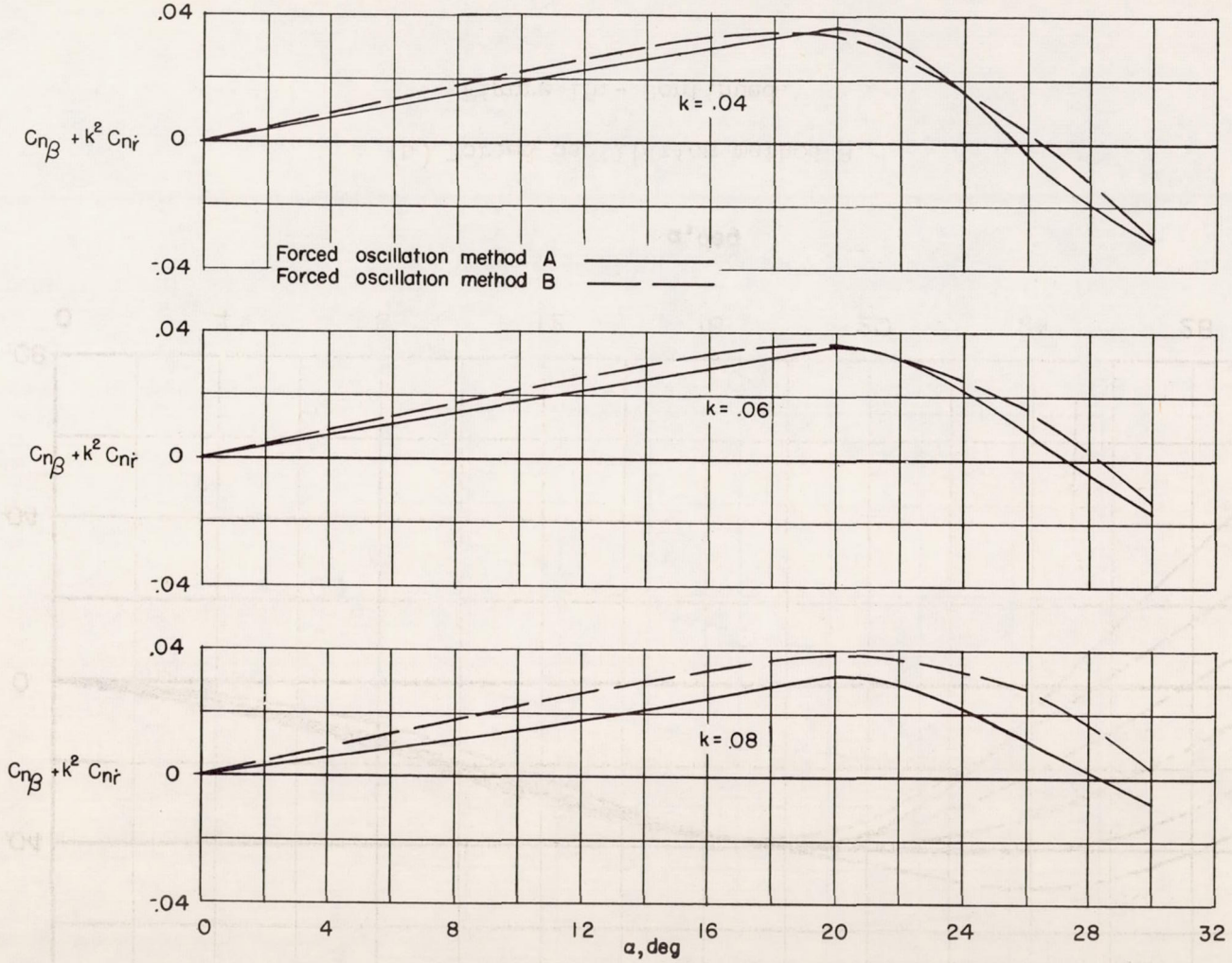

(c) Comparison of data obtained with two methods.

Figure 15.- Concluded.

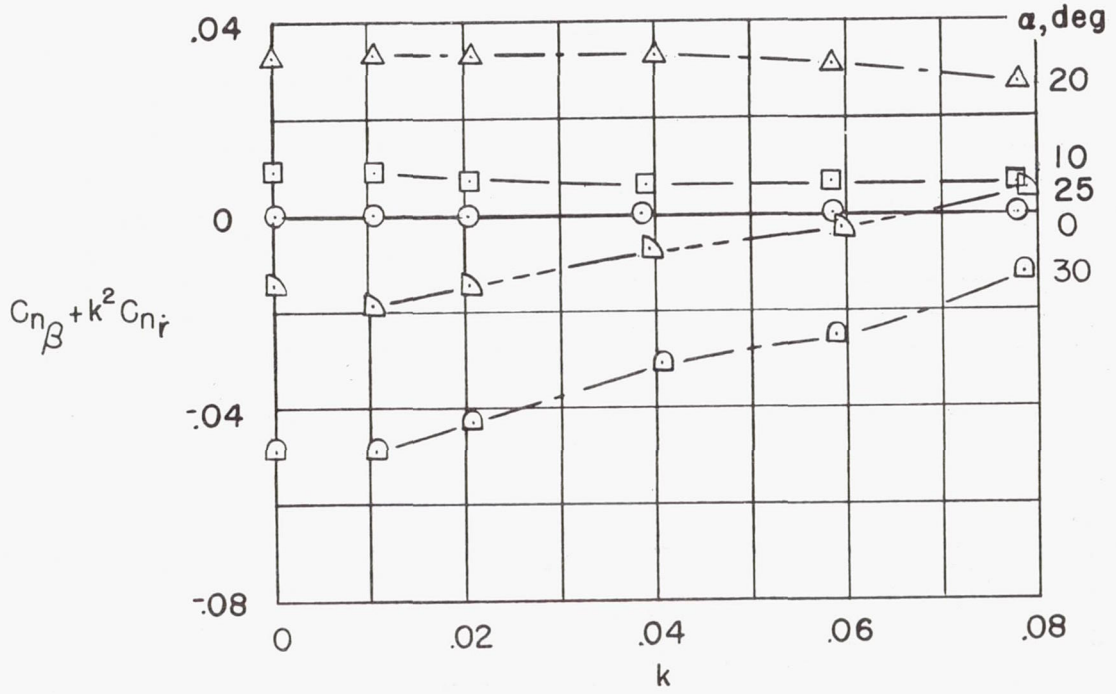

(a) Variation with frequency.

Figure 16.- Variation of $C_{n_\beta} + k^2 C_{n_{\dot{r}}}$ with frequency and angle of attack for the swept wing as determined by forced oscillation method A.

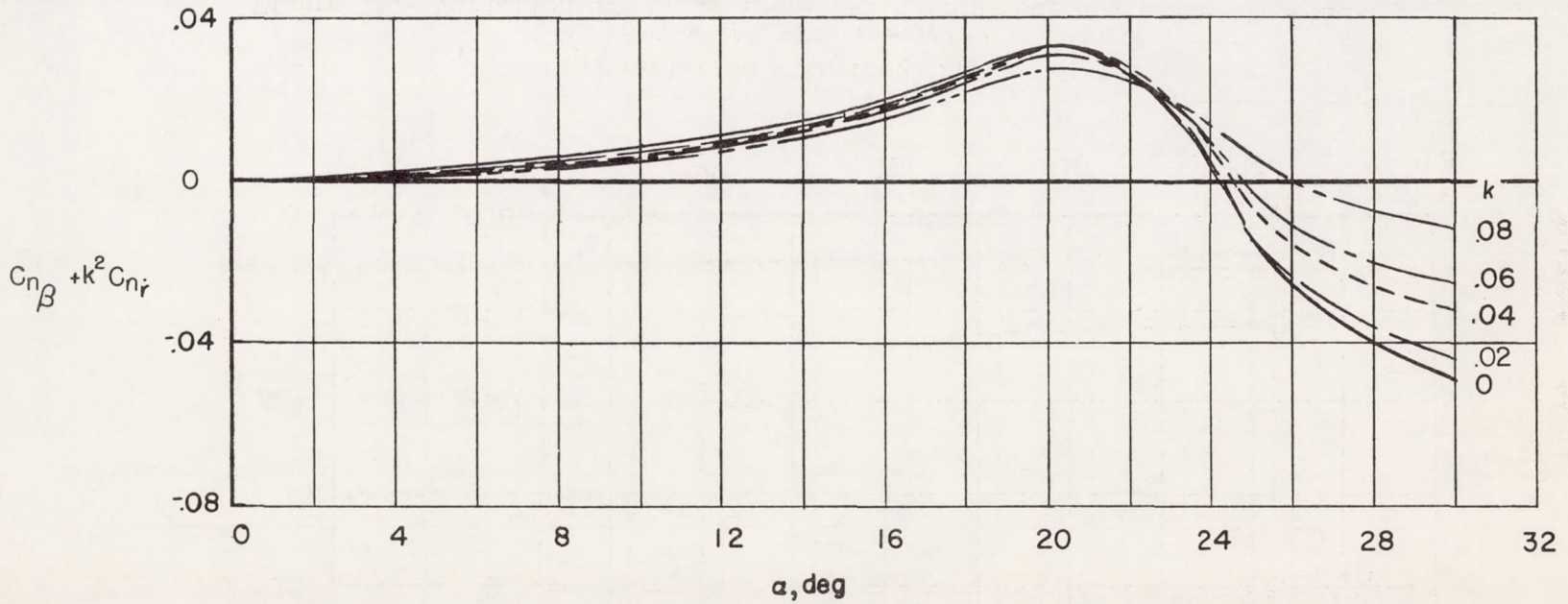

(b) Variation with angle of attack.

Figure 16.- Concluded.

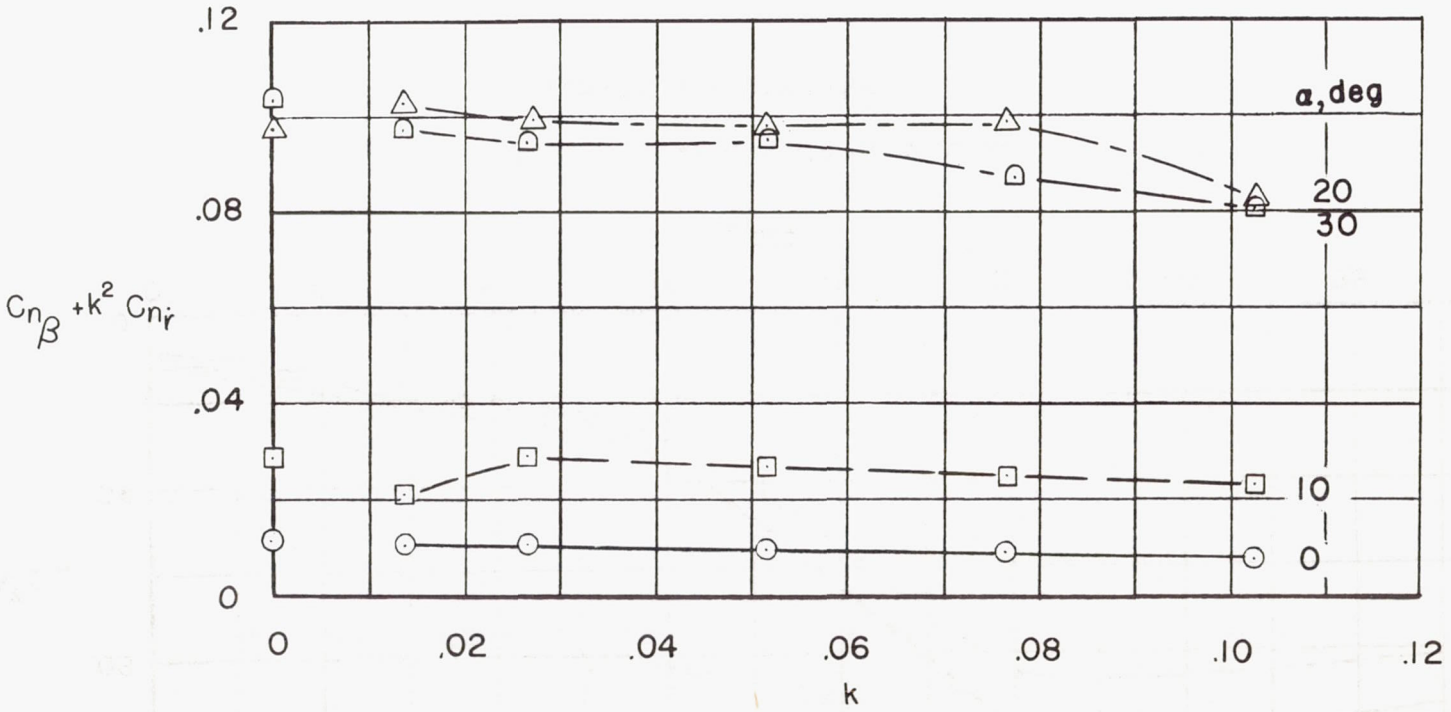

(a) Variation with frequency.

Figure 17.- Variation of $C_{n_\beta} + k^2 C_{n_{\dot{r}}}$ with frequency and angle of attack for the unswept wing as determined by forced oscillation method A.

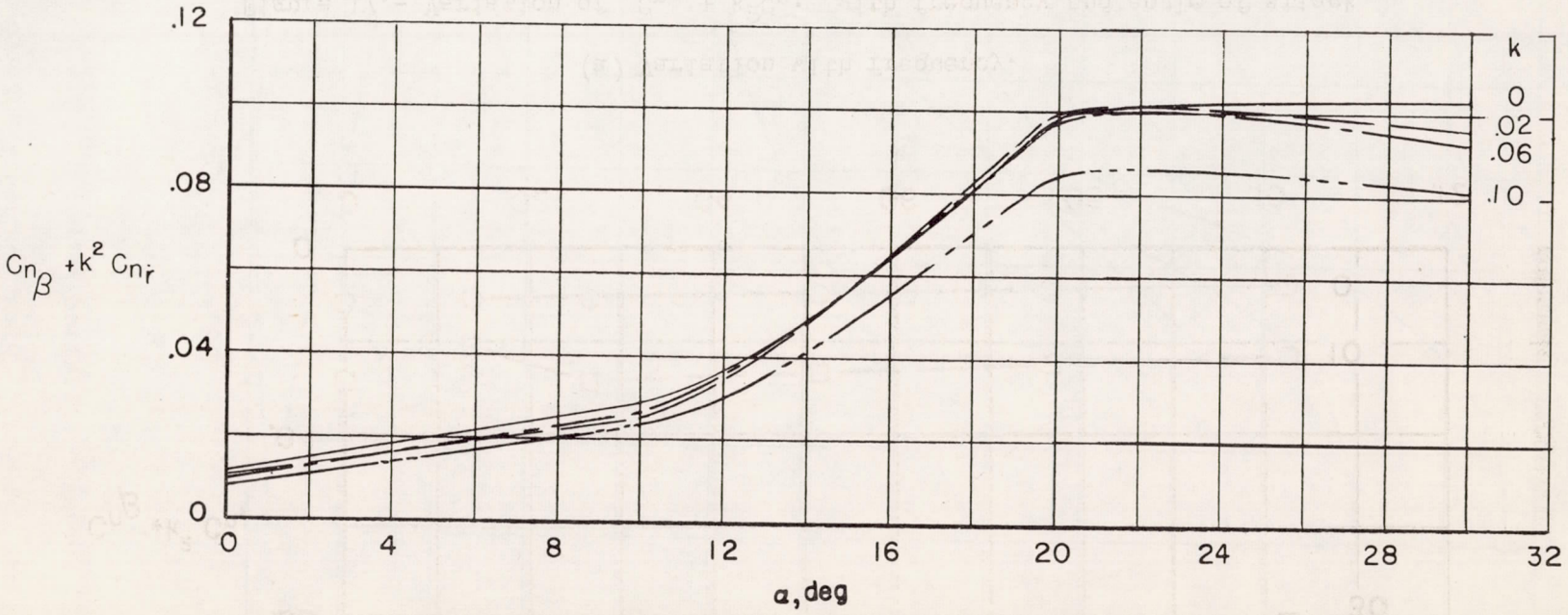

(b) Variation with angle of attack.

Figure 17.- Concluded.

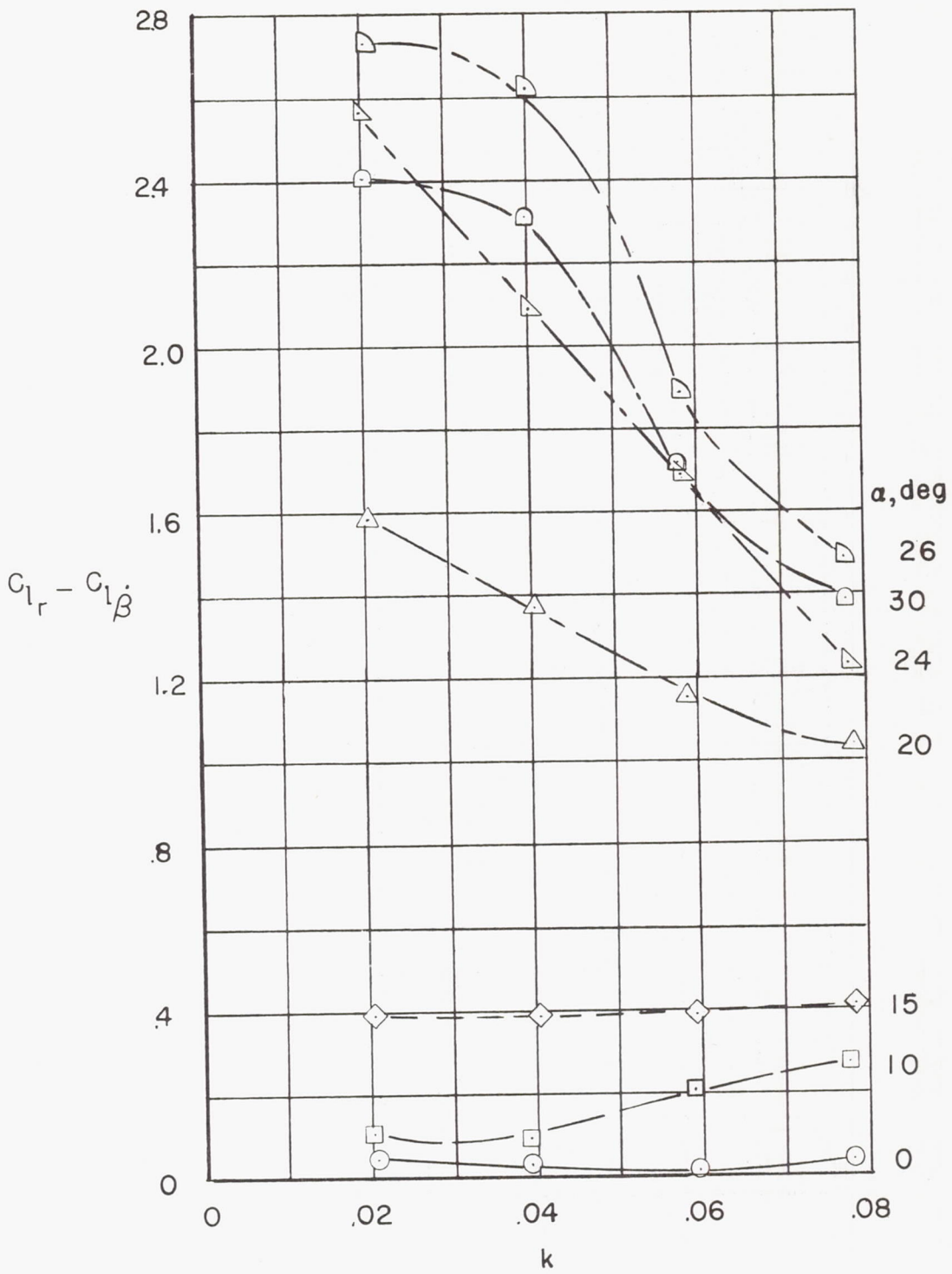

(a) Forced oscillation method A.

Figure 18.- Variation of $C_{l_r} - C_{l_{\dot{\beta}}}$ with frequency for the delta wing.

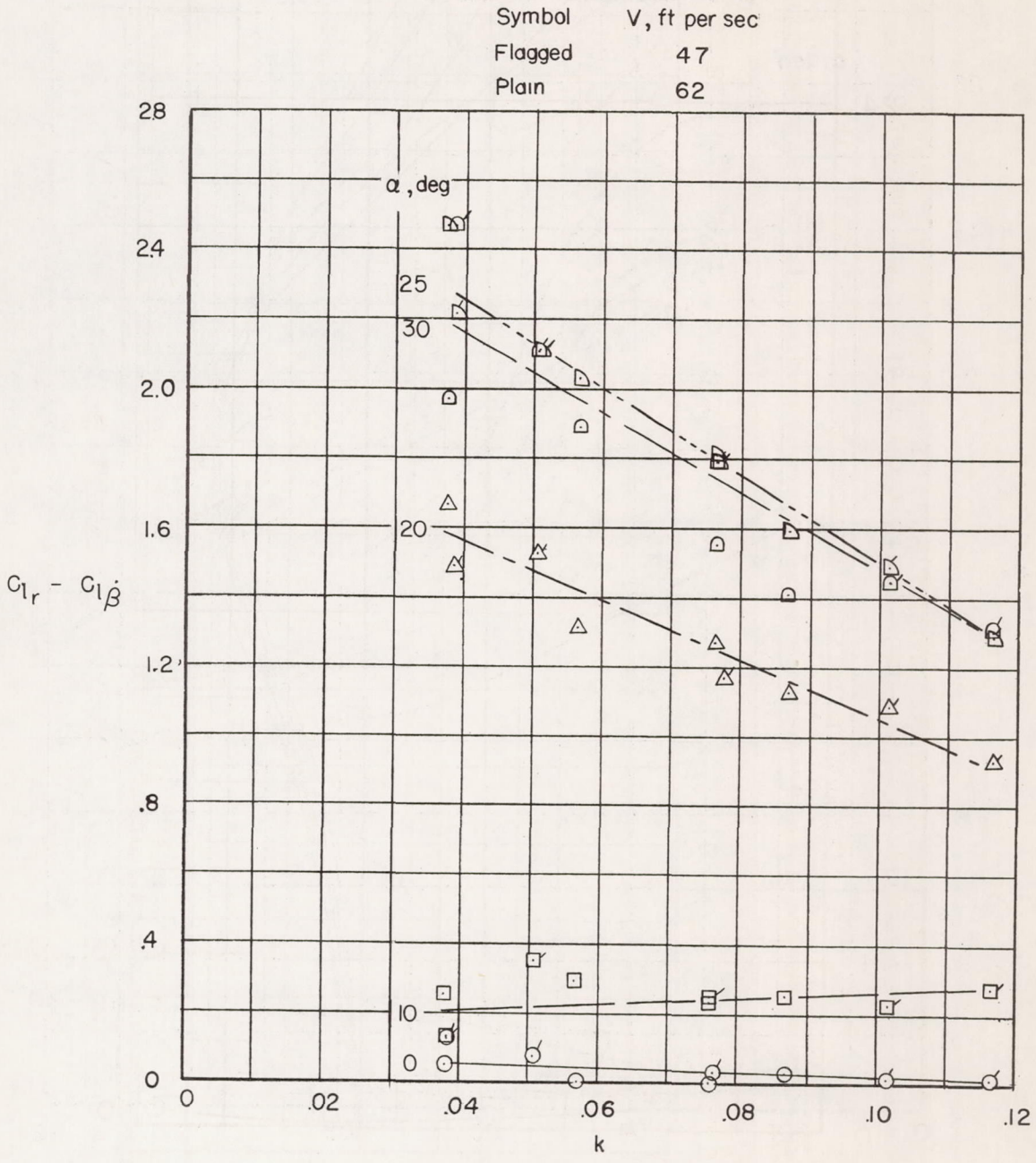

(b) Forced oscillation method B.

Figure 18.- Continued.

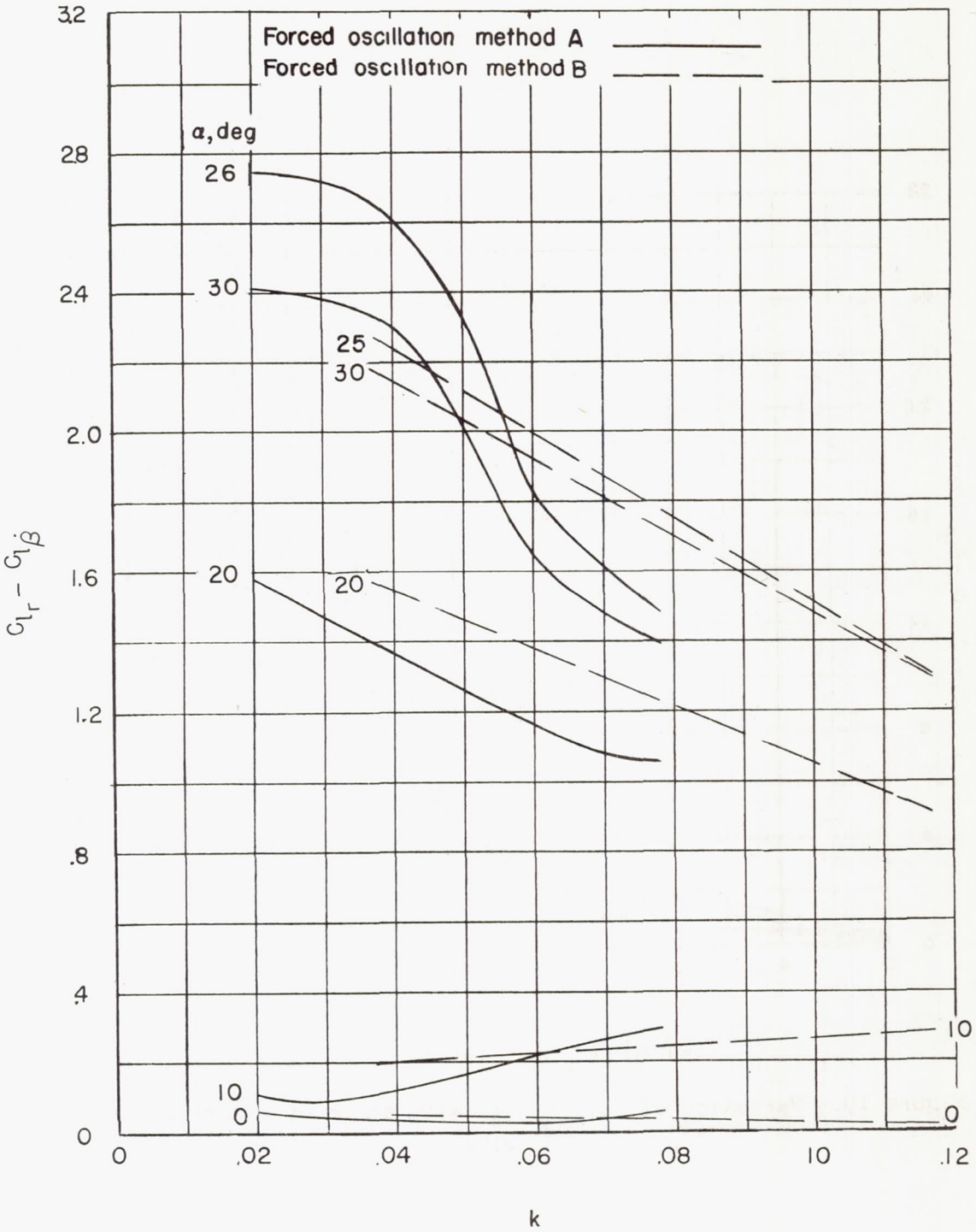

(c) Comparison of data obtained with two methods.

Figure 18.- Concluded.

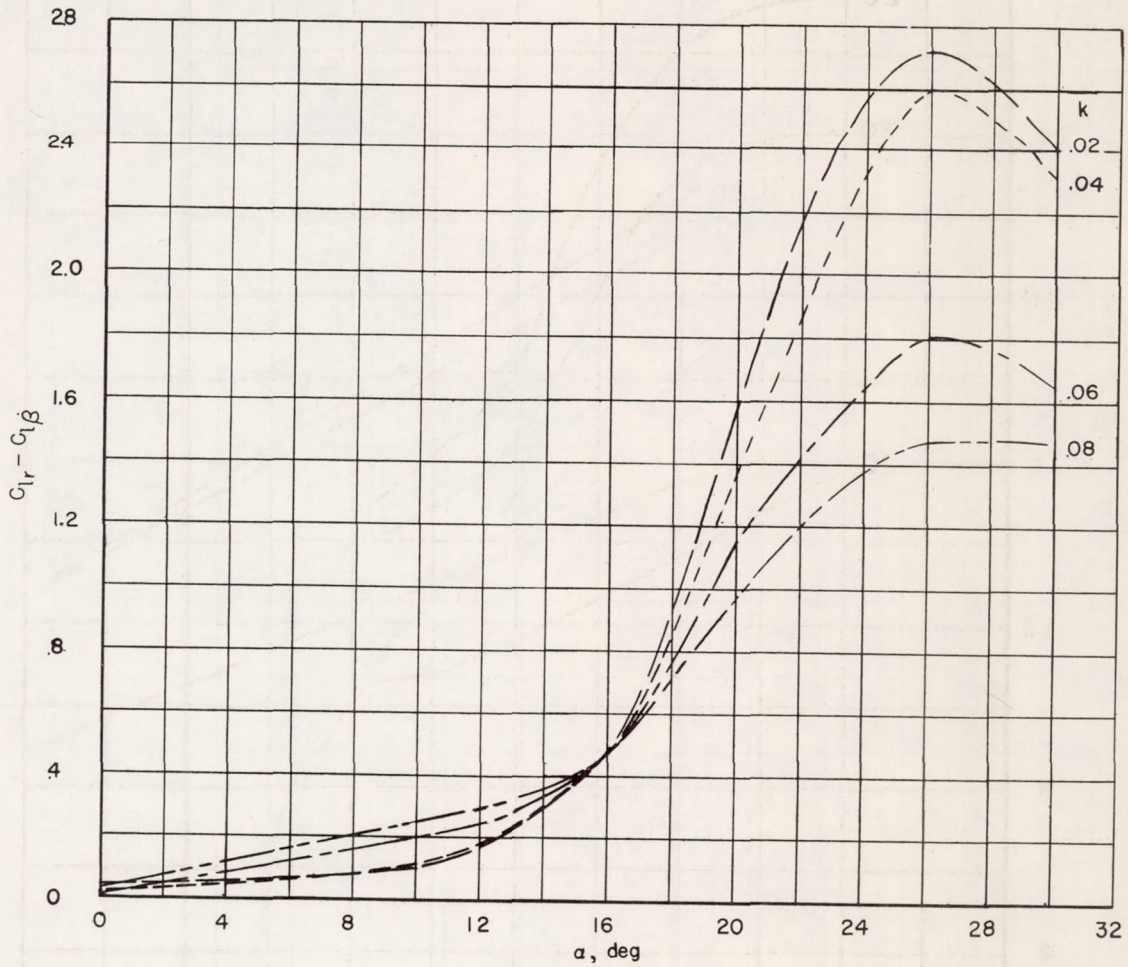

(a) Forced oscillation method A.

Figure 19.- Variation of $C_{l_r} - C_{l_{\dot{\beta}}}$ with angle of attack for the delta wing.

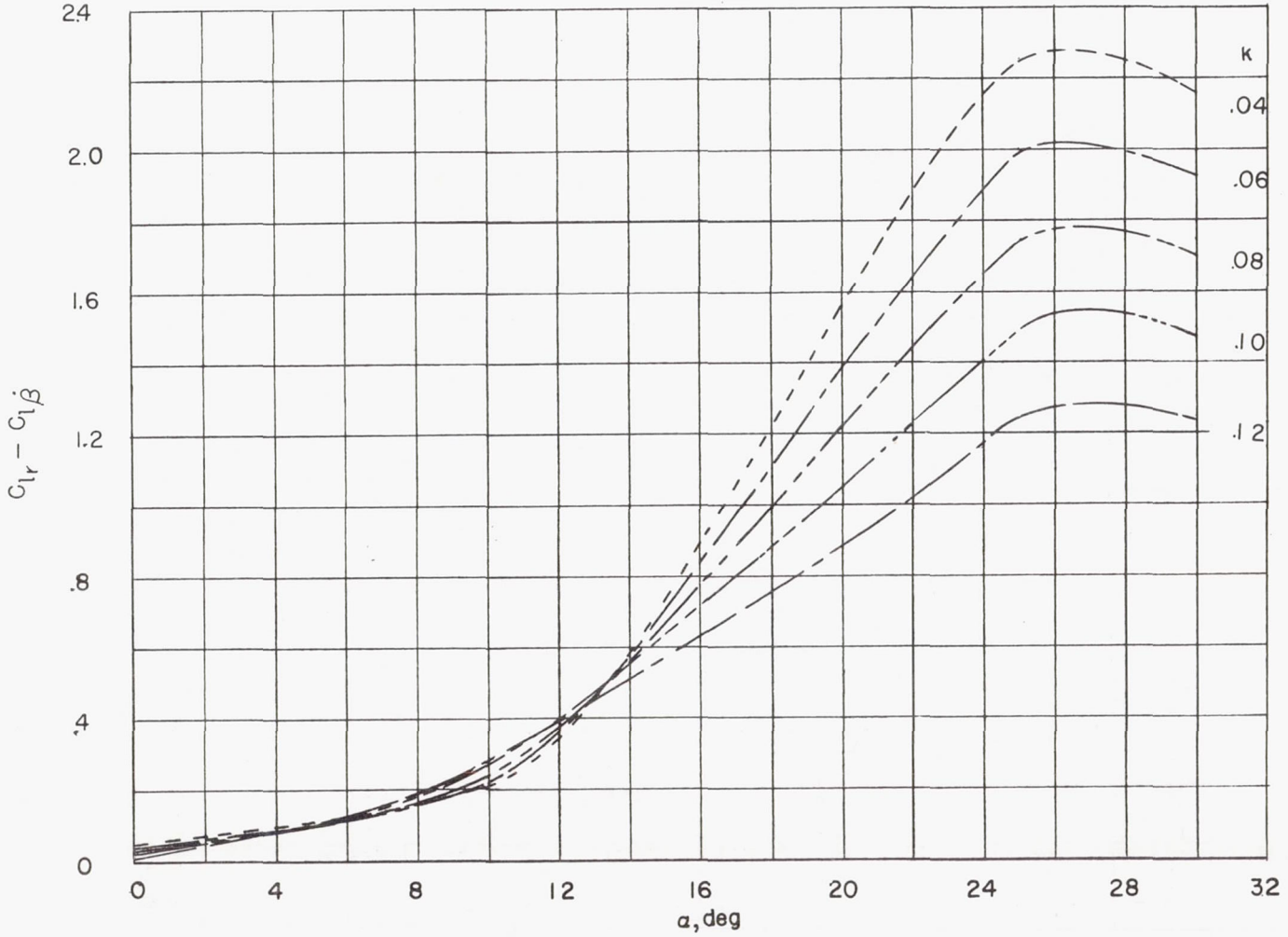

(b) Forced oscillation method B.

Figure 19.- Continued.

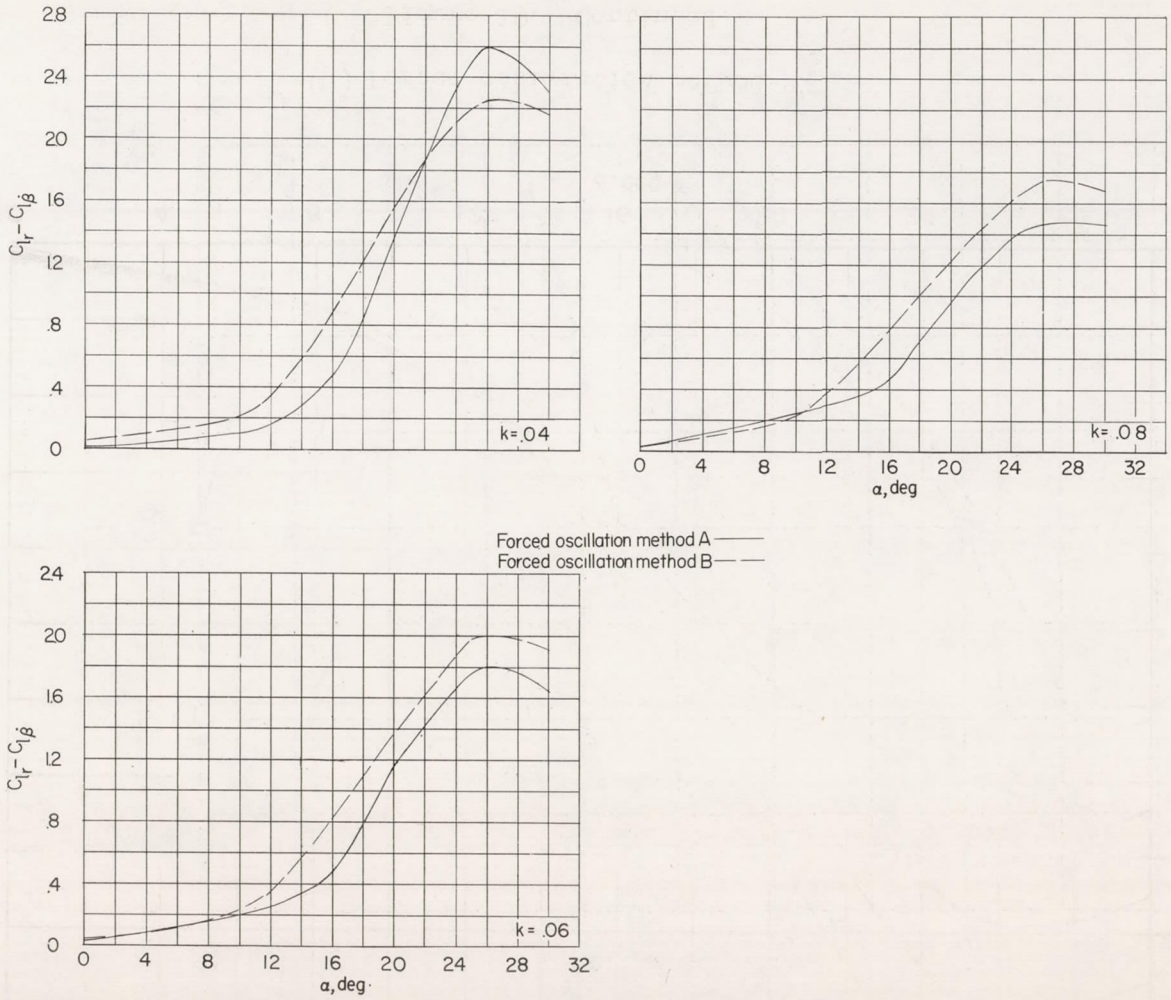

(c) Comparison of data obtained with two methods.

Figure 19.- Concluded.

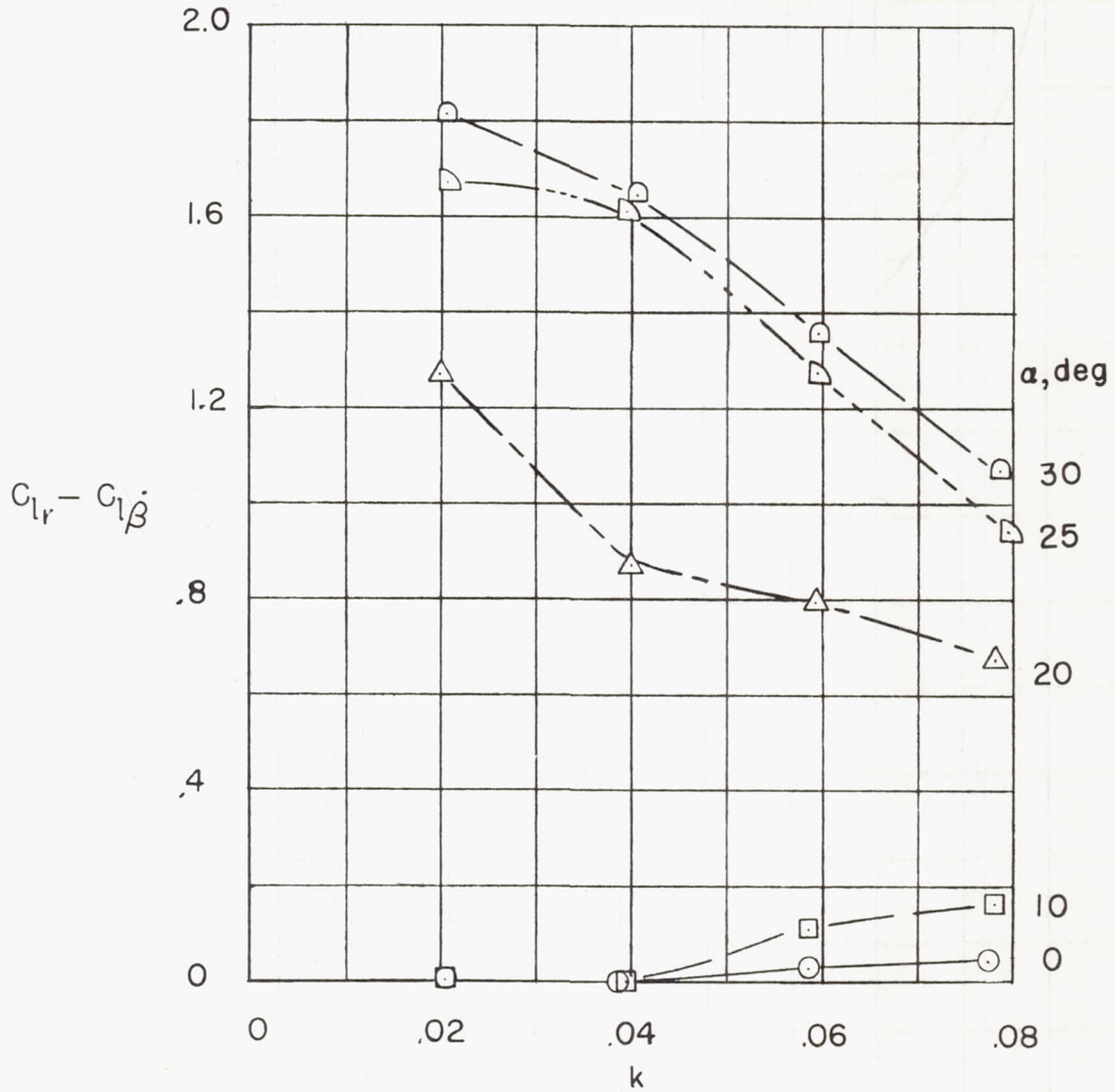

(a) Variation with frequency.

Figure 20.- Variation of $C_{l_r} - C_{l_{\dot{\beta}}}$ with frequency and angle of attack for the swept wing as determined by forced oscillation method A.

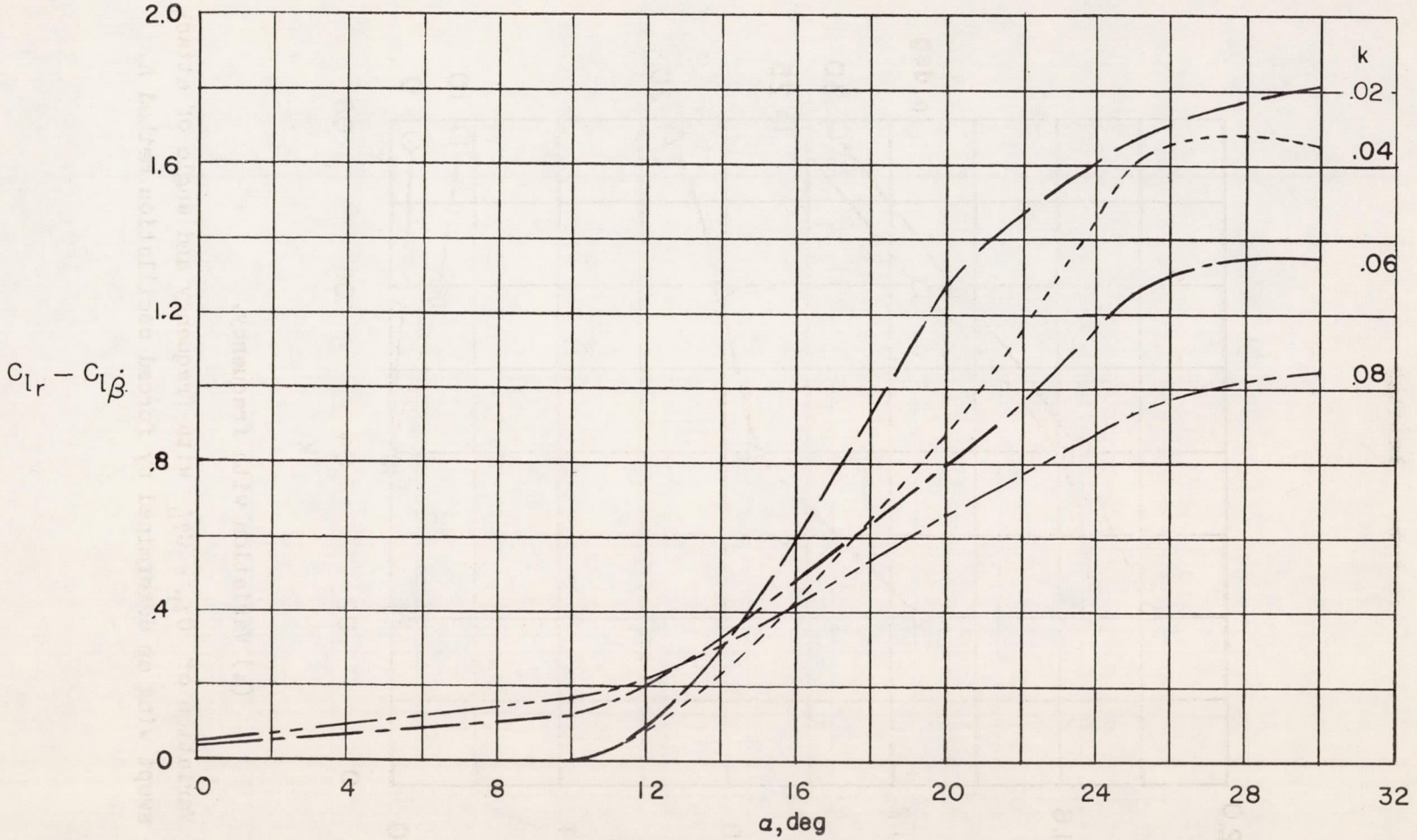

(b) Variation with angle of attack.

Figure 20.- Concluded.

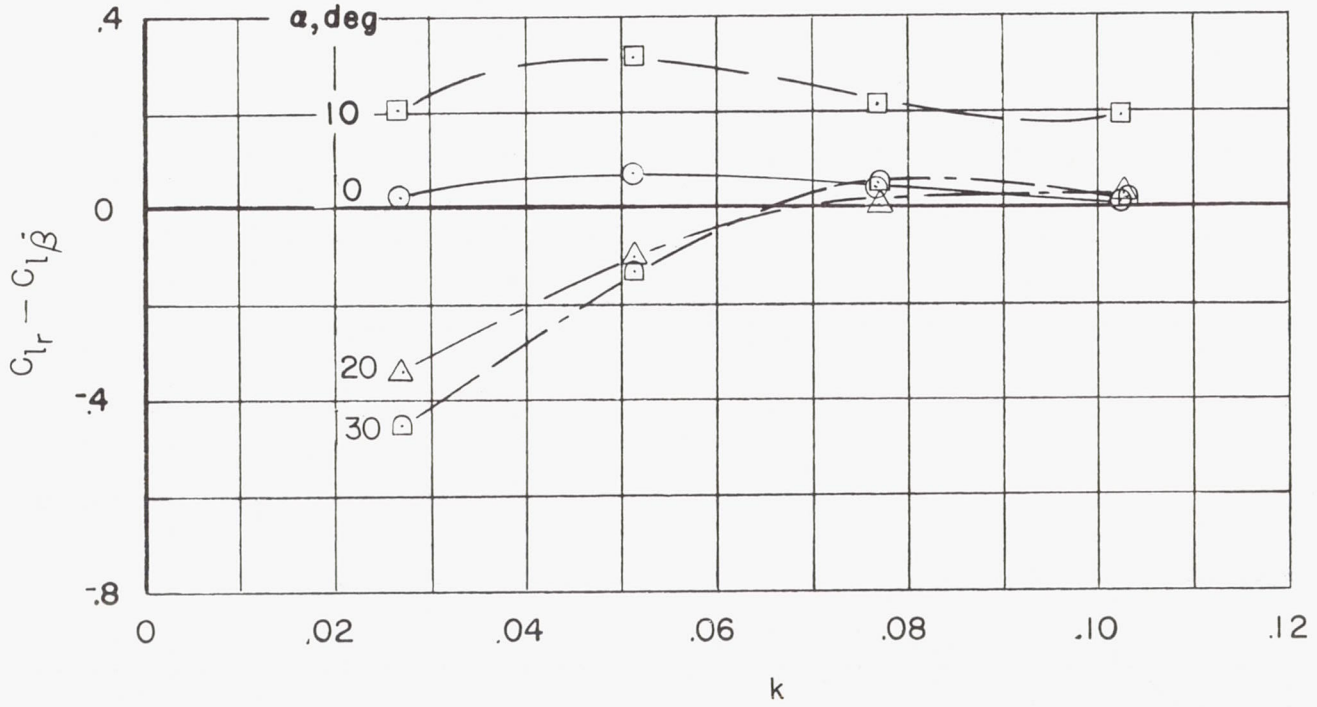

(a) Variation with frequency.

Figure 21.- Variation of $C_{l_r} - C_{l_{\dot{\beta}}}$ with frequency and angle of attack for the unswept wing as determined by forced oscillation method A.

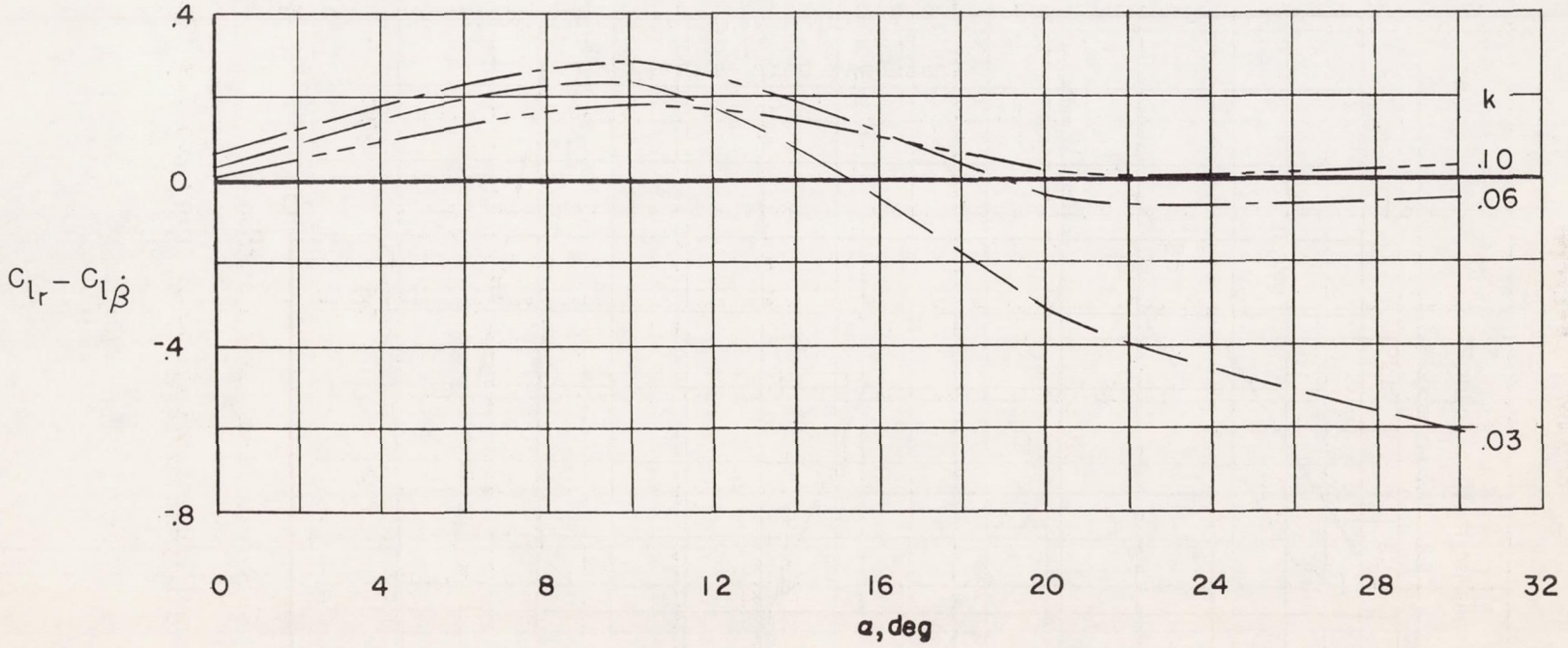

(b) Variation with angle of attack.

Figure 21.- Concluded.

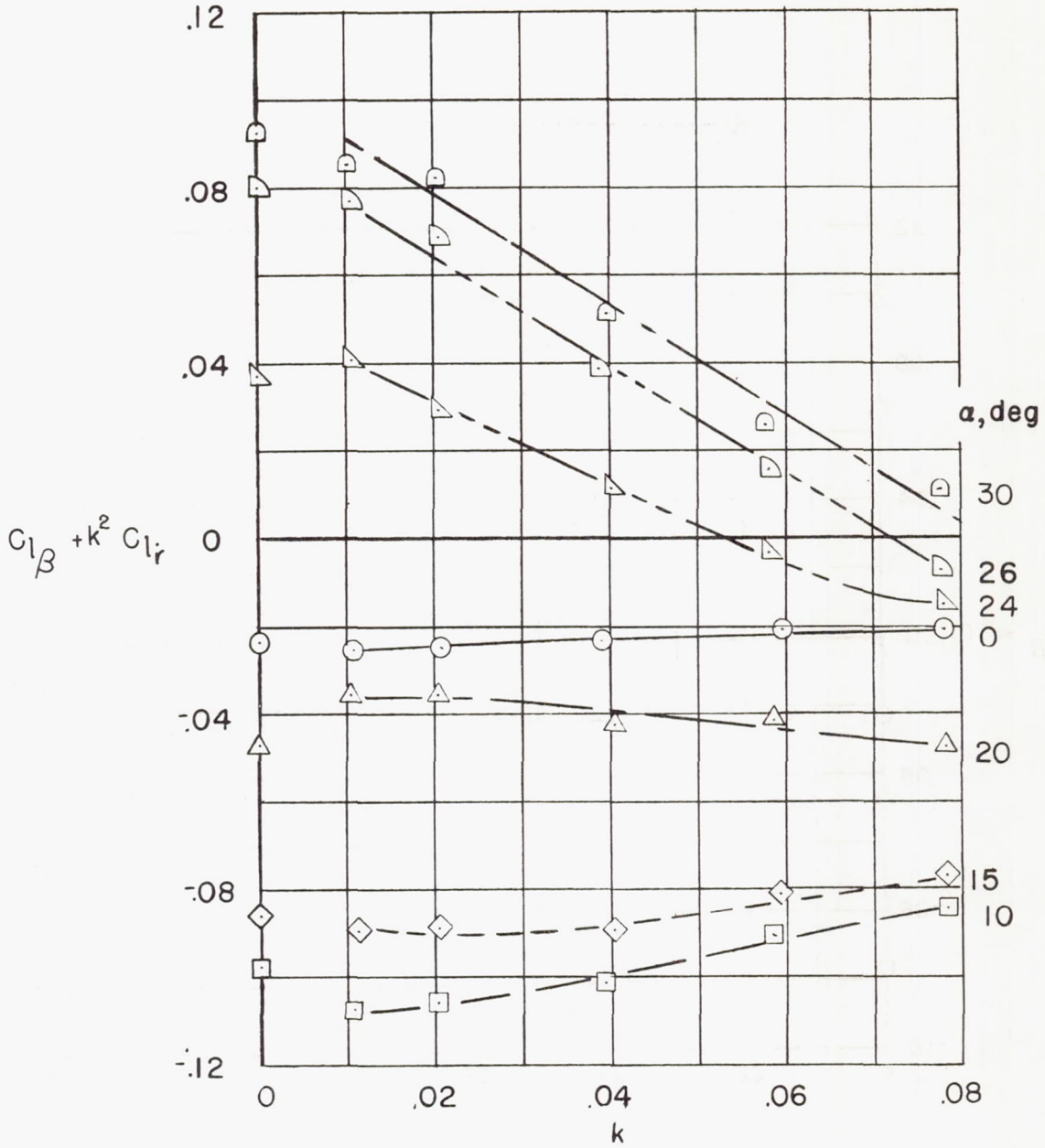

(a) Forced oscillation method A.

Figure 22.- Variation of $C_{l_\beta} + k^2 C_{l_{\dot{r}}}$ with frequency for the delta wing.

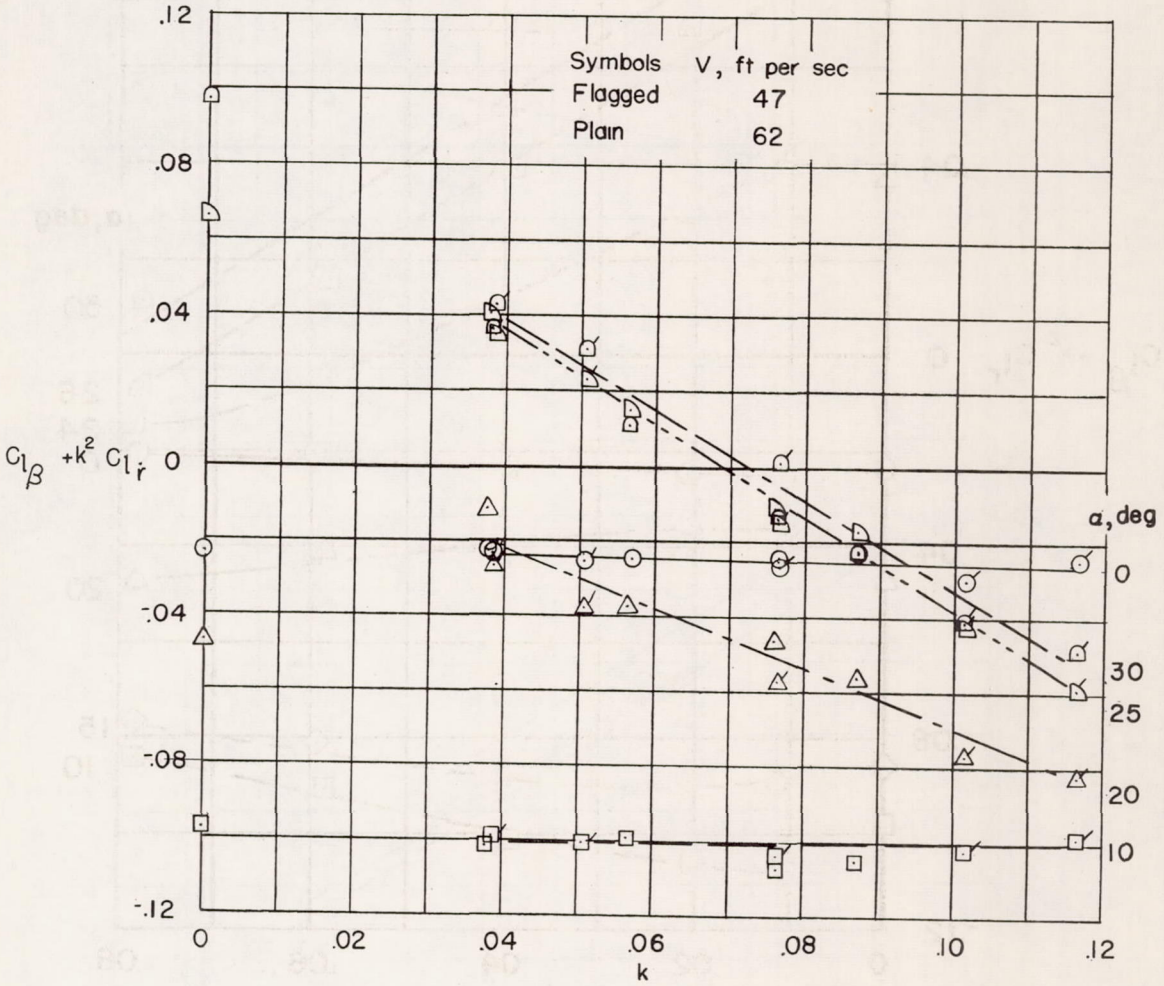

(b) Forced oscillation method B.

Figure 22.- Continued.

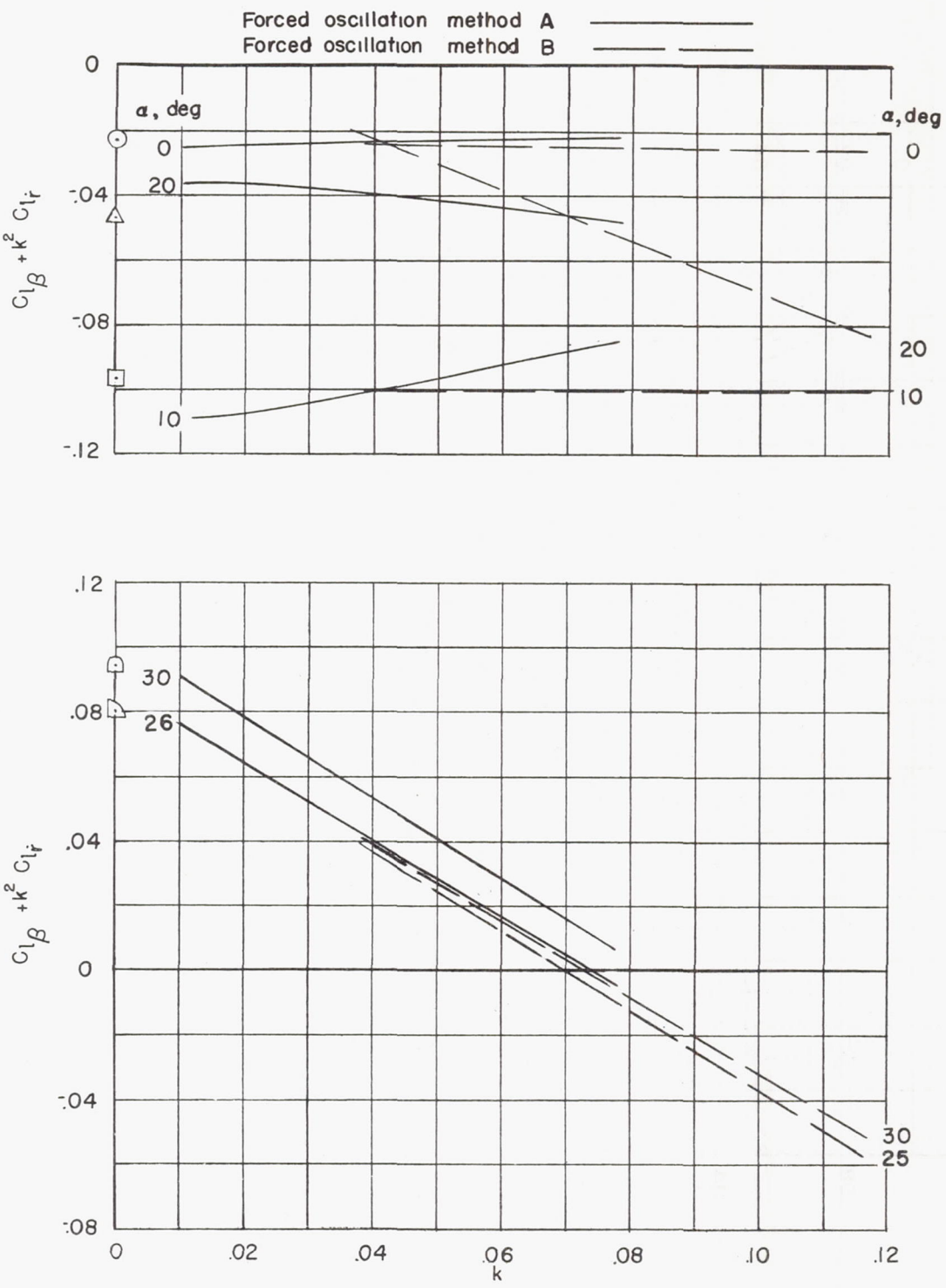

(c) Comparison of data obtained with two methods.

Figure 22.- Concluded.

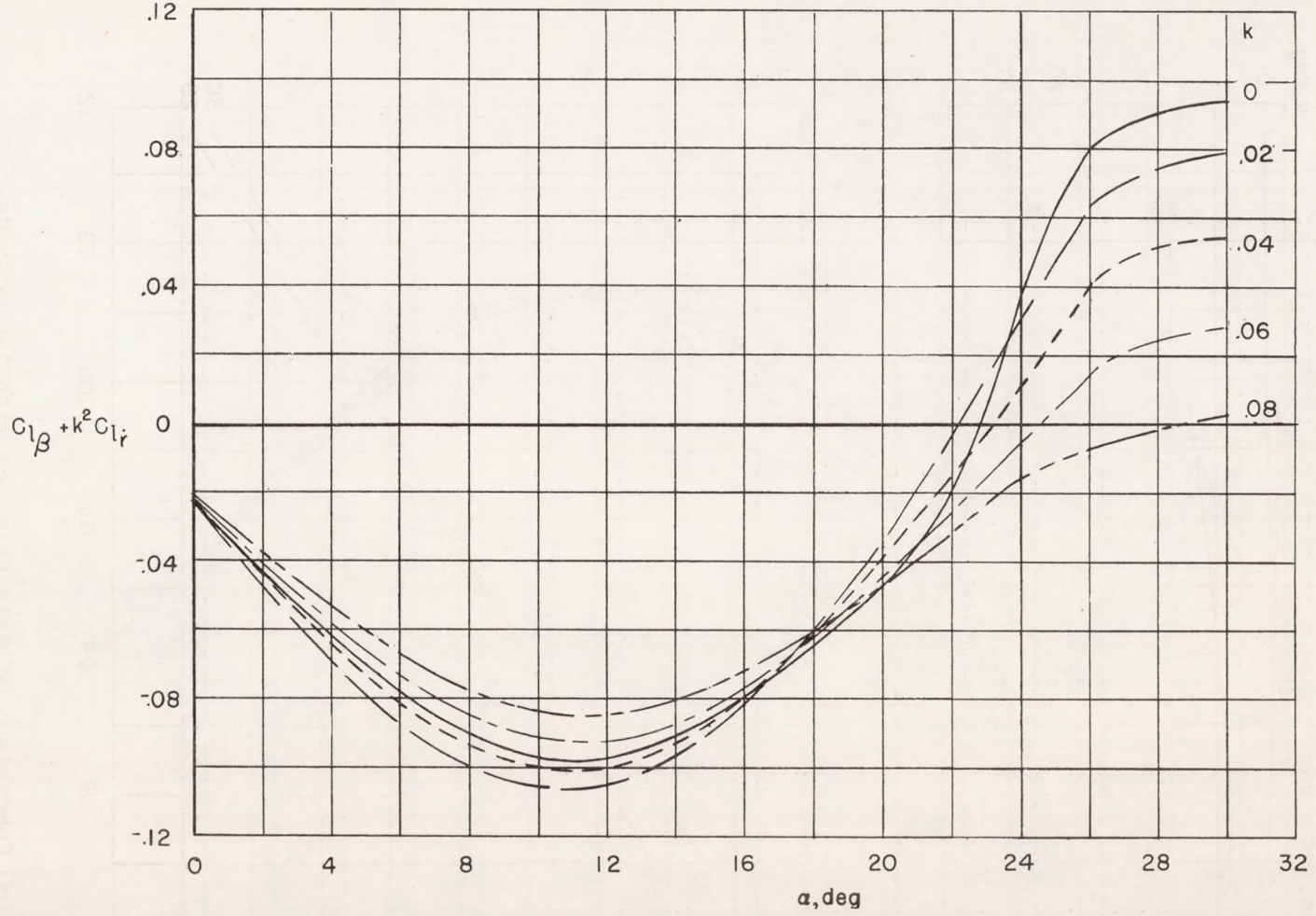

(a) Forced oscillation method A.

Figure 23.- Variation of $C_{l_\beta} + k^2 C_{l_{\dot{r}}}$ with angle of attack for the delta wing.

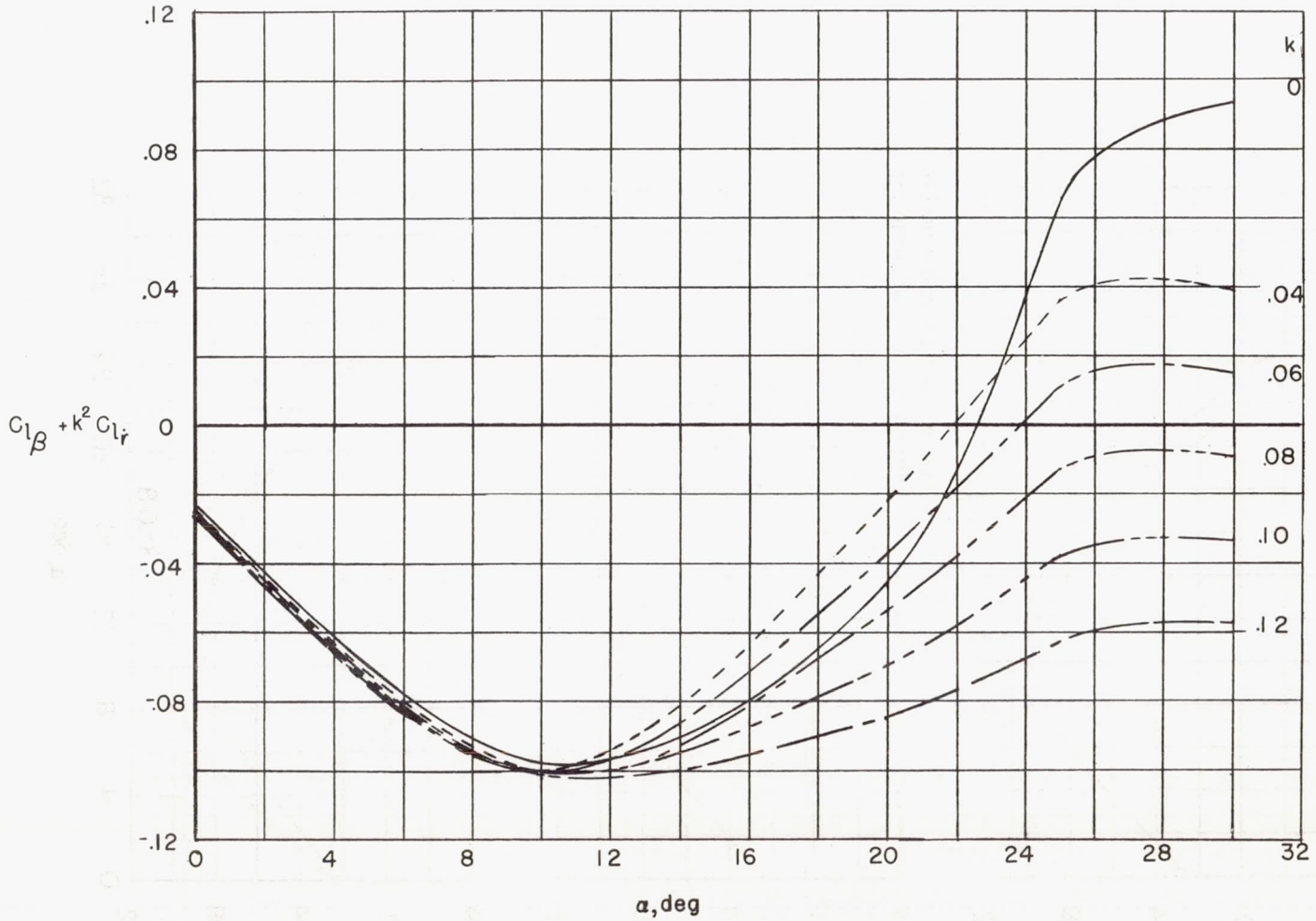

(b) Forced oscillation method B.

Figure 23.- Continued.

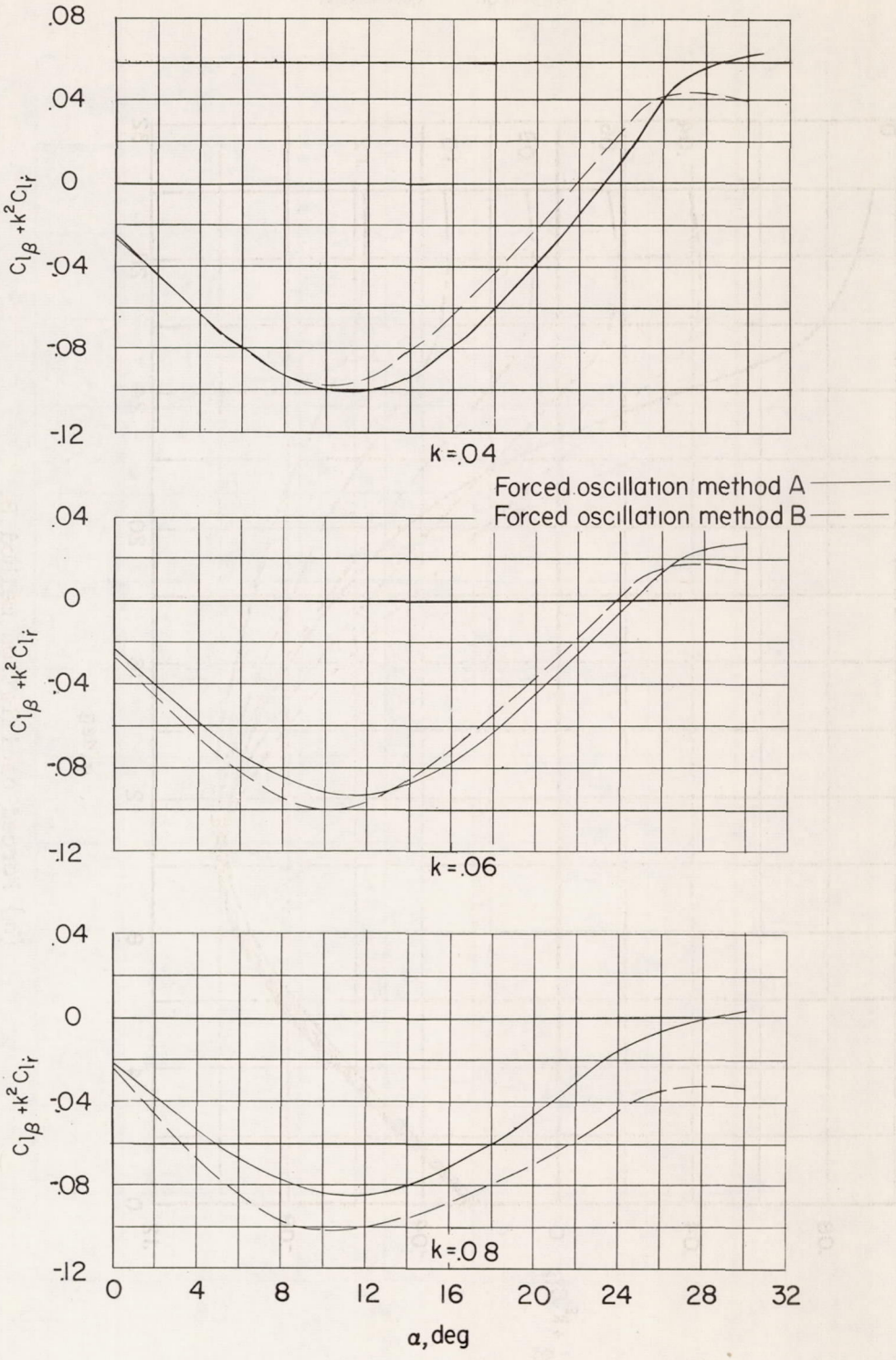

(c) Comparison of data obtained with two methods.

Figure 23.- Concluded.

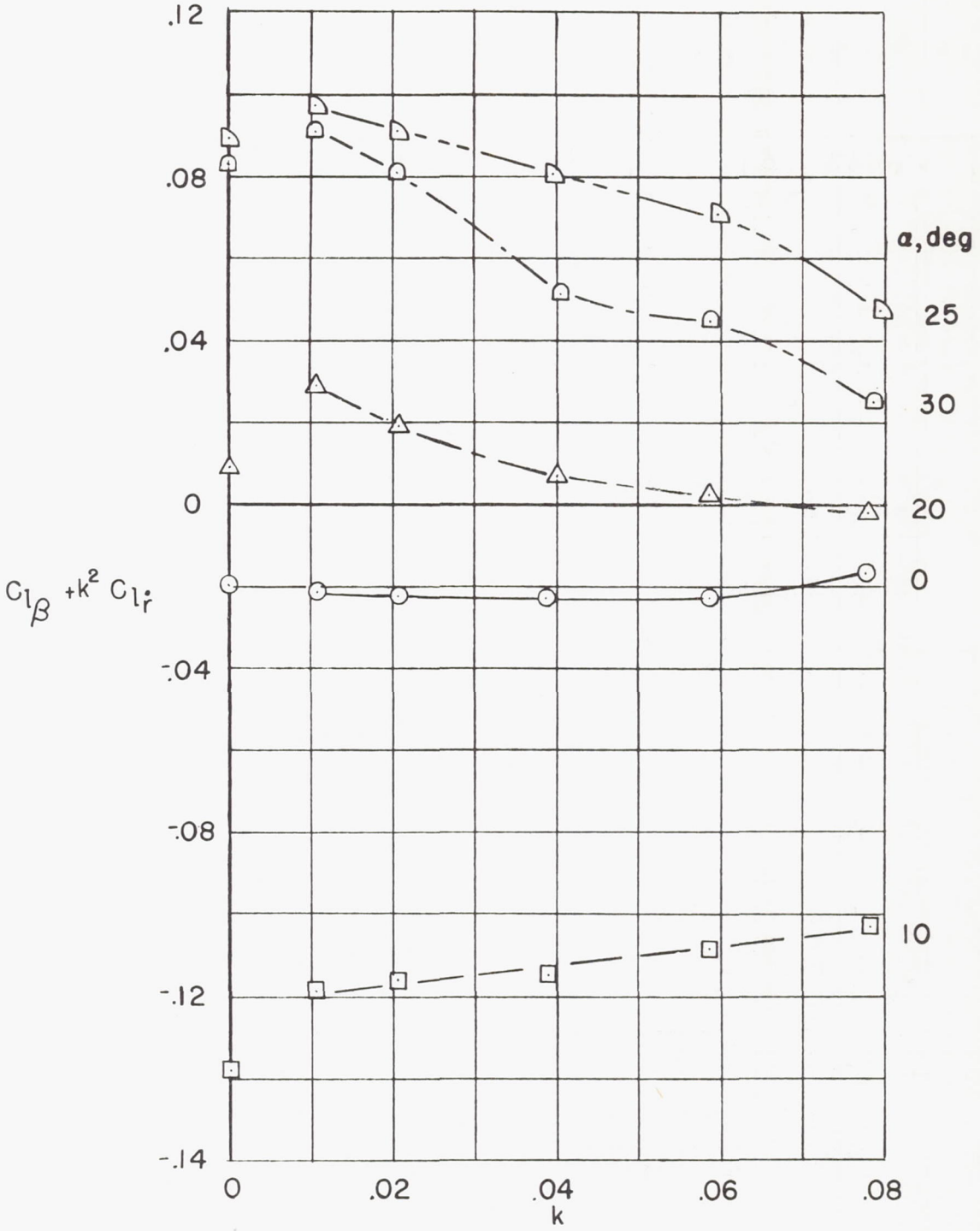

(a) Variation with frequency.

Figure 24.- Variation of $C_{l_\beta} + k^2 C_{l_{\dot{r}}}$ with frequency and angle of attack for the swept wing as determined by forced oscillation method A.

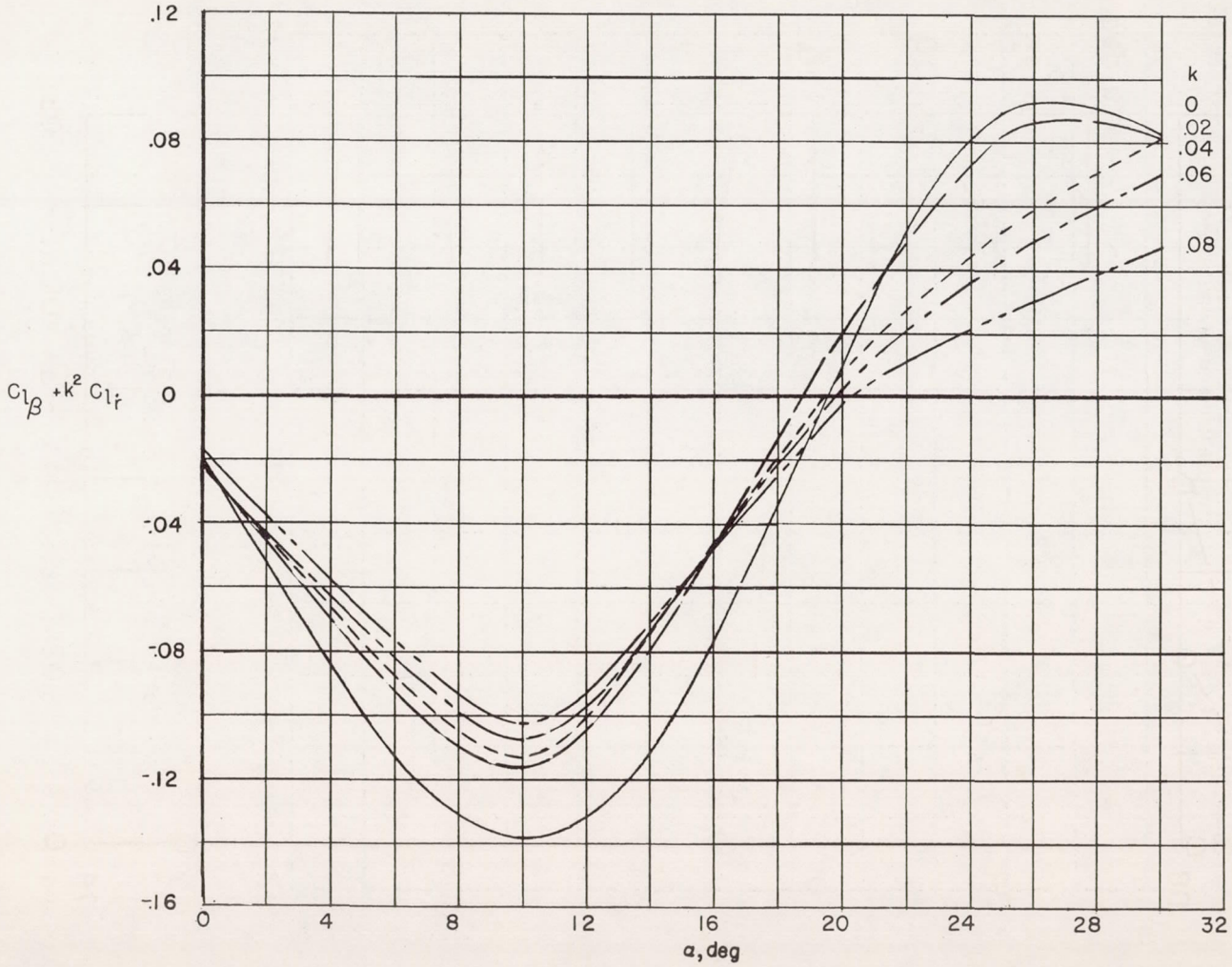

(b) Variation with angle of attack.

Figure 24.- Concluded.

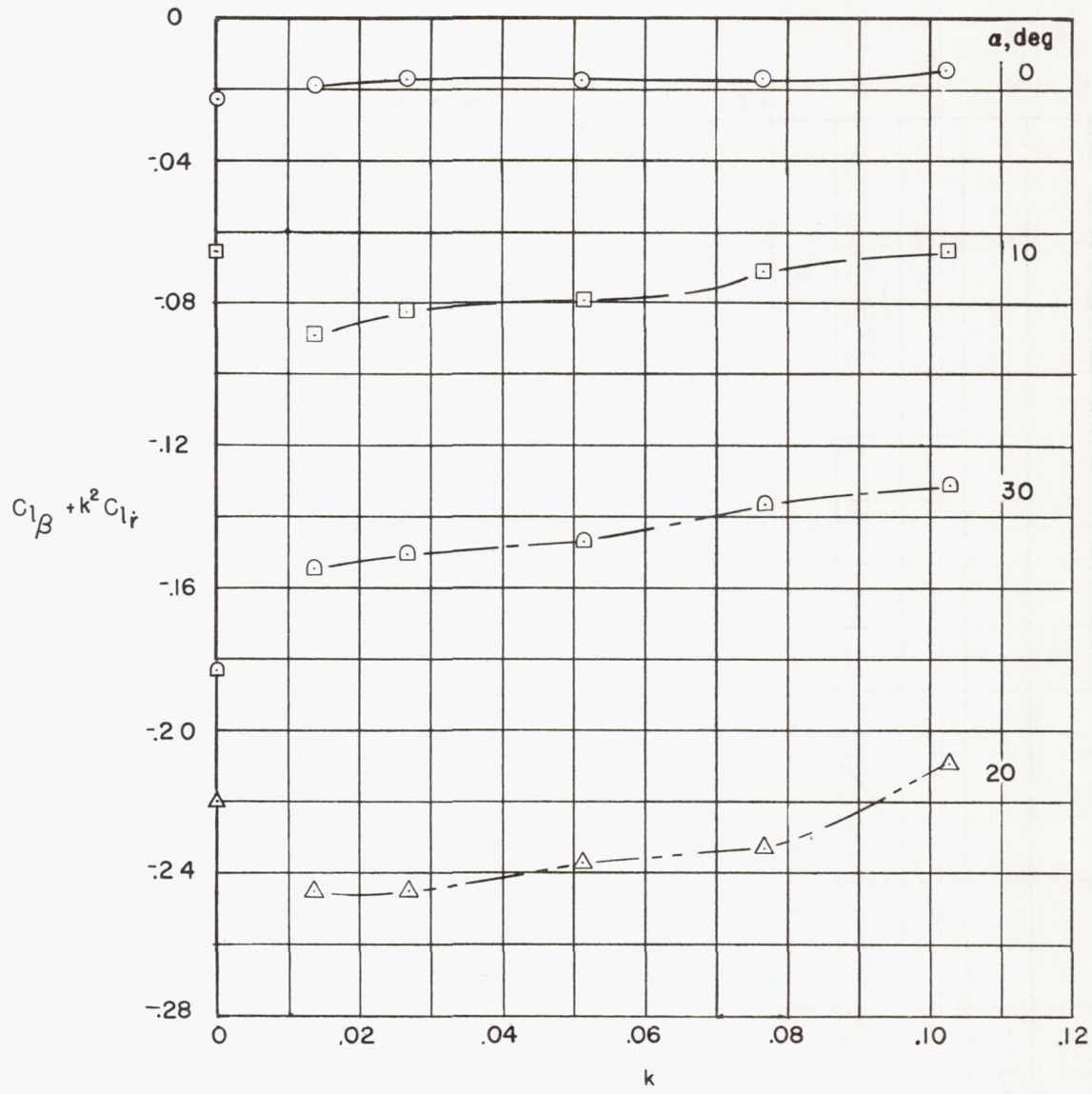

(a) Variation with frequency.

Figure 25.- Variation of $C_{l_\beta} + k^2 C_{l_{\dot{r}}}$ with frequency and angle of attack for the unswept wing as determined by forced oscillation method A.

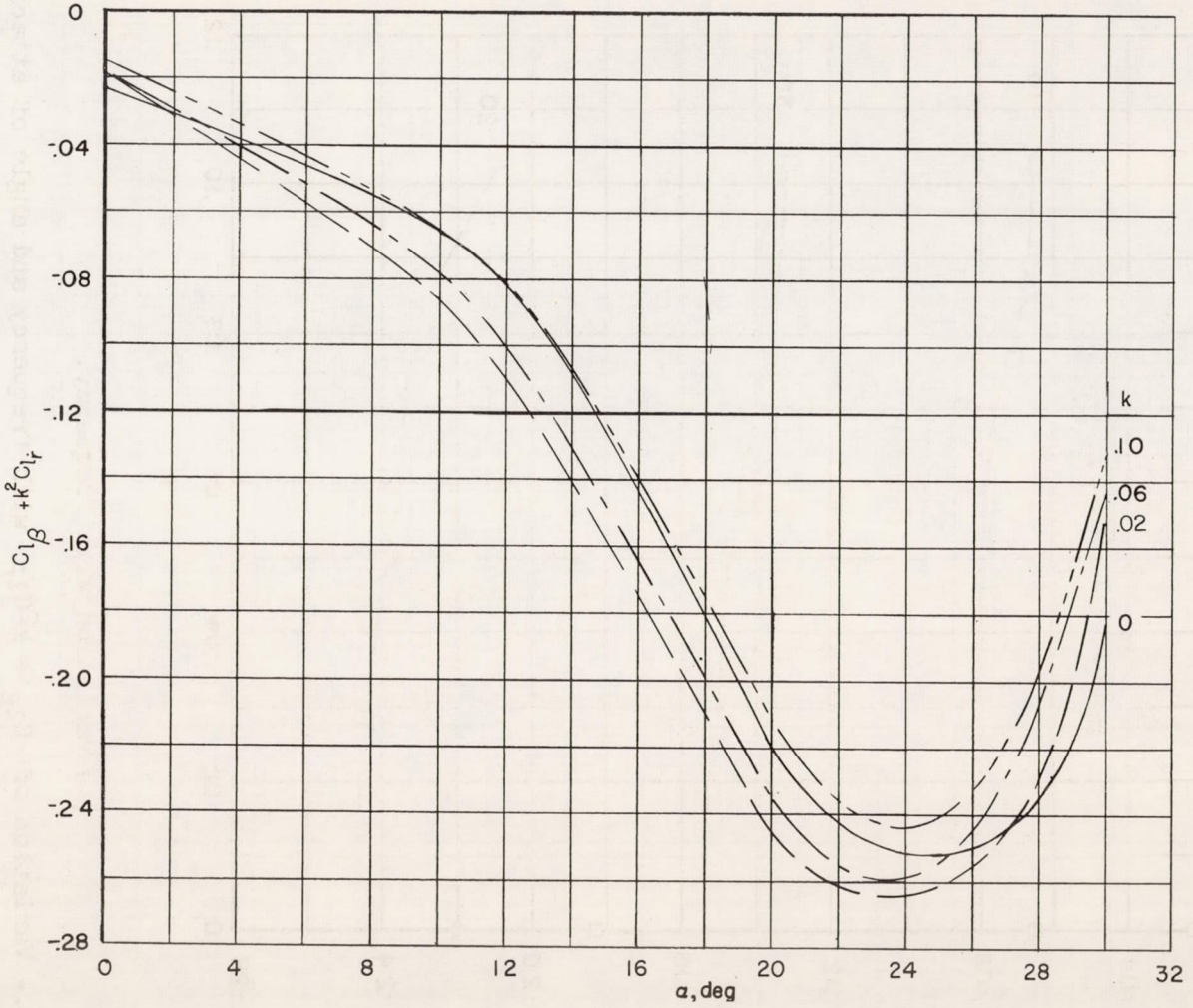

(b) Variation with angle of attack.

Figure 25.- Concluded.

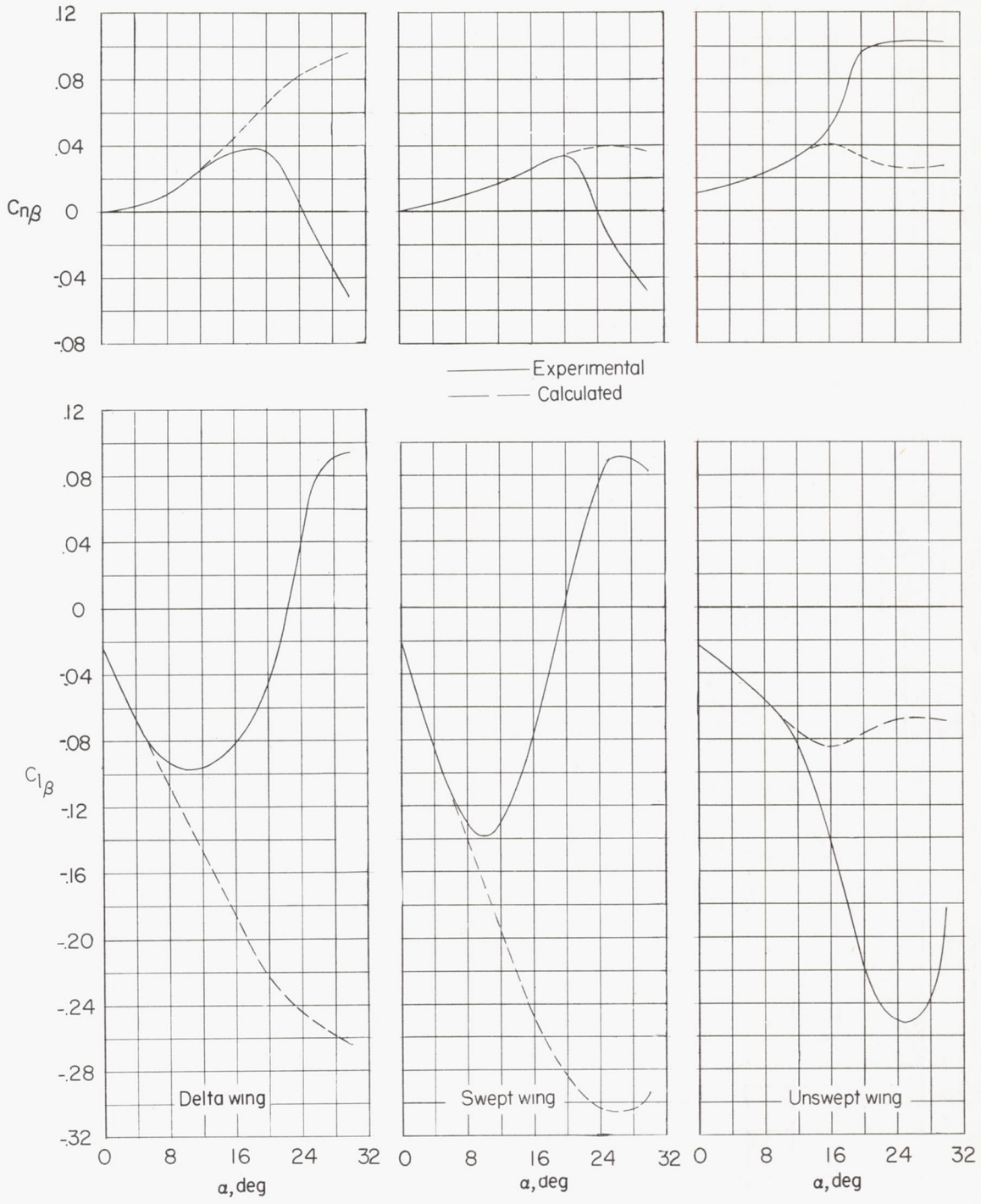

Figure 26.- Experimental and calculated values of C_{n_β} and C_{l_β} for the three wings.

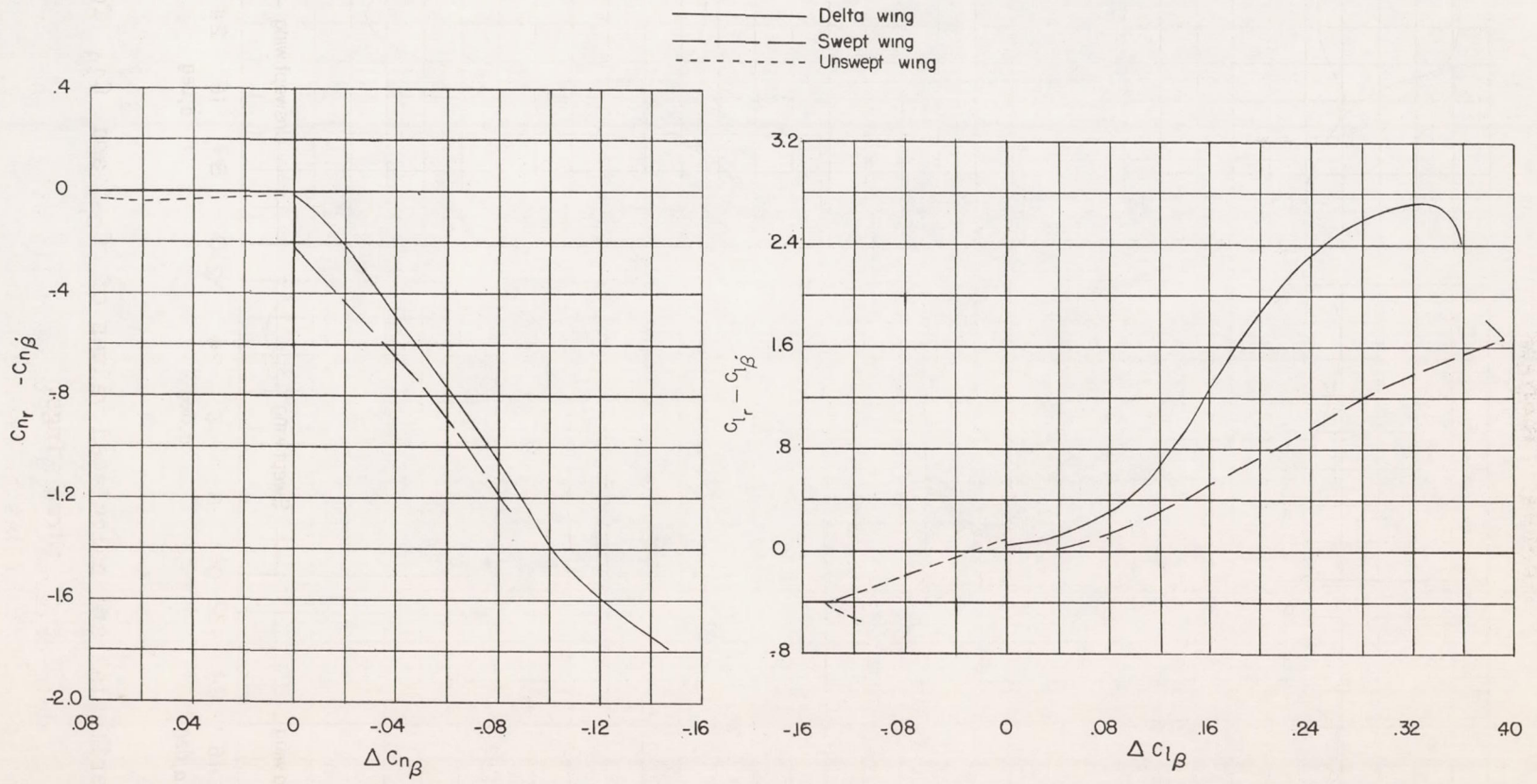

Figure 27.- Variation of $C_{n_r} - C_{n_{\dot{\beta}}}$ with ΔC_{n_β} and $C_{l_r} - C_{l_{\dot{\beta}}}$ with ΔC_{l_β} for the three wings. k = 0.02. (Values of ΔC_{n_β} and ΔC_{l_β} obtained from fig. 26.)

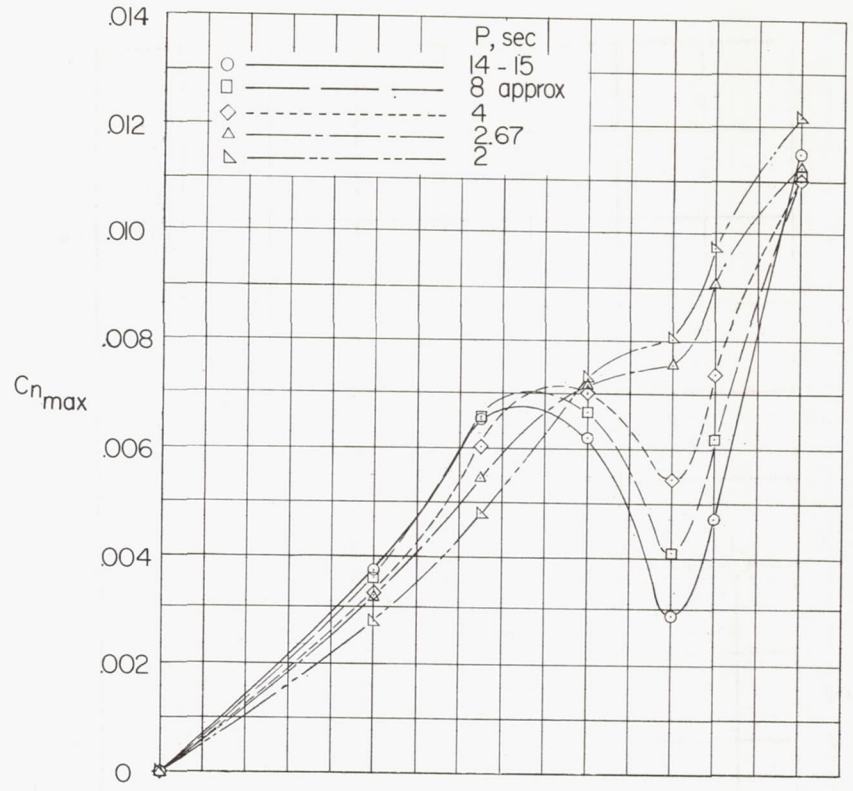

(a) Variation of $C_{n_{max}}$ with angle of attack.

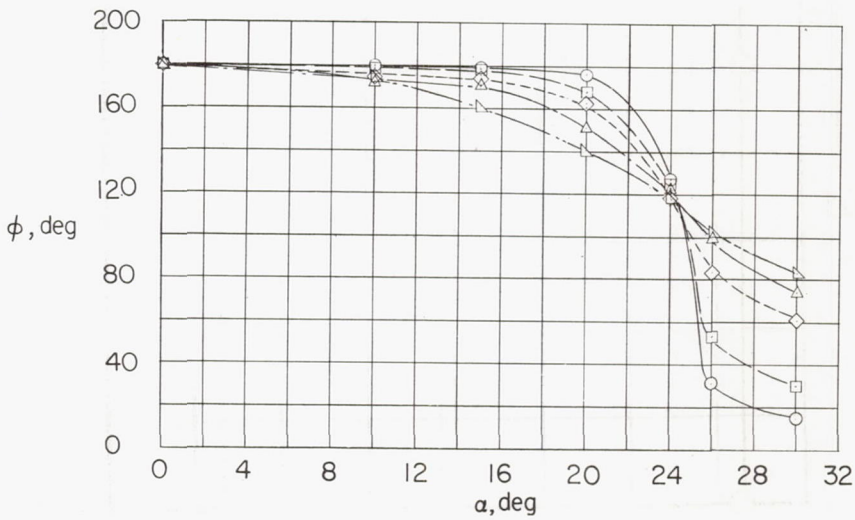

(b) Variation of phase lag with angle of attack.

Figure 28.- Basic data obtained from tests of delta wing using forced oscillation method A.

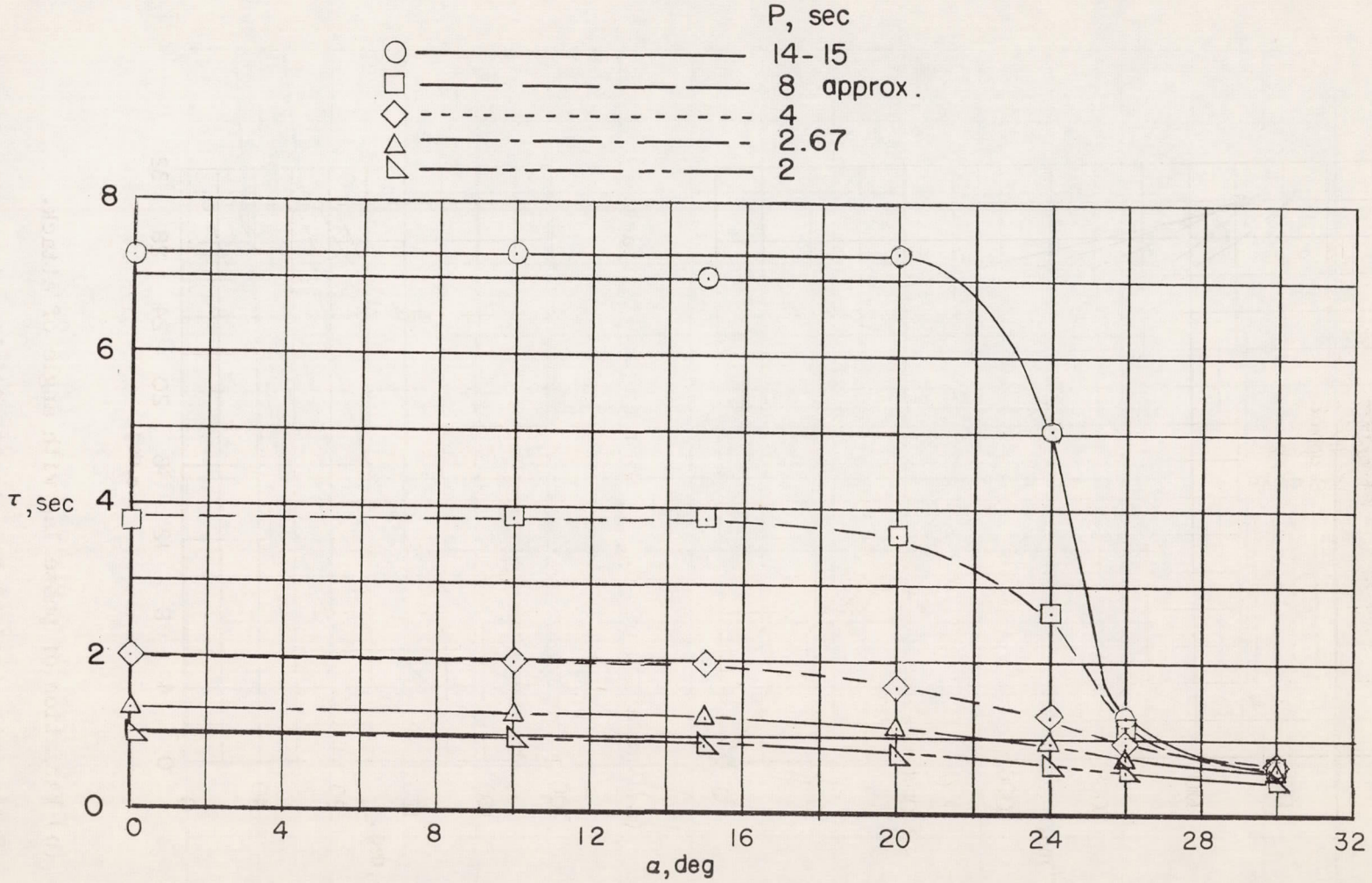

(c) Variation of time lag with angle of attack.

Figure 28.- Continued.

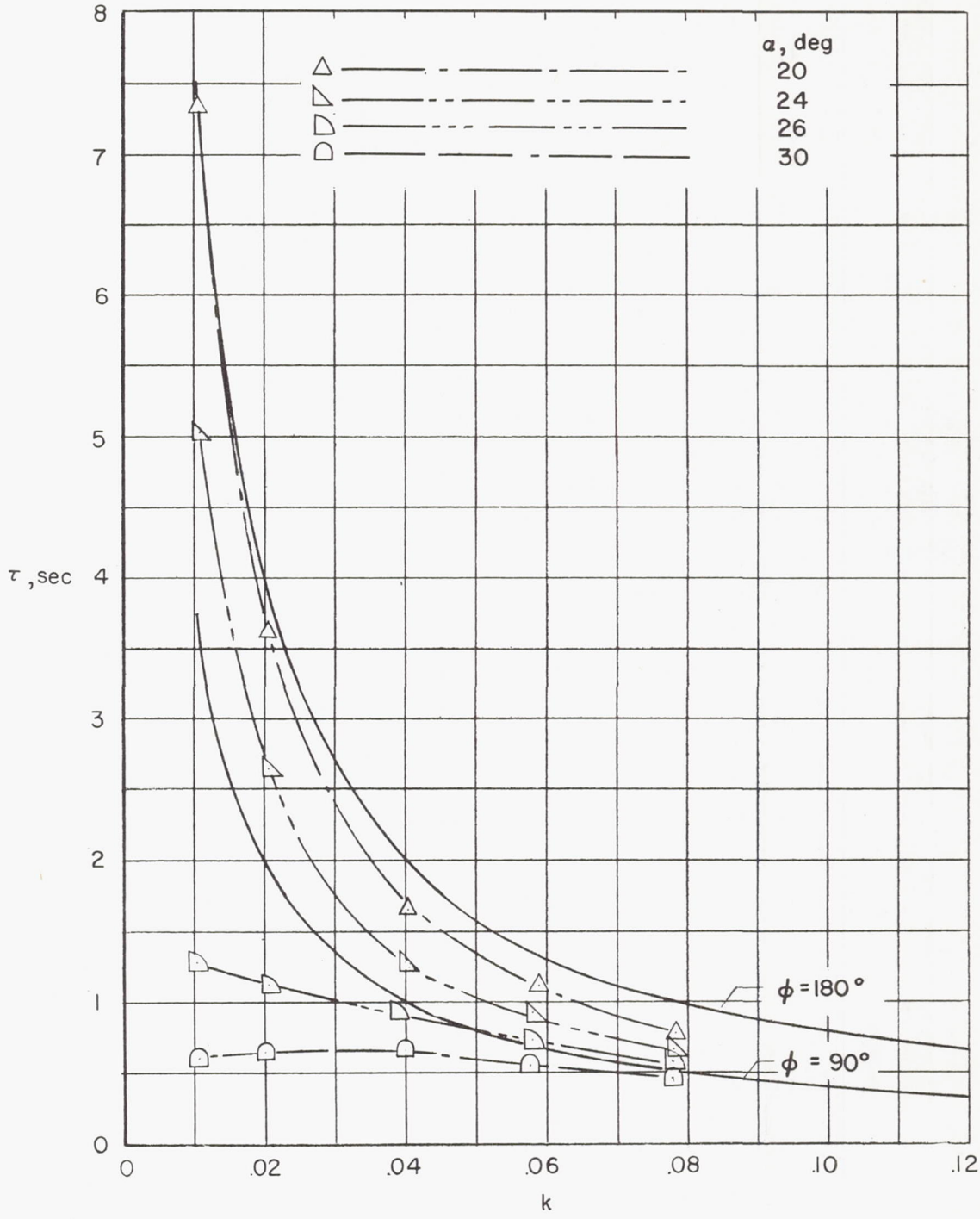

(d) Variation of time lag with frequency.

Figure 28.- Concluded.

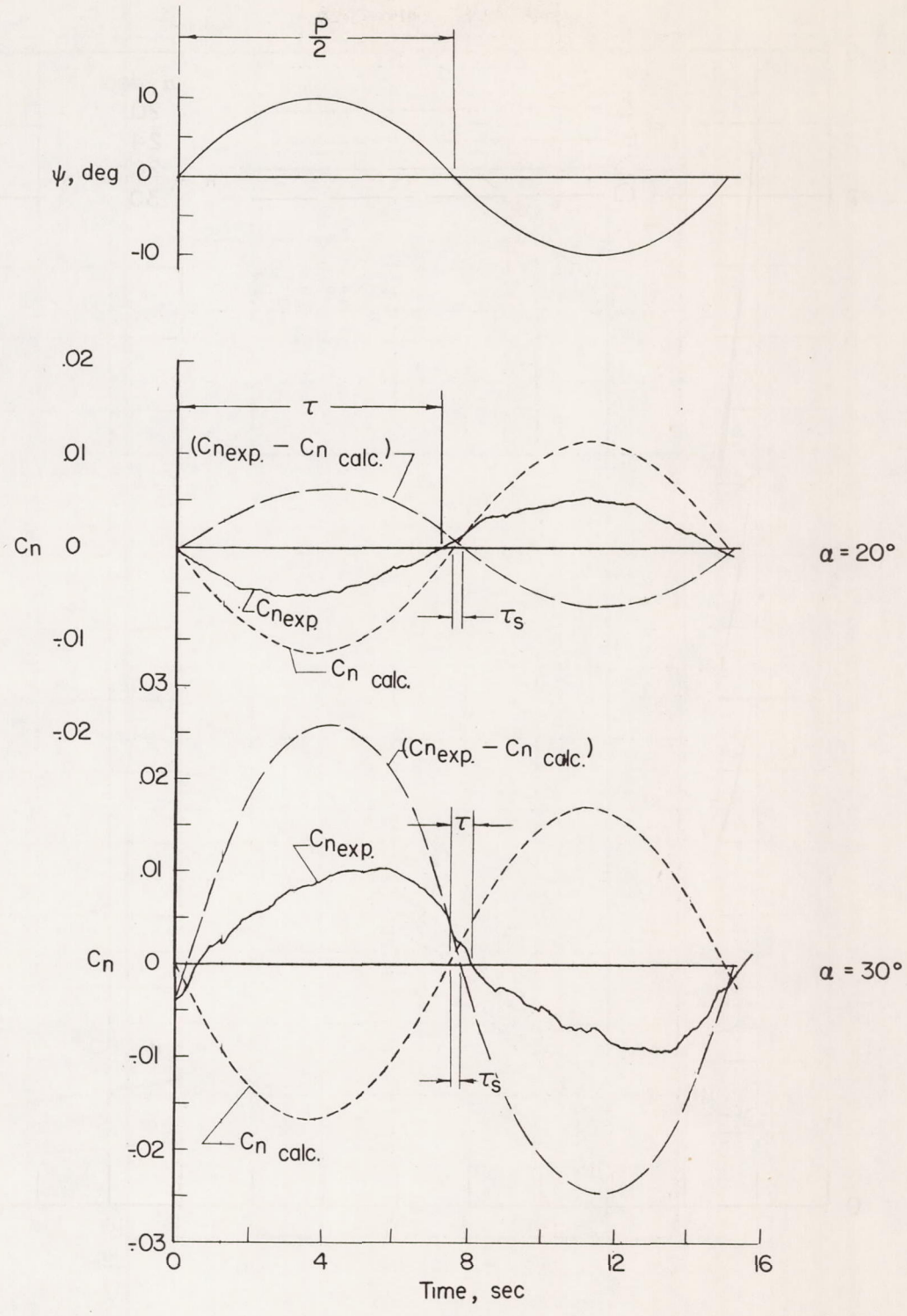

Figure 29.- Illustration of method used to determine effects of separation on the yawing moments measured during a yawing oscillation. Delta wing. P = 15 seconds.

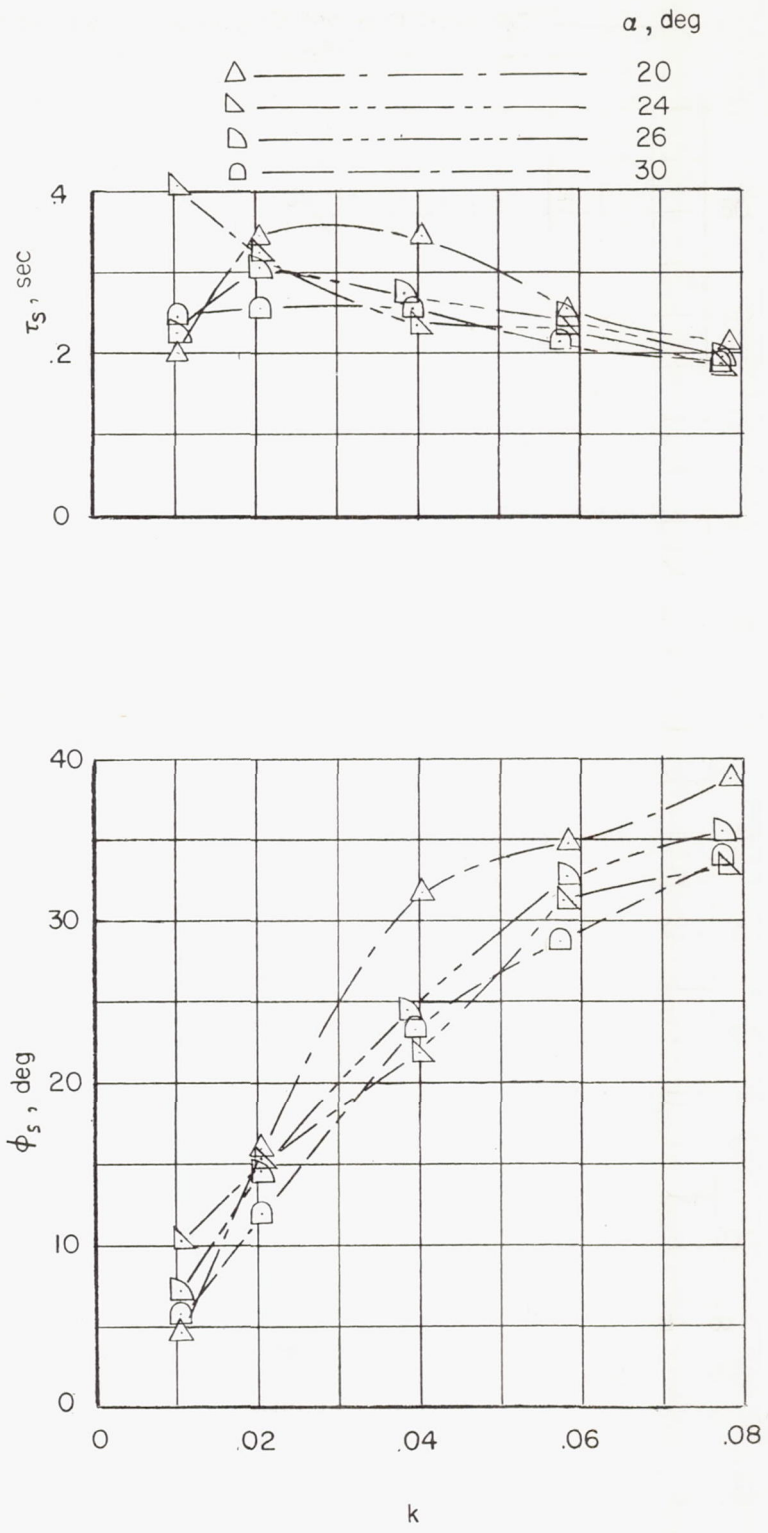

Figure 30.- Effect of frequency and angle of attack on the lag determined by the method illustrated in figure 29. Delta wing.

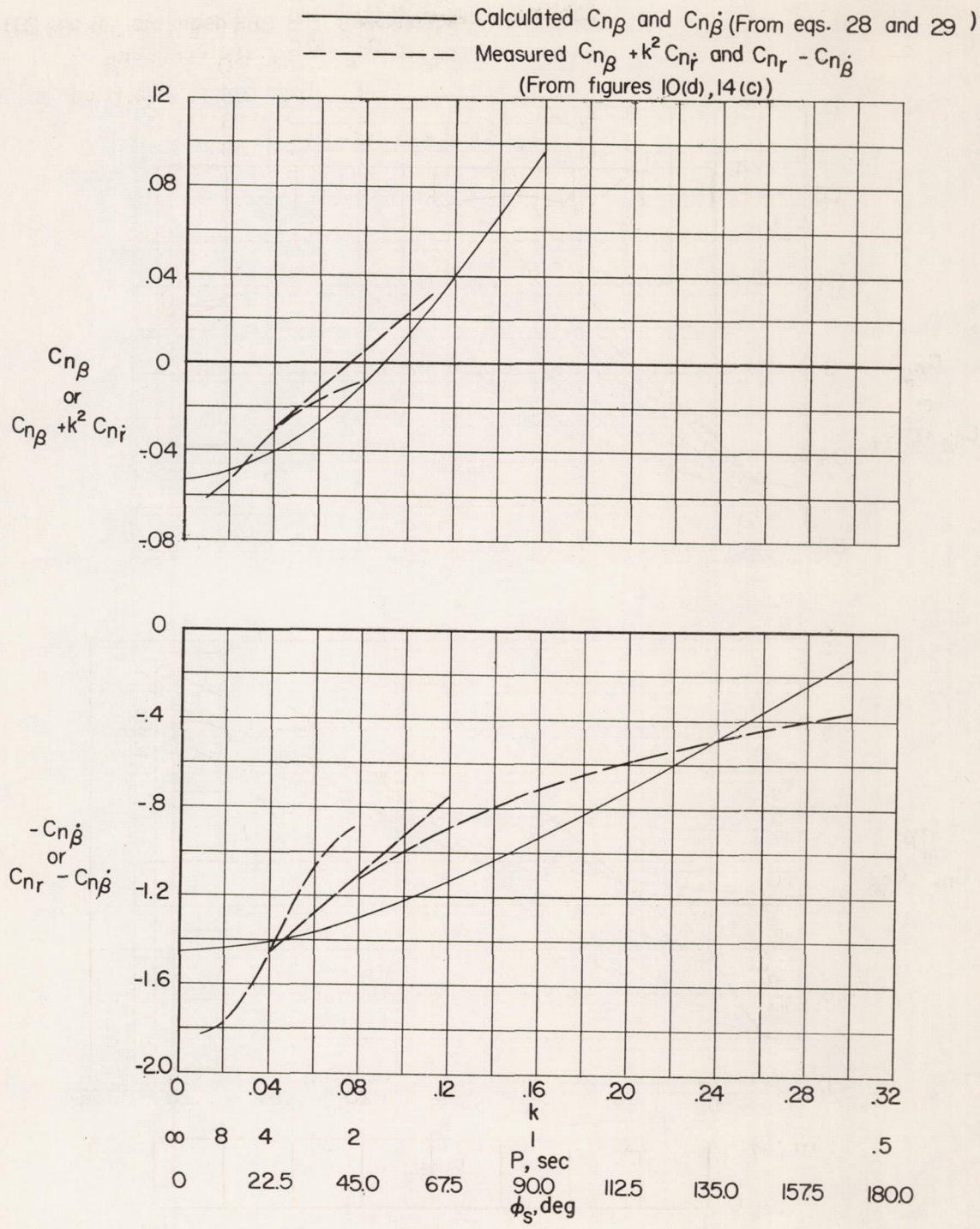

Figure 31.- Calculated effect of frequency on C_{n_β} and $C_{n_{\dot\beta}}$ for a time lag τ_s of 0.25 second and comparison with experimental data for $C_{n_\beta} + k^2 C_{n_{\dot r}}$ and $C_{n_r} - C_{n_{\dot\beta}}$. Delta wing, $\alpha = 30^\circ$. (For calculations, V = 60 ft/sec.)

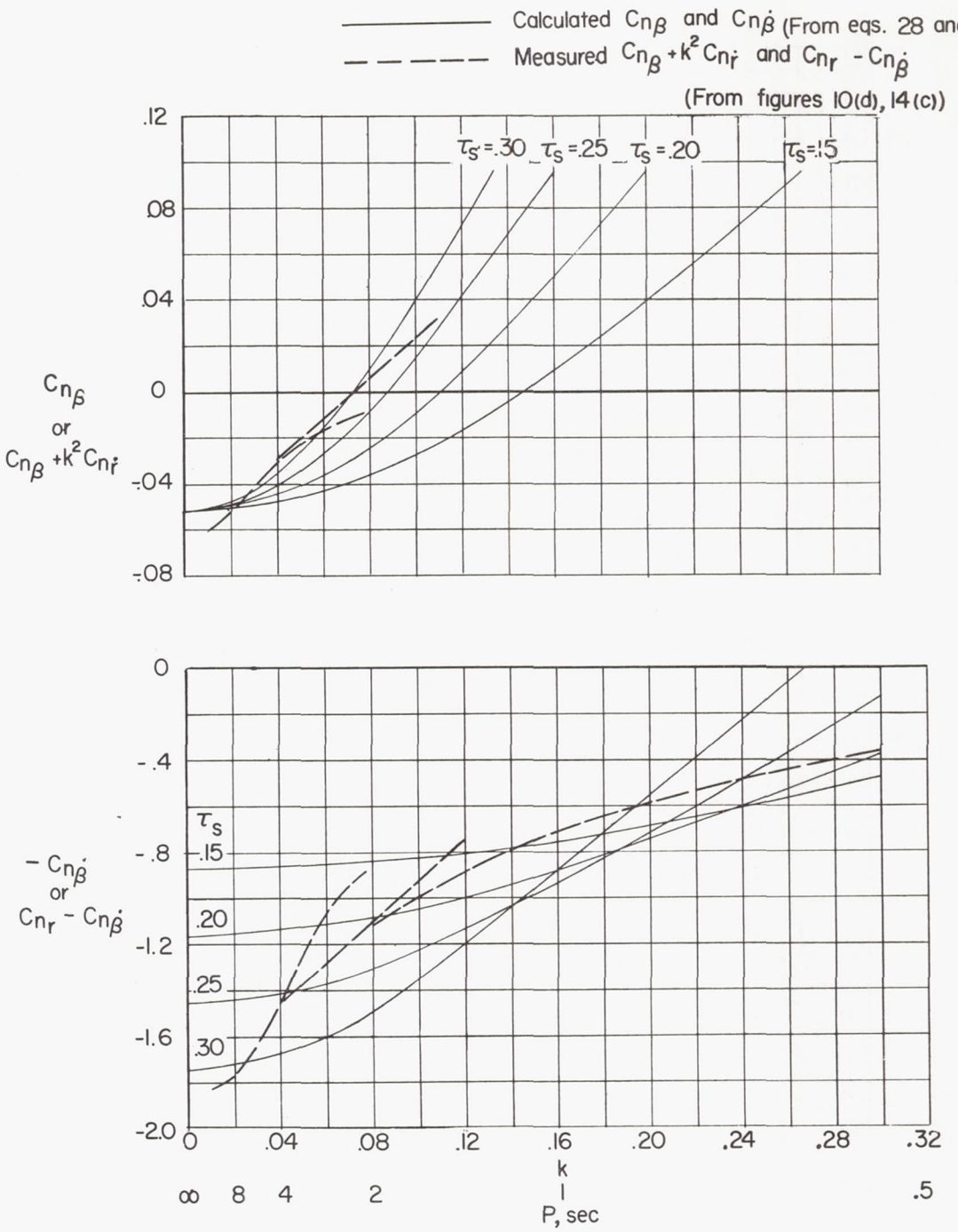

Figure 32.- Calculated effect of frequency on C_{n_β} and $C_{n_{\dot\beta}}$ for time lags of 0.15, 0.20, 0.25, and 0.30 second and comparison with experimental data for $C_{n_\beta} + k^2 C_{n_{\dot r}}$ and $C_{n_r} - C_{n_{\dot\beta}}$. Delta wing, $\alpha = 30^\circ$.

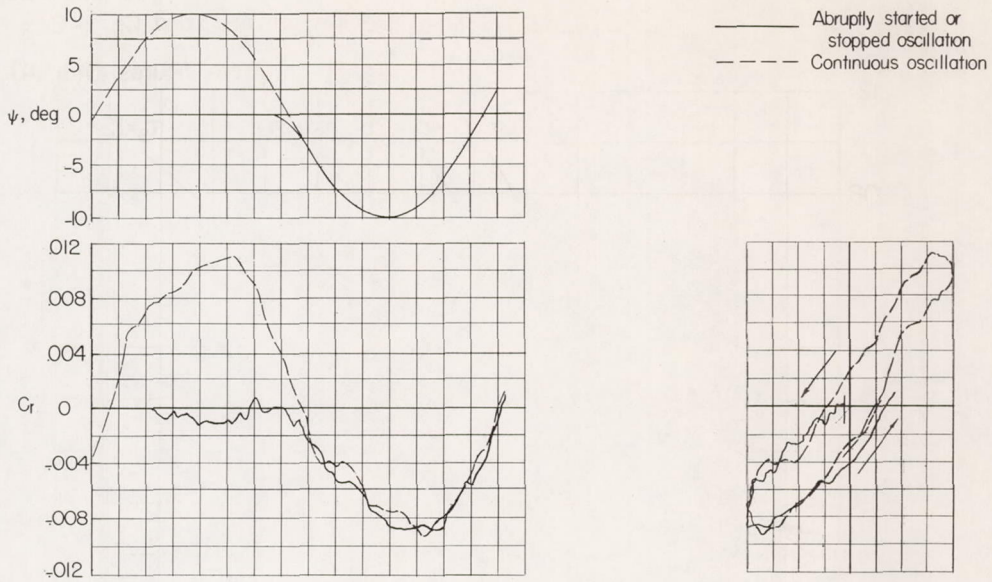

(a) Abruptly started oscillation.

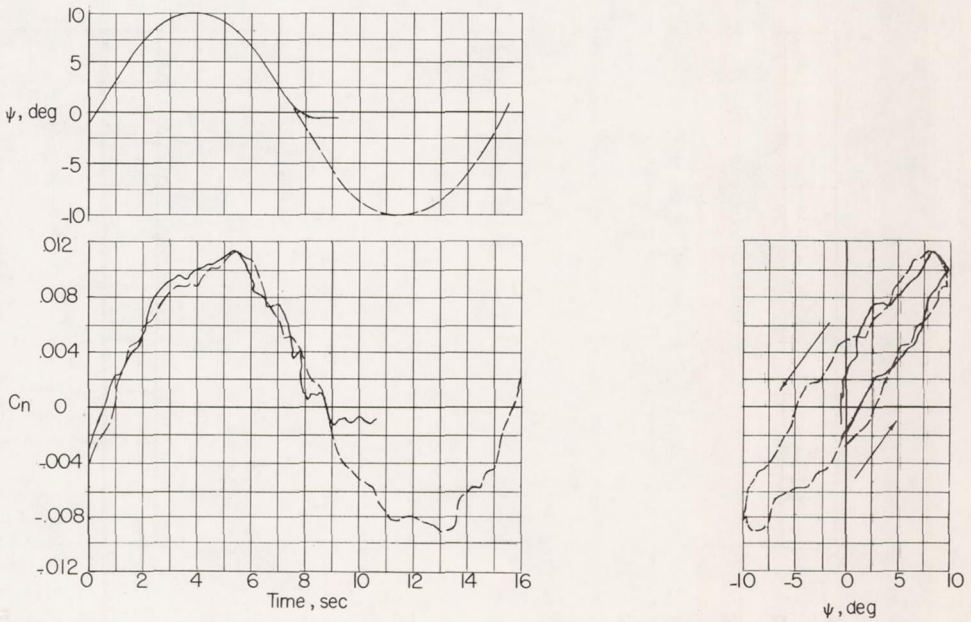

(b) Abruptly stopped oscillation.

Figure 33.- Illustration of the variation of yawing moment during sudden starting and stopping of a yawing oscillation. Delta wing, $\alpha = 30^{\circ}$; P = 15 seconds.